4-2012

Supercritical CO2 Extraction of Oil from Henna Flower: Experimental, Mathematical Modeling, and Antioxidant Activity

Bushra Saeed Mohammed Dohai

UAEU Faculty of Engineering

جامعة الإمارات العربية المتحدة
United Arab Emirates University

United Arab Emirates University
Faculty of Engineering
M.Sc. Program in Petroleum Science & Engineering

SUPERCRITICAL CO_2 EXTRACTION OF OIL FROM HENNA FLOWER: EXPERIMENTAL, MATHEMATICAL MODELING, AND ANTIOXIDANT ACTIVITY

By

Bushra Saeed Mohammed Dohai

A thesis Submitted to
United Arab Emirates University
In Partial fulfilment of the requirements
For the Degree of M.Sc in Petroleum Science & Engineering

April 2012

UAEU Faculty of Engineering

جامعة الإمارات العربية المتحدة
United Arab Emirates University

United Arab Emirates University
Faculty of Engineering
M.Sc. Program in Petroleum Science & Engineering

SUPERCRITICAL CO_2 EXTRACTION OF OIL FROM HENNA FLOWER: EXPERIMENTAL, MATHEMATICAL MODELING, AND ANTIOXIDANT ACTIVITY

By

Bushra Saeed Mohammed Dohai

A thesis Submitted to
United Arab Emirates University
In Partial fulfilment of the requirements
For the Degree of M.Sc in Petroleum Science & Engineering

Supervisor

Ali H. Al Marzouqi
Associate Professor in chemical Engineering
Department of Chemical & Petroleum Engineering
Collage of Engineering
United Arab Emirates University

April 2012

ABSTRACT

Henna is a plant that has been used traditionally for coloring nail, skin, and hair, and as medicinal plant. The supercritical fluid technology offers a considerable promise as extraction media due to its advantages over other conventional extraction techniques. The extraction of volatile components from flowers of henna was studied using supercritical carbon dioxide at temperatures and pressures ranging from 35 to 55 °C and 80 to 120 bar, respectively. A maximum extraction yield of 31% from 2g of henna flowers was obtained at 45 °C and 120 bar. The composition of the extracts was investigated by gas chromatography technique. Furthermore, the extracts were tested for their antibacterial and antioxidant activities. No inhibition zone was observed in the antibacterial study; however, the extracts obtained at most of the extraction conditions exhibited antioxidant activity.

A mathematical model of the extraction curve based on mass transfer principles was developed at all extraction conditions. Powell optimization method was used to obtain the model parameters by adjusting to experimental results. The calculated extraction yields were in good agreement with experimental results.

ACKNOWLEDGEMENT

Praise be to God for his unlimited graces and help to complete the requirements of this work.

First and foremost, I would like to extend my deepest gratitude to my supervisor Dr. Ali Al Marzouqi for his guidance, encouragement, valuable suggestions, support, and advices that are useful in personal and professional life. I would especially like to thank him for sharing his knowledge in supercritical fluid extraction (SFE), essential oils, mathematical modeling, and programming.

Secondly, I would like to thank the assistance of the following individuals who supported me in the analysis, Dr. Agnes Sonnevend from Faculty of Medicine and Health Sciences for her assistance in conducting the antibacterial test. I thank Mr. Babucarr Jobe, and Mr. Sajid Maqsood from Faculty of Food and Agriculture for sharing their knowledge on conducting antioxidant tests. The assistance of Dr. Ali Dowaidar in Gas Chromatography and particle characterization is also greatly appreciated.

I would like also to thank my close friend Eng. Hanifa Taher; a PhD student from Chemical and Petroleum Engineering Department for her support and assistance on using EndNote software. Also I would like to acknowledge my friend Negin Farah, a master student from Chemical and Petroleum Engineering Department for reviewing the English writing of this thesis.

Also, I wish to thank all the faculty members and staff of the Chemical and Petroleum Engineering Department at UAE University for supporting me during my research studies.

Last but definitely not the least; I thank my family members, who I can never thank enough for believing in me and helping me to go through the challenging period of my studies at UAE University.

TABLE OF CONTENTS

LIST OF FIGURES

LIST OF TABLES

Nomenclature

SCF	Supercritical Fluid
SFE	Supercritical Fluid Extraction
SC-CO_2	Supercritical carbon dioxide
GC	Gas Chromatography
HPLC	High Pressure Liquid Chromatography
T	Temperature, Kelvin
P	Pressure, bar
ε_b	Bed porosity
ε_p	Particle porosity
C_p	Concentration of solute in the particle phase, kg/m^3
C_{po}	Initial Concentration of solute in the particle phase, kg/m^3
C_{pR}	Concentration of solute at the particle surface, kg/m^3
C	Concentration of solute in the fluid phase, kg/m^3
C_o	Initial concentration in the fluid phase, kg/m^3
q	Concentration of solute in the solid phase, kg/m^3
q_o	Initial Concentration of solute in the solid phase, kg/m^3
d_p	Particle diameter, m
r	Particle radius, m
R	Bed radius, m
L	Bed length, m

D	Bed diameter, m
A	Bed cross sectional area, m^2
V	Bed volume, m^3
F	Flow rate of SC-CO_2, kg/s
u_s	Superficial velocity, m/s
u_i	Interstitial velocity, m/s
z	Axial coordinate, m
M_{sample}	Weight of charged sample, kg
M_o	Initial mass in the sample, Kg
y	Extraction yield percentage
f_o	fraction of oil initially dissolved in the fluid phase
ρ	Density of SC-CO_2, kg/m^3
μ	Viscosity of SC-CO_2, Pa.s
T_c	Critical temperature of CO_2, K
V_c	Critical volume of CO_2, m^3/mol
ρ_c	Critical density of CO_2, kg/m^3
μ_c	Critical viscosity of CO_2, Pa.s
ρ_r	Reduced density of CO_2
μ_r	Reduced viscosity of CO_2
D_{ax}	Axial diffusivity coefficient, m^2/s
D_e	Effective diffusivity coefficient, m^2/s

k_f	Film coefficient, m/s
K	Equilibrium constant, $m^3_{void}/m^3_{s.p}$
k_a	Adsorption coefficient, $s^{-1}m^3_{void}/m^3_{s.p}$
r	Radius coordinate, m
Δr	Size of particle increment, m
Δz	Size of bed increment, m
Δt	Time increment, m
N_r	Number of particle increments
N_z	Number of bed increments
N_t	Number of time increments

1 INTRODUCTION

1.1 Problem statement

Henna plant (*Lawsonia inermis)* extracts have historical usages in cosmetics and medicine fields. The plant extracts give temporary color, which is used for tattooing especially in Middle East region. Moreover, the extracts of henna exhibit biological activities, including antimicrobial, antioxidant, and anticancer activities.

Conventionally, chemical solvents are employed for extraction of components from henna leaves, seeds, and roots. Only few studies are available for the extraction from henna flowers using solvent extraction. These toxic and expensive chemical solvents hinder the explorations on valuable extracts from henna. Furthermore, separation processes are not efficient enough, and are risky, especially when extracts are used for food or medicine. Moreover, volatile components can thermally degrade if other conventional techniques such as steam distillation are used.

The supercritical fluid technology is a promising field, which has in some application replaced the traditional extraction techniques. This is typically due to the favorable transport properties of supercritical fluids. In particular, supercritical carbon dioxide has gained a great deal of attention since it is nontoxic, inexpensive, inert chemical, and nonflammable. In addition to these properties, supercritical conditions of carbon dioxide are easily reachable (31 ^{o}C and 73 bar).

1.2 Scope

Supercritical carbon dioxide can be utilized to extract volatile components from henna flowers with comparable quality and yield to conventional extraction techniques. Furthermore, the effect of extraction on extract solubility and yield is investigated. The physical trend of the extraction curve is studied by proposing a mathematical model based on laws of conservation of mass.

1.3 Objectives

The main target of this thesis is to examine the validity of supercritical fluid to extract volatile components of henna flowers. This main target has the following specific targets:

1. Optimization of supercritical extraction conditions.
2. Compositional analysis of the extracts by gas chromatography
3. Investigation of antibacterial and antioxidant activities of the extract.
4. Development of mathematical model for the supercritical extraction process.

2 BACKGROUND AND LITERATURE SURVEY

2.1 Henna plant (Syn. Lawsonia inermis Linn. Lytheraceae)

Henna is a flowering plant grown in dry tropical and subtropical regions such as Middle East, North Africa, India, and Srilanka. The plant extracts are traditionally used for cosmetic purposes and applied to hands, feet, nails and hair to give temporary color. The major component of the extract is the lawsone (2-hydroxy-1,4-naphthoquinonel) which is the dying molecule that supplies red-orange pigment. In addition it is used to reduce body temperature in case of high fever. Hanna's extracts are prepared by finely grinding the dried leaves and mixing them with water at room temperature.

In addition to the cosmetic purposes, henna is considered as medicinal plant since the extracts showed biological activities including antimicrobial (Hsouna et al., 2011; Jallad & Espada-Jallad, 2008; Priya et al., 2011), antifungal (Chaudhary et al., 2010; Sharma & Sharma, 2011), anti-inflammatory and antipyretic (BH. et al., 1995; Mikhaeil et al., 2004), and antioxidant (Hsouna et al., 2011; Uddin et al., 2011). Henna extracts are used as medicine for jaundice, leprosy, smallpox, and skin complaints. Moreover, it was asserted by Priya and co-authors that the ethanol extracts of henna roots exhibited significant antitumor activity, which explained the fact that henna has a long history for the treatment of cancer (Priya et al., 2011).

The leaf extracts took the attention of most henna investigators. The biological activities of the leaf extracts from henna trees were scanned. Anis and his colleagues figured out that the chemical components of L.inermis leaves have good antioxidant capacities, and it is possible to use those extracts as a potential source of new natural

antioxidant (Hsouna et al., 2011). Furthermore, leaf samples were analyzed for their antimicrobial potential and showed obvious antibacterial activity against Escherichia coli (Hsouna et al., 2011; Jallad & Espada-Jallad, 2008; Priya et al., 2011). Besides, isolation of Lawsone from leaves' extract revealed strong antifungal activity (Sharma & Sharma, 2011). The extracts showed anticancer activity as well against liver and colon cancer cells (Endrini et al., 2007; Uddin et al., 2011).

On the other hand there is only one study published on the flower part. Wong and Tong, 1995 extracted the volatile components of henna flowers by solvent extraction. They analyzed the extract and identified the major components by GC and GC-MS for red and yellow flowers. The research revealed the presence of volatile components in the yellow flowers such as: (E)-3-hexenol, diethyl oxalate, linalool, dihydro-β-ionone, benzyl alcohol, 2-phenylethanol, β-ionone, and dihydro-β-ionol. Other volatile components were detected in the red flower including; hexanal, eugenol, and ethyl linolenate. Volatile components in yellow and red henna flowers with their corresponding composition are presented in Table 1.

Table 1 Major volatile components in henna flower (Wong & Tong, 1995)

Component	Composition in yellow flower (wt %)	Composition in red flower (wt %)
Hexanal	-	1.4
Hexanol	1.6	1.5
(E)-2-hexenal	-	5.4
(E)-2-hexenol	-	2.2
(E)-3-hexenol	5.4	3
Diethyl oxalate	1.4	3.1
Linalool	19.8	12.7
Methyl salicylate	-	1.8
Ethyl nicotinate	-	1.2
Dihydro-β-ionone	2.5	-
Benzyl alcohol	3.3	6
2-phenylethanol	5.8	11.5
β-ionone	48.6	2.5
Dihydro-β-ionol	1.4	-
Eugenol	-	1.1
Ethyl palmitate	-	1.1
Ethyl linoleate	-	2.5
Ethyl linolenate	-	8.9

2.2 Supercritical fluids (SCFs)

A supercritical fluid is a substance beyond its critical pressure and temperature where only one phase exists. Figure 1 illustrates a phase diagram for carbon dioxide. SCFs physical and chemical properties intermediate between gases and liquids. As indicated in

Table 2, SCFs have diffusivities higher than pure liquids, and viscosities higher than those for pure gases. A SCF has the gaseous property of being able to penetrate and the liquid property of being able to dissolve materials into their components. SCFs possess

no surface tension hence no capillary forces will appear during extraction. The solvating power of the SCF follows the changes in the density.

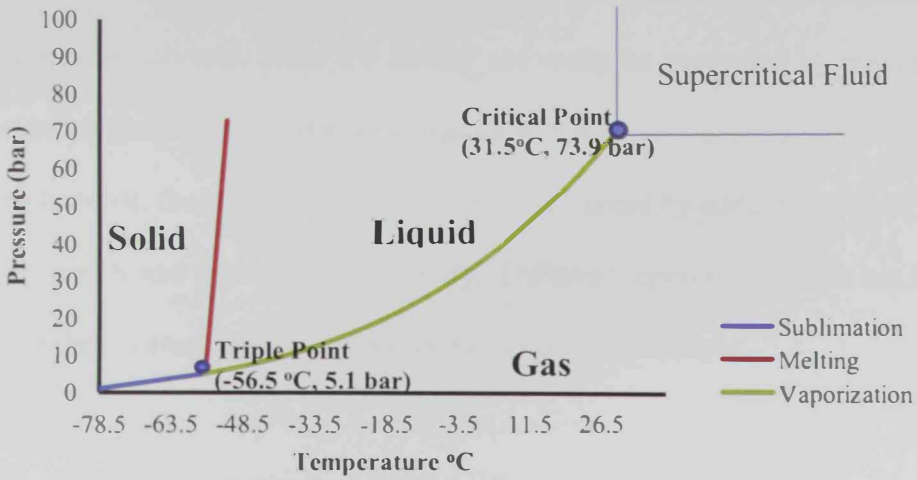

Figure 1 Phase diagram of CO_2

Table 2 Some of the physical properties of gas, liquid and supercritical fluid

Physical State	Density (kg/m^3)	Viscosity (cp)	Diffusivity (mm^2/s)
Gas	1	0.01	1-10
Supercritical Fluid	100-800	0.05-0.1	0.01-0.1
Liquid	1000	0.5-1	0.001

Around the critical point, the density, viscosity and diffusivity of the fluid are tunable and sensitive to pressure, for example, a small change in the pressure results in large changes in densities and hence large change in the solvating power of the fluid. Figure 2 presents the change of density of carbon dioxide with pressure at 15 °C and 32 °C. It is clear from the figure that at 15 °C, pressure has small influence on density of the fluid, however at 32 °C, which is close to the critical temperature; the change is drastic around the critical pressure (73.9 bar).

Such combination of fluid properties provides the drive for applying SCFs as a preferable alternative to conventional organic solvents. The higher diffusion coefficient of SCFs compared to that of liquids allows SCFs to penetrate into solid materials easier than organic solvents. Since the density can easily be controlled by pressure, separation of substances from SCFs is easy to handle which reduces separation costs. In addition to these benefits, the solubility in SCFs can be enhanced by adding modifiers to change the fluid polarity and improve its selectivity. Different supercritical fluids are listed in Table 3 with their corresponding critical conditions and applications.

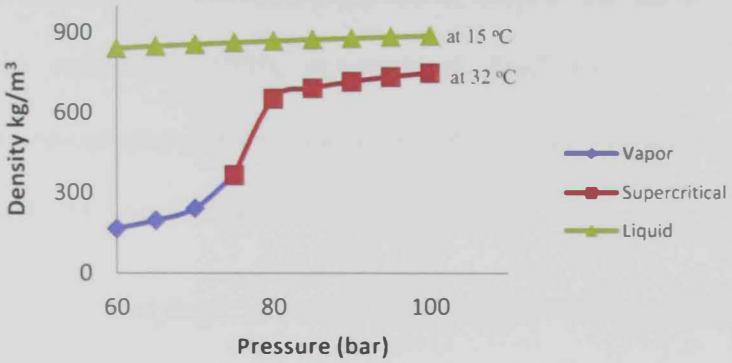

Figure 2 The change in density of CO_2 with pressure

Among all listed supercritical fluids in Table 3, the most commonly used fluid is the carbon dioxide due to its benign chemical and physical characteristics which are; the easily reachable critical temperature which saves energy, being nontoxic, inflammable, and noncorrosive. In addition, from economic aspects it is readily available with low cost compared to other fluids. Supercritical carbon dioxide is hydrophopic which allows easy dissolution of light hydrocarbons. The low polarity of SC-CO_2 increases its stability which is environmentally acceptable.

Although the special characteristics of supercritical fluids were first discovered in 1879 by Hannay and Hogarth, applications of supercritical fluid technology marked crucial place on the research areas over the last three decades. SCFs have been used in different industries: Neutracuetical, Pharmaceuticals, Cosmetics, Polymers, textiles and clothing, soil remediation, and renewable energy (McHugh & Krukonis, 1994).

Researchers have used SCFs in different unit operation techniques including extraction and impregnation, fractionation, chromatography, drying, coating, dying, and as reaction media. It is worth mentioning that SCF techniques are available in commercial scale with more than 200 plants around the world. Most of the industrial techniques are supercritical fluid extraction (SFE), supercritical fluid fractionation (SFF), supercritical fluid chromatography (SFC), and supercritical fluid reaction (SFR). These techniques are briefly discussed in the following paragraphs.

In analytical chemistry supercritical chromatography is prefered approach to liquid chromatography due to its shorter time consumption, safety since it acquires lower organic solvents, and simple decompression is needed to obtain the products (García-Risco et al., 2011). Supercritical chromatography is employed for separation of mixtures, determination of binary diffusion coefficients of solutes (Guiochon & Tarafder, 2011) and detection of dyes in food samples (Rezaei & Temelli, 2000).

Table 3 Most Common Supercritical fluids

Compound	T_c (°C)	P_c (bar)	Application	Reference
Nitrogen	-147	33.98	Polymer processing due to its inert properties , Gass assisted injection moulding process	(Okubo, 2005; Zhang et al., 2011)
Ethylene	282.4	48.2	Polymer processing	(Yeo & Kiran, 2005)
Carbon dioxide	31.5	73.9	coffee and tea decaffeination, extraction of essential oils: spices, fragnces, dyes, pharmacuetical compounds, and polymerization	(B.Gupta & Shim, 2007)
Nitrous oxide	36.4	72.5	As a solvent and oxidant for organic functional group since the byproduct is N_2 which is environmentally acceptable, Extraction of: Amines, pharmacuetical compounds from animal feed, and lipids from human plasma.	(Ashraf-Khorassani et al., 1990; Poh et al., 1999)
Butane	91.8	46.2	Production of: isoparaffins byFischer-Tropsch synthesis from synthesis gas, and emulsifiers by enzyme-catalyze glycerlysis reaction	(Ceni et al., 2010; Valerio et al., 2009; Yoneyama et al., 2009)
Propane	96.6	42.5	Deasphaltation of petroleum, regeneration of activated carbon fiber in liquid petroleum gas processes (LPG), and Manufacture of metallocene catalysts in polyolefin production	(Chihara et al., 2012; J. Wang et al., 2004)
Ammonia	132.5	112.8	Synthesis of carbon nanotubes, heterogenous catalytic processes, ammonothermal growth of GaN in the manufucture if light emitting devices (LEDs)	(Fischer et al., 1999; Hashimoto et al., 2005; Shao et al., 2009; Vyalov et al., 2011; S. Wang et al., 1999)
Acetone	235	46.9	Biodiesel production : to ketalise the byproduct glycerol into slketal, Chemical recycling of polymers, thermal dehydration of fructose, and thermal degradation of cellulose	(Hwang et al., 1999; Royon et al., 2011)
Methanol	239.4	81	Chemical recycling of polymers, Biodiesel production, and synthesis of metal and metal oxide nanoparticles, and nanofluids	(Okubo, 2005; Quesada-Medina & Olivares-Carrillo, 2011; Sawangkeaw et al., 2009; Tan et al., 2010; C. Wang et al., 2011; Zhou et al., 2010)
Ethanol	243	63.8	Biodiesel production, and polymer processing	(Gonen et al., 2011; Gui et al., 2009)
Tetrahydrofuran (THF)	267	51.8	Chemical recycling of polymers	(Lee & Hong, 1998)
Toluene	318.6	41	Chemcial recycling of polymers, extraction of petroleum pitch, oil shale processes, and liquefaction of coal	(Abourriche et al., 2009; Joung et al., 1999; Pan et al., 2006; Sangon et al., 2006; Zhuang & Thies, 1999)
Water	374	221	Supercritical water oxidation in waste treatment processes, hydrothermal synthsis of multicomponents oxide in particle formation, gasification and reforming of biomass, and reaction media fo polymerization and conversion processes	(Brunner, 2009; Kipcak et al., 2011; Kruse & Dinjus, 2007; Lachance et al., 1999; Letellier et al., 2010; Leusbrock et al., 2010; Marias et al., 2011; Otsu & Oshima, 2005; Savage, 2009; van Bennekom et al., 2011; Vogel et al., 2005; Yoshida et al., 2004; Zheng et al., 2008)

Supercritical fluids also act as good reaction media due to their beneficial physical characteristics, which were discussed earlier. The reason behind carrying out reactions under supercritical conditions is the possibility of controlling reaction conditions via temperature and pressure. In multi-step reactions the supercritical media can be the choice in the case of diffusion limited reactions due to the high diffusion coefficients of SCFs. A supercritical media can also shift the reaction balance towards the products when the later one is prefered to dissolve in certain phase, thus the selectivity can be enhanced. Many researchers have investigated the use of supercritical media in chemical reactions such as; ethylbenzene disproportionation (Sotelo et al., 2010), synthesis of vitamin E (S. Wang et al., 2000), desulfurization and demetallizaiotn of gasoil (Vogelaar et al., 1999).

2.3 Extraction Technologies

Extraction is used to recover compounds from raw materials. The raw material can be solid such as herbs and meats, or liquid such as crude oil and gels. The phenomenon behind extraction is the solubility of the desired compounds can dissolve in another substance or phase according to their molecular properties such as polarity. Many industries are using extraction among which are; pharmaceutical, food, cosmetics, environmental & petroleum industries. The most common extraction technique is Soxhlet extraction and steam distillation or hydro-distillation. The new extraction technology which has taken a great attention recently is the supercritical fluid extraction. Theses extraction techniques are discussed below with extended detail for SCF extraction.

2.3.1 Soxhlet Extraction

Soxhlet extraction also known as solvent extraction was first introduced by Von Soxhlet in 1879 as a solid-liquid extraction technique. It has been used for more than a century and considered as the main reference to evaluate the performance of other extraction methods. In Soxhlet extraction an organic solvent is used to dissolve a desired compound from solid raw material. The criteria for selecting appropriate solvent are: high solvent power, selectivity, and chemical stability, being recyclable, inexpensive, nontoxic and noncorrosive, low viscosity, avoid emulsion, and allow formation of immiscible liquid phases (Luque de Castro & Priego-Capote, 2010).

In Soxhlet extractor the solvent is placed in a reservoir and heated up to evaporation and is passed through a distillation tube. The solvent vapor is condensed indirectly by cold water and dripped into the chamber holding the solid sample. During dripping, the extraction takes place and once the sample chamber is filled with the warm solvent, the later one returns back to its starting reservoir via siphon arm holding the desired extract. A further separation is acquired to obtain the extract. Figure 3 shows the schematic diagram for Soxhlet extractor.

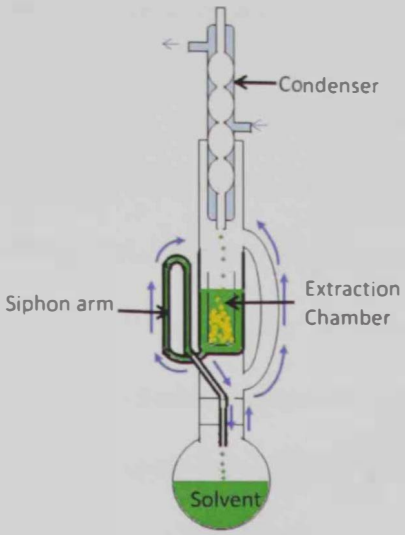

Figure 3 Soxhlet Extractor

Using this extraction approach one can ensure the continuous contact between sample and fresh solvent which improves the driving force and hence the mass transfer. Also the equipment is economical compared to microwave-assisted extraction and supercritical extraction. Moreover, the selectivity can be enhanced by altering the solvent polarity. The drawbacks of this technique include: time consumption, large amount of solvent which increases the cost and environmental impact, and thermal degradation of some compounds which may happen since the process is performed at a temperature close to the boiling point of the solvent (Luque de Castro & Garcia• Ayuso, 1998).

2.3.2 Hydrodistillation

One of the oldest extraction methods is hydrodistillation which uses water as solvent for the extraction of water soluble compounds. Adequate amount of water is poured into the vessel containg the solid sample. Heat is supplied to boil water and steam is allowed to penetrate into the sample to release the desired compounds from its raw material. The leaving steam containing the extract (distillate) is condensed by indirect

cooling and flows into a separator where extract is automatically isolated from distillate water.

The main advantages of this technique is its feasibility and low solvent cost. Bearing in mind that it suffers from serious disadvantages including; low extraction efficiency since steam cannot penetrate into the inner pores, time consumption, and degradation of volatile components which are thermally sensitive materials (Damjanovic et al., 2005; Khajeh et al., 2005). In addition to these drawbacks, the long contact time of plant material can cause the hydrolysis of essential oil compounds such as esters into acids and alcohols (Handa et al., 2008).

2.3.3 Microwave- Assisted Extraction (MAE)

Microwave- Assisted extraction is a new technique applied firstly in 1986 by Salgo et al for extraction of organic compounds. MAE is being commercialized with two types; closed extraction vessels and focused microwave ovens (Mandal et al., 2007). MAE is mainly based on converting the electromagnetic energy in microwaves into heat energy at frequency of 2450 MHz. It saves energy since heating occurs in closed systems, and saves time compared to other conventional extraction techniques (Armstrong, 1999; Duvernag et al., 2005; Franke et al., 1996; Ganzer et al., 1986). The extraction takes place when moisture inside the sample cells is heated up and evaporates pushing the cells walls from inside. As a result of the pressure, the walls stretch and rupture releasing the active compounds into the surrounding solvent (Mandal et al., 2007) .

The process is limited by the solvent nature since only polar solvents can absorb microwave heating. Therefore, MAE is not a favorable technique for recovery of non

polar compounds. Moreover, MAE has lower selectivity than SFE, hence fractionation cannot be avoided to enrich or purify the extract. After extraction cooling and depressurizing of the vessels are required which consume energy and time (Sun & Lee, 2003; Taathke & Y.Jaiswal, 2011). Another drawback is the environmental impact due to solvent usages. Another disadvantage mentioned is the significant thermal degradation of analytes extracted by MAE (Chan et al., 2011) .

2.3.4 Supercritical Fluid Extraction (SFE)

SFE is simply carried out by passing a SCF (usually CO_2) through sample material such as dried plants. Due to the transport properties, the compound of interest transfers into SCF phase. The process is restricted by temperature, pressure, fluid flow rate, time, and sample size. The SFE process is schematically shown in Figure 4. CO_2 flows from the cylinder into a pump and a heater where temperature and pressure are adjusted to reach the supercritical state. The SC-CO_2 passes through the extraction vessel which is charged by the sample material. The desired compounds dissolve in the supercritical fluid as a result of contact between the two phases. The SC solution (SC-CO_2 containing the extract) leaves the extraction vessel. Finally, the extract is collected by venting SC-CO_2 at ambient condition into a vial. It should be noted that CO_2 can be recycled and the process can be performed continuously to reduce the cost and facilitate the operation work.

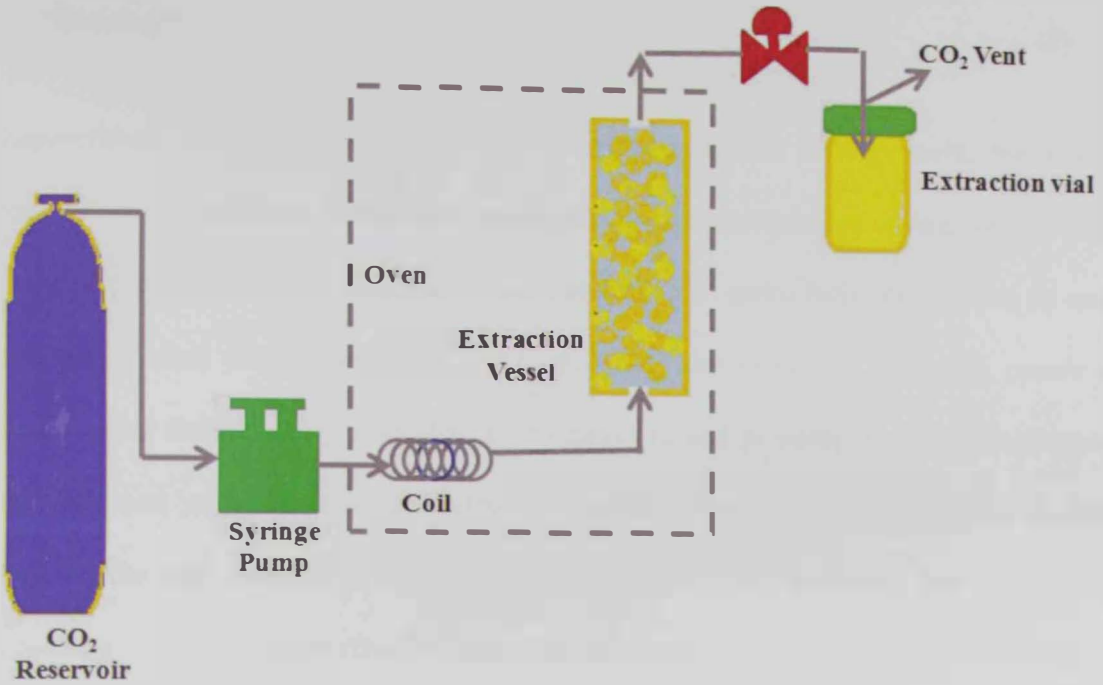

Figure 4 Schmatic diagram of SFE apparatus

The performance of SCF process can be assessed by three parameters which are; product yield, product quality, and efficiency. Yield is defined as the amount of extract obtained by SFE over the amount of sample charged in the extraction vessel.

$$\%\ \text{Yield} = \frac{W_{extract}}{W_{sample}} \times 100 \qquad (1)$$

On the other hand the product quality is described by analytical techniques such as gas chromatography (GC) and high performance liquid chromatography (HPLC). The product has high quality when high removal of impurities or high abundance of desired compounds was obtained from extraction process. Extraction efficiency is defined as the amount of extract obtained by SFE over the amount of extract initially present in the charged sample. The amount of extract initially present in a sample is found by a reference conventional extraction technique such as Soxhlet extraction..

$$\% \text{ Efficiency} = \frac{W_{extract}}{W_{extract\ in\ charged\ sample}} \times 100 \qquad (2)$$

Supercritical fluid extraction has numerous advantages that can be useful for several applications in different fields; food, cosmetics, pharmaceuticals, clothing, and etc. The process is environmentally acceptable and considered as green technology since no toxic solvent is used thus reducing harmful residues. Moreover the solvating power of supercritical fluid is easily controlled by temperature and pressure. Another advantage is that isolation of SCFs from the extract is feasible since SCFs are separable at room temperature and thus reduces the separation expenses. In addition, due to the high solvating power of supercritical fluids, extraction of high boiling point compounds is achievable at lower temperatures. Thermal degradation of sensitive valuable compounds can be avoided in supercritical fluid extraction.

The main reported drawback of supercritical fluid extraction is the high capital cost of the equipment which can be covered by the recovery of valuable and commercial compounds with higher yield and quality. A disadvantage of SC-CO_2 is that it is a good solvent only for non polar compounds; however, addition of modifiers such as ethanol could increase the solubility of polar compounds.

2.3.4.1 Extraction parameters

The extraction process strongly depends on several factors including; temperature, pressure, time, solvent flow rate, and particle size. Effects of these factors are discussed bellow.

Pressure Effect

The effect of pressure on the extraction process is related to solvent density and solvent power. It is well known that when the pressure is increased, the solvent density increases elevating the solvent power, thus reducing amount of solvent needed. In other words increasing the extraction pressure will result in more molecules being forced into the solution, therefore more solutes will dissolve in the supercritical fluid. This behavior is favorable when higher extraction yield is desired. It should be brought to attention that an increase in extraction pressure will reduce the extraction selectivity since higher solubility means dissolving more compounds. Consequently, the extraction pressure can be used to tune the selectivity since density is sensitive in supercritical region.

Temperature Effect

The extraction yield is strongly influenced by extraction temperature. It is obvious that change in extraction temperature is associated by change in supercritical fluid density and solute volatility which affect the solute solubility in opposite ways. Such behavior of the extraction temperature is commonly known as the crossover phenomena where both parameters (density and volatility) are competing factors are dominant. By increasing the extraction temperature the volatility of the extract increases, which increases the solubility, hence extraction yield goes up. The extraction yield goes down with increasing temperature when density of supercritical fluid decreases causing reduction in the solubility.

Effect of solvent flow rate and extraction time

The solvent flow rate is inversely proportional to extraction time. Increasing the solvent flow rate will make the extraction process faster. At higher solvent flow rates, the contact time between solvent and sample will be lower, and the solvent may not have enough time to penetrate into sample pores effectively. As a result lower amount of dissolved compounds will exist in the supercritical fluid, thus reducing extraction yield.

Effect of particle size

In most cases sample preparation is needed before performing the extraction process. One of the preparation steps is grinding the sample into smaller size. It is well known that when the sample particle size is decreased, the surface area increases and the contact between the solvent and sample material will be more. As a result of increasing the contact between the sample and solvent, more extract will be released from the sample cells and hence extraction yield is enhanced.

Several investigators reported that in some cases decreasing the sample particle size can lead to lower yield. The reason behind this behavior is that the small particles are packed together forming bed caking allowing the solvent to flow through channels along the extraction bed (Bernardo-Gil et al., 2007; Jia et al., 2009b; Langa, Cacho et al., 2009; Langa, Porta et al., 2009; Liu et al., 2010).

2.3.4.2 Mathematical Modeling

The potential interest in supercritical fluid extraction is the need for mathematical and theoretical description of the extraction process. A mathematical model of a process helps in predicting the process design parameters such as solvent flow rate, particle size,

and equipment dimensions. Moreover, due to high capital investment of SFE, a mathematical prediction is needed to assess the process scale-up feasibility. The mathematical model of the process reflects the physical trend of the experimental data.

The extraction process is mainly described by an extraction curve; a plot of extract weight versus CO_2 volume. Simulation of extraction curve can be accomplished by understanding the extraction mechanism and solute behavior in the SCF phase. Briefly, in the extraction process the transport of solute occurs in three phases namely; solid phase, particle phase, and fluid phase. First, the solute moves from the solid particle the pores, then, diffuses inside the pores will take place, and the final step is the axial diffusion along the bed. The extraction process is affected by the solubility and diffusion of the solutes in supercritical fluid phase.

2.3.4.2.1 Solubility of solute in Supercritical fluid phase

Solubility data of the interested compounds are needed to model the supercritical fluid processes. Investigators have used many approaches to observe the behavior of a solute in the supercritical fluid region. Those approaches can be divided into two main categories; mathematical and experimental depending on the nature of the existing compounds. The mathematical approach uses two main tools; empirical correlations and thermodynamic models.

- *Thermodynamic solubility*

The thermodynamics models for solubility or phase equilibrium data are based on equations of state along with various mixing rules. Typically, a system reaches equilibrium state when it meets one of the three conditions; minimum Gibbs free energy,

same chemical potential of each specie in all phases, and the equality of the fugacity of pure solute to its fugacity in supercritical fluid phase. The equilibrium data can be described by the fugacity coefficient which is obtained by equations of state. The calculations start with common assumptions including; the solubility of the fluid in solute phase is negligible and the molar volume of solute phase is constant. At equilibrium the fugacity of the solute in the solid phase is equal to the fugacity of the solute in the supercritical phase (Eq. 3). The fugacity of pure species at solute phase and supercritical phase are calculated using equation 4 and 5, respectively.

$$f_i^{solid} = f_i^{supercritical} \quad (3)$$

$$f_i^{solid} = P_i^{sat}\varphi_i^{sat} exp\left[\frac{v_i^{solute}(P-P_i^{sat})}{RT}\right] \quad (4)$$

$$f_i^{supercritical} = y_i\varphi_i P \quad (5)$$

Where f is the fugacity and i refers to component i in the mixture, P is the pressure, T is the temperature, v is solute molar volume, R is the universal gas constant, P_i^{sat} is the saturation pressure found either in literature or calculated using Antoine equation (Eq. (6)) , φ_i^{sat} is fugacity coefficient for species i at saturation and can be taken as unity, and φ_i is the fugacity coefficient of species i in supercritical fluid phase which is calculated by equations of state such as; Peng-Robhinson, Van der waals, and Redlich-Kwong equation of state.

$$\log P^{sat} = A - \frac{B}{T(K)-C} \quad \text{Eq.(6)}$$

where A, B, and C are Antoine constants for pure species, T is the operating temperature

Several investigators used equations of state for solubility calculation. Recently, Yazdiadeh et al., 2011 modeled the solubilities of 52 mostly used solid compounds in supercritical carbon dioxide. In their model, they applied the Peng-Robinson and Esmaelizadeh-Roshanfekr equations of state along with several mixing rules including Wong-Sandler and Van der vaals. Their results showed good agreement with experimental data found in literature (Yazdizadeh et al., 2011). Gracia et. al, 2009 studied the phase behavior of vegetable oils in supercritical carbon dioxide. In their approach, they considered that any vegetable oil consists of two key components; oleic acid and triolein. The cubic equations of state Soave-Redlich-Kwong and Peng-Robinson-Boston-Mathias were used along with mixing rules with modifications. The equations were included in Aspen-Plus software package and the results fitted the experimental data fairly well (Gracia et al., 2009). Another group, Esmaelizadeh et al. (2009) developed a new mixing rule to simulate the solubilities of aromatic hydrocarbons, aliphatic carboxylic acids, aromatic acids, aromatic and aliphatic alcohols in supercritical carbon dioxide. Their new excess Gibbs free energy (G^{ex}) mixing rule was employed along with PR and SRK and compared with five mixing rules namely; Wong-Sandler, Orbey-Sandler, Van der waals with one adjustable parameter, Van der Waals with two adjustable parameters, and covolume dependent rules. Their model gave satisfactory results with minimum deviation from experimental results compared with other models(Esmaeilzadeh et al., 2009). Madras (2004) proposed a thermodynamic model for the solubility of fatty acids in supercritical carbon dioxide. He used Redich-Kwong equation of state coupled with Kwak-Mansoori mixing rules with one adjustable parameter. Furthermore, he correlated the interaction parameter to the chain length of the

fatty acid by linear relationship and concluded that the model can be used to predict the solubility of various fatty acids. His results matched experimental data published in literature (Madras, 2004). In addition, Correa et al. (2010) reported new solubility data for squalene in supercritical carbon dioxide. They used combination of Peng-Robinson equation of state and Van der Waals mixing rules and their results agreed with experimental solubility data (Martinez-Correa et al., 2010).

- *Empirical solubility*

Various studies have been conducted on relating the solubility of materials in supercritical fluids by empirical correlations. In 1982 Chrastil could relate the solubility of various components directly to the density of supercritical carbon dioxide by the equation:

$$y = \rho^k exp\left(\frac{a}{T} + b\right) \quad (7)$$

where y is the solubility of solute expressed in g/L, ρ is density of the supercritical fluid in g/L,T is the temperature in K, k is association number, and the constants a and b are related to vaporization and solvating heat and molecular weights of solute and supercritical fluid. The model is based upon the fact that one molecule of solute A associates with k molecules of solvent B and combine to give the complex AB_k. The Chrastil equation fitted the experimental solubilities of the interested compounds fairly well over temperature range from 40 to 80 °C and pressure range from 80 up to 250 atm (Chrastil, 1982). Further modification was employed to Chrastil equation by Del Valle and Aguilera (1988) to be more general and valid for wider range of temperatures and pressures. Their equation can be applied for calculating the solubility of vegetable oils in

supercritical carbon dioxide for temperatures from 20 to 80 °C, pressures from 150 atm to 880 atm, and solubilities lower than 100 g/L. The Del Valle and Aguilera equation is expressed:

$$\ln y = 10.724 \ln \rho \, exp\left(40.36 - \frac{18708}{T} + \frac{2186840}{T^2}\right) \quad (8)$$

Gong and Cao (2009) used Chrastil and Mendez-Santiago-Teja empirical models to correlate experimental solubility data of artimisinin in supercritical carbon dioxide. The Mendez-Santiago-Teja model is based on the theory of dilute solutions (Santiago & Teja, 1999). They compared the empirical models with the experimental measurements and obtained an average deviation of 8% for both models. The model is expressed by the following equation, where the constants A, B and C are adjustable parameters (Gong & Cao, 2009).

$$T ln(yP) = A + B\rho + CT \quad (9)$$

Another empirical model is the one proposed by Adachi-Lu involving five adjustable parameters. Savova et al. (2001) used Adachi-Lu model to quantify the solubility of grape and blackcurrent oils in supercritical carbon dioxide in addition to Chrastil Del Valle and Aguilera models. The Adach-Lu model fitted the experimental data fairly well but the other models showed better agreement. The Adachi-Lu model with Savova's adjustable parameters is expressed by Eq. (10)

$$y = \rho^{1.4+0.0048\rho-0.000002\rho^2} \exp\left(\frac{-5000}{T-10.14}\right) \quad (10)$$

- *Experimental solubility*

Solubility of pure components can be measured experimentally as described in literature (Anitescu & Tavlarides, 1997; Chen et al., 2011; Chrastil, 1982; Del Valle & Aguilera, 1988; Sovova et al., 2001). However these systems are limited for solubility of pure compounds not mixtures. In addition solubility measurements are time consuming since they are carried out at low flow rates. A typical experimental approach to determine the solubility is from the experimental extraction curve. The solubility is simply equal to the initial slope of the linear part of the extraction curve. This approach is preferable especially if the extract consists of different unknown compounds.

The mathematical solubility models are limited to common compounds and pure species. The thermodynamic models can be complicated when the extract is a mixture of several species. When the extract contains many compounds, there will be a need for the physical properties which are not widely available. Moreover, physical properties are not always measurable or computable. Correlations and formulas for physical properties can be valid only within a certain range. For example, the saturation pressure which is calculated by Antoine equation is limited for temperature and pressure ranges, and also the Antoine constants are not available for all compounds. Besides the lack of physical properties, the behavior of a component is different when it is in a mixture. For example, diffusivity and heat capacity parameters for pure components vary when they are in a mixture due to the effect of other components diffusivity and heat capacity based on their compositions.

Usually the empirical models are not widely accepted in the scientific community because they are limited by process conditions, e.g. temperature and pressure ranges.

Moreover, the adjustable parameters cannot be generalized for all kinds of extracts. Furthermore, the adjustable parameters are applicable to common extracts and fitted without physical significance. In other words, the adjustable parameters do not reflect the physical behavior of the compounds and do not explain the theory behind the extraction curve to facilitate process scaling–up.

As a result of the limited mathematical tools for getting the solubility, the appropriate approach is the initial slope of the extraction curve which ensures sufficient accuracy of solubility value and demonstrates the physical behavior of solutes in supercritical extraction process.

2.3.4.2.2 Modeling the extraction curve

Numerous studies simulated the extraction curve of the supercritical extraction process. The available models in the literature vary depending on different scientific views and different postulations. Recently, Grosso et al. (2010) published a study dealing with different mathematical models for supercritical CO_2 extraction of volatile oils from aromatic plants. In general the models are found in four main categories; empirical models, shrinking core models, models based on heat transfer analogies, and models based on differential mass balances (Grosso et al., 2010).

General assumptions common to almost all models types include; 1) isobaric and isothermal process, 2) constant physical properties along the process; porosity and initial oil content, 3) uniform superficial velocity and solvent flow rate, 4) extract content is distributed uniformly between particles, all solid particles have the same uniform shape, and 5) linear relationship between solid and fluid phase.

Moreover, the adjustable parameters cannot be generalized for all kinds of extracts. Furthermore, the adjustable parameters are applicable to common extracts and fitted without physical significance. In other words, the adjustable parameters do not reflect the physical behavior of the compounds and do not explain the theory behind the extraction curve to facilitate process scaling–up.

As a result of the limited mathematical tools for getting the solubility, the appropriate approach is the initial slope of the extraction curve which ensures sufficient accuracy of solubility value and demonstrates the physical behavior of solutes in supercritical extraction process.

2.3.4.2.2 Modeling the extraction curve

Numerous studies simulated the extraction curve of the supercritical extraction process. The available models in the literature vary depending on different scientific views and different postulations. Recently, Grosso et al. (2010) published a study dealing with different mathematical models for supercritical CO_2 extraction of volatile oils from aromatic plants. In general the models are found in four main categories; empirical models, shrinking core models, models based on heat transfer analogies, and models based on differential mass balances (Grosso et al., 2010).

General assumptions common to almost all models types include; 1) isobaric and isothermal process, 2) constant physical properties along the process; porosity and initial oil content, 3) uniform superficial velocity and solvent flow rate, 4) extract content is distributed uniformly between particles, all solid particles have the same uniform shape, and 5) linear relationship between solid and fluid phase.

- *Empirical models*

An empirical model was proposed by Naik et al. in 1989 to describe the extraction of perfumes and flavors from plant materials. They illustrated the variation of the extraction yield versus time by simple mathematical Eq. (11). This model describes the extraction yield versus extraction time by a Langmuir gas adsorption isotherm. Langmuir assumed monolayer coverage of the solid matrix including the solutes, which forces a constraint to the maximal amount of solute in the substrate depending on its specific surface. Despite the good agreement with experimental data, this model doesn't consider both the interactions between solute and solid matrix and the fractionation of oil during the process. Several researchers employed this empirical model and optimized the adjustable parameter; they found that parameter b varies with mass flow rate, pressure, and temperature (Esquivel et al., 1999; Papamichail et al., 2000).

$$Y = \frac{Y_\infty t}{b+t} \qquad (11)$$

where Y is extraction yield defined as the ratio of the mass of oil extracted in kg at time t (s) to the initial mass feed, Y_∞ is Y after infinite extraction time, , and b is adjustable model parameter.

Linearization of Eq. (11) leads to linear relationship between the inverse of the yield and inverse of the extraction time with a slope equals $\frac{Y_\infty}{b}$ and intercept equals to $\frac{1}{Y_\infty}$. In addition, Y_∞ can be assumed to be the maximum yield obtained experimentally, thus the number of adjustable parameters will reduce. Furthermore, Huang et al. (2011) defined the recovery r as $\frac{Y}{Y_\infty}$ and obtained the relation shown in Eq. (12). They determined

parameter b from the slope of the curve reciprocal recovery versus reciprocal of the extraction time.

$$r = \frac{t}{b+t} \tag{12}$$

(Huang et al., 2011) described the extraction rate as a first order chemical reaction was Eq. (13). According to the model, the extract available in the solid matrix is decreasing with time exponentially by rate constant k and expressed mathematically by Eq. (14) with initial concentration C_{s0}. The extraction rate constant (k) is related to diffusivity and particle dimensions by Eq. (15). In this model Y_0 and k can be obtained by fitting the model to experimental data (Naik et al., 1989).

$$\frac{dC_s}{dt} = -kC_s \tag{13}$$

$$C_s = C_{s0}\exp(-kt) \tag{14}$$

With overall extraction yield given by

$$Y = Y_0[1 - \exp(-kt)] \tag{15}$$

Where

$$k = \frac{DS}{Vd} \tag{16}$$

And

$$\frac{S}{V} = \frac{6(1-\varepsilon_P)}{d_P} \tag{17}$$

where C_s is the extract concentration in the solid matrix in g/l, d_P is particle diameter in m, d is the bed diameter in m, D is solute diffusion coefficient, ε_P is particle porosity, S and V are particle surface area in m^2 and volume in m^3, respectively.

Regardless of the simplicity and the large capacity of the empirical models, which are the only advantages, such models suffer from lack of theoretical or physical meanings. As a result empirical models are not suitable for scaling up the supercritical extraction (Bernardo-Gil & Casquilho, 2007).

- *Heat transfer analogies models*

These models describe the extraction phenomena as a heat transfer phenomena by considering each solid particle as a hot sphere cooling in a uniform cool medium. This cooling of hot spheres is used to simulate the concentration profile as a function of time. Derivation of this model is carried out by applying Fick's second law for diffusion along with heat-mass transfer analogy using Fourier transforms. The model was proposed by Crank and represented by Reverchon using the following equation (Campos et al., 2005; Crank, 1975; Doker et al., 2004; Ernesto Reverchon, 1997; Ernesto Reverchon et al., 1993):

$$\frac{q}{q_o} = \frac{6}{\pi^2}\sum_{n=1}^{\infty}\frac{1}{n^2}exp\left(-\frac{n^2\pi^2 Dt}{r^2}\right) \quad (18)$$

where q is the solute concentration in solid phase (Kg/m^3), q_o is the initial solute concentration in solid phase (Kg/m^3), n is an integer, D is solute diffusivity in solid sphere (m^2/s), t is extraction time (s).

Gaspar et al. (2003) simulated the extraction curve using heat transfer analogy model with the assumption of the plate like particles, so called simple single plate model (SSP). They slightly modified the model proposed by Bartle et al. (1990) where the extractable oil is considered to minimize the deviations from experimental data. It is worth mentioning that the proposed model by Bartle et al. for the extraction of rosemary leaves oil showed deviations from experimental data as a result of neglecting the equilibrium stage (early extraction stage) where the majority of oil was extracted. The model was rewritten in terms of extraction degree and expressed by Eq. (19). (Gaspar et al., 2003). Esquivel et al. (1999) used the same approach to describe the extraction of olive husk oil. They reported that the model gave satisfactory agreement with experimental data at high superficial velocities while at low superficial velocities the fitting was very poor (Ernesto Reverchon et al., 1993).

$$E(t) = E_{\infty}\left[1 - \sum_{0}^{\infty} \frac{8}{(2n+1)^2} e^{\left(\frac{-D_m(2n+1)^2\pi^2 t}{\delta^2}\right)}\right] \qquad (19)$$

where $E(t)$ and E_{∞} are the extraction degree (%) after time t (s) and infinite, D_m is solute diffusivity on the particle plate (m^2/s), δ is the thickness of the particles (plates) (m) and n is an integer.

- *Shrinking core model*

This model divides the porous solid matrix into two zones; inner zone which is oil rich core, and outer zone. The extraction proceeds as a result of irreversible desorption of solute from the core to the particle pores followed by diffusion within the pores (intra-particle diffusion), and diffusion through the bulk fluid phase. When the solute

concentration in the outer zone is much higher than the solubility in the fluid phase; a sharp boundary (shrinking boundary) exists between the two zones. During the extraction process the core of the inner region shrinks with time. The model was proposed by Goto at al. (1996) for describing the extraction curve of oil from rape seeds. The model assumes no adsorption of solute into the solid matrix and has two fitting parameters; effective diffusivity and mass transfer coefficient. Goto et al. (1996) expressed the shrinking core model using dimensionless material balances in the fluid phase and solid phase by set of equations shown below and solved the differential equations numerically using Crank-Nicholson's method (Goto et al., 1996; Oliveira et al., 2011).

Material balance in the bulk fluid phase:

$$\frac{\partial X_b}{\partial \theta} + a\frac{\partial X_b}{\partial Z} = \frac{a}{Pe}\frac{\partial^2 X_b}{\partial Z^2} - 3Bi\left(\frac{1-\varepsilon}{\varepsilon}\right)\left[\frac{X_b - 1}{\left(1 - Bi\left(1-\frac{1}{\xi_c}\right)\right)}\right] \tag{20}$$

Material balance in the particle phase:

$$\varepsilon_P \frac{\partial X_P}{\partial \theta} + (1-\varepsilon_P) b \frac{\partial Q}{\partial \theta} = \frac{1}{\xi^2}\frac{\partial}{\partial \xi}\left[\xi^2 \frac{\partial X_P}{\partial \xi}\right] \tag{21}$$

with an extraction yield expressed as

$$Y = \frac{ab\varepsilon}{1-\varepsilon}\int_0^\theta X_b \, d\theta \tag{22}$$

$X_b, X_P, Q, \theta, Z, \xi$ are dimensionless groups of concentration in bulk phase, concentration in particle phase, solid phase concentration, time, axial bed coordinates and particle coordinate, respectively, defined as:

$$X_b = \frac{C_b}{C_{sat}}, \qquad X_P = \frac{C_P}{C_{sat}}, \qquad Q = \frac{q}{q_o}$$

$$\theta = \frac{tD_e}{R^2}, \qquad Z = \frac{z}{L}, \qquad \xi = \frac{r}{R}, \qquad \xi_c = \frac{r_c}{R}$$

where C_b is the solute concentration in the bulk phase (mol/m^3), C_P is solute concentration of the particle phase (mol/m^3), C_{sat} is saturated solute in fluid phase (mol/m^3), q is solute concentration in solid phase (mol/m^3), q_o is initial solute concentration in solid phase (mol/m^3), Bi is Biolt number, Pe is Peclet number, ε is bed porosity, ε_P is the particle porosity, t is time (s), D_e is the effective diffusivity (m^2/s), r is radial coordinate (m), r_c is the core radius (m), R is the initial radial coordinate, z is the axial coordinate in the extractor (m), L is the extractor length (m), and V is the interstitial velocity of the solvent (m/s). The model constants a and b are defined as follows:

$$a = \frac{VR^2}{D_e L}$$

$$b = \frac{q_o}{C_{sat}}$$

Machmudah et al. (2006), Salgin et al. (2006), and Doker et al. (2010) employed the shrinking core model for the extraction of nutmeg oil, sunflower oil, and sesame seed oil respectively. In their work they fairly validated the model by fitting the effective diffusivity since the mass transfer coefficient can be estimated using correlations published in literature.

- *Differential mass transfer models*

These models have more reasonable explanations for the theory behind the supercritical extraction process. They acquire more physical properties and coefficients of the solid and solvent matrices such as; particle and bed porosity, mass transfer

coefficients, and diffusivity coefficients. They are based on two main mechanisms; the equilibrium which occurs at the early stage of the extraction curve, and the mass transfer mechanism at later stage. The equilibrium is the mechanism where the solubility of the solute in the supercritical region is dominant. The second stage of the extraction stage occurs when the concentration gradient became more dominant and it is described by mass transfer phenomena.

It is clear that the mass transfer mechanism may be controlled with two resistances; external and internal mass transfer resistances. Many researchers simulated the extraction curve based on mass transfer balances. Different assumptions where employed in order to simplify the models. Based on these various assumptions; the mass transfer balances models can be classified into three groups according to the hypothesized controlling step namely; the external mass transfer resistance model, the internal mass transfer resistance model, and both mass transfer resistances control the extraction process. Such deviations on these assumptions can be attributed to the different structures of the material being extracted for example different plant parts (e.g. flowers, seeds, leaves, roots etc.) can yield to different mass transfer phenomena.

Reverchon and Marrone (1997) formulated a mathematical model for the supercritical extraction of clove bud oil considering that external resistance is the controlling step. They studied the influence of both resistances and found that only slight deviation was observed, which suggested that the internal mass transfer resistance can be ignored. They asserted that the internal resistance can be ignored since it is insensitive to solvent flow rate; on the other hand the external resistance is sensible to solvent flow rate. Wu and Hou (2001), Perrut et al. (1997), and Kim et al. (2007) followed the same scheme for

modeling the extraction of sunflower seed oil, egg yolk, canola oil, and caffeine, respectively.

Later on, internal mass transfer resistance was taken into account and considered as the controlling step in the supercritical extraction process. The reason behind this consideration was explained by Reverchon et al. (2000) when they investigated the structure of hip rose seed using scanning electron microscope (SEM). The structure revealed that only solutes near to the opening channels are readily available for extraction. Therefore, supercritical solvent faces resistance due to the diffusion at the channels as it penetrates deeply within the inner channels.

Moreover, it was stated that as the extraction time increases, more extract content is obtained. In other words, at the beginning of the process, the solute located at the particle surface are extracted, while solutes located inside the particle are transferred later on when easily extractable solutes are depleted (Nei et al., 2008; Park et al., 2007; Reis-Vasco et al., 2000; Vaquero et al., 2006).

The third group proposed models that consider both resistances control the supercritical extraction process simultaneously which was described by Savova in 1994. She articulated the extraction curve by assuming that solutes are stored in the particle cells and protected by the cell walls. During milling, some of those walls are broken (broken cells) and solutes became easily accessible, however the solutes present in the intact cells are inaccessible. Two resistances exist and face the extraction; the first is an external resistance in the fluid phase and controls the process up to all essential oil in the broken cells is recovered. The second resistance lies in the intact cells and controls the

remaining extraction part which resists the diffusion of the inaccessible oil. Based on these postulations, three differential mass balances are driven addressed; two for the particle phase; one in the broken cells and another one in the intact cells, and the third balance is in the fluid phase. The differential equations were integrated numerically with three adjustable parameters; mass transfer coefficient in the solid phase, mass transfer coefficient in the fluid phase, and the fraction of oil initially exist in the cells. The model was adopted for the extraction of various oils including; plumula nelumbinis by Jia et al (Jia et al., 2009a), apricot kernel by Ozkal et al. (Ozkal et al., 2005), and Spanish sage by Langa et al (Langa, Porta et al., 2009)..

Later some modifications were employed to the broken and intact cells. Reverchon and Marrone extended this model by a parallel resistance model where solutes are transferred with different kinetics in both broken and intact cells (E. Reverchon & Marrone, 2001). The difference between series and the parallel models is that the solutes are extracted directly to the fluid phase in the latter one. Fiori et al. (2009) combined the shrinking core model with the broken intact cells model. They considered the oil existence in the intact and broken cells, and as the extraction process progresses each cell is irreversibly depleted causing the solutes to move towards the internal shell, which is described by the shrinking core model.

3 EXPERIMENTAL SET UP AND METHODOLOGIES

3.1 Sample preparations

Henna flowers were picked from henna tree located at Al-Jimi area in Al Ain city, UAE during blooming season in October. The flowers were dried to reduce the moisture content using a freeze dryer (Eyela, FDU 1200, Japan) at -48 °C for 12 hours. Dried flowers were stored in a fridge until further use.

3.2 Supercritical fluid extraction

The experimental setup shown in Figure 5 was used for the supercritical carbon dioxide extraction of volatile components from henna flowers. The apparatus consists of a 260 ml syringe pump with controller system (ISCO 260D), and an ISCO series 2000 SCF Extraction system (SFX 220) including a dual chamber extraction module with two 10 ml stainless steel extraction cells. Each 10 ml stainless steel cell has diameter of 1.5 cm and 5 cm length. In a typical experiment, about 2 g of dried henna flower was weighed using an electronic balance (Precisa, Swiss), mechanically grinded (Moulinex, France), and placed in the extraction cell. The particle diameter measured by microscope (Nikon eclipe lve100pol, Japan) was obtained to be on average 0.504 mm. The particle and bed porosity were calculated and their values were 0.79 and 0.5, respectively. After placing the sample in the cell and setting the extraction temperature and pressure, the sample was allowed to equilibrate for 15 min with SC-CO_2. Supercritical CO_2 flowed along the extraction cell with flow rate of 1 ml/min. The extract collector was immersed in cold methanol (-40 °C) provided by a chiller (ULTRA-KRYOMAT, Germany) to trap the extract while the CO_2 was vented to the atmosphere. The extract weight was recorded for different CO2 amounts passing through the sample until no more extract was obtained

at which time the apparatus was stopped. The apparatus was thoroughly cleaned after each experiment by flushing methanol and 300 ml of CO_2.

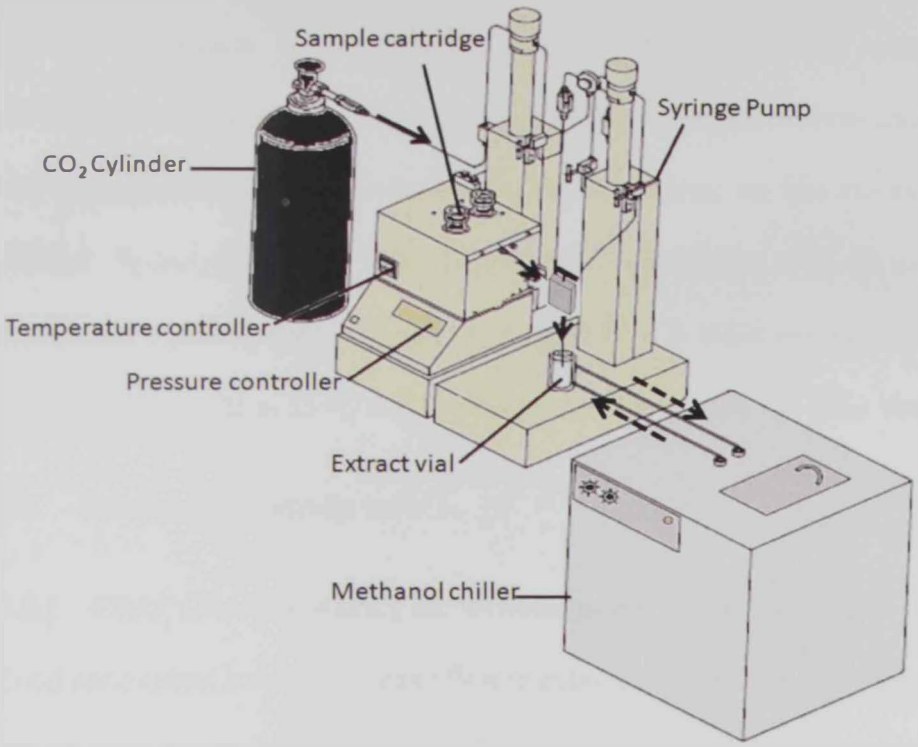

Figure 5 Supercritical Extraction Experimental Set up

3.3 Gas Chromatography analysis

The extracts from flowers of henna obtained by SFE were subjected to Gas chromatography (GC) compositional analysis. Gas chromatographic (GC) analysis was performed with a CP 3800 Varian instrument equipped with flame ionization detector and a column (CP-Select 624 CB, DF = 1.8, Id = 0.32 mm, length = 60 m). The conditions were as follows: carrier gas (helium); Oven temperature program: Initial Temp: 40 °C for 1 min, Ramp 1: heating up to 60 °C with heating rate 20 °C/min, Ramp 2: heating up to 140 °C with heating rate 2 °C/min, Ramp 3: Heating up to 250 °C with heating rate 5

°C/min and hold at 250 °C for 40 min, Injector temperature: 300 °C, Injection Mode: splitless, Inlet pressure: 20 psi, Detector Temperature: 280 °C.

3.4 Antibacterial Activity Test

The extracts were tested for their antibacterial activity using disc diffusion method. Gram positive and Gram negative bacteria (*Staphylococcus aureus* ATCC25923 and Escherichia coli 25922) were spread as lawn culture on Mueller-Hinton Agar plates (MAST, Merseyside, UK). Filter paper discs impregnated with 10 µL of each herbal extract were placed onto the agar with maximum 6 discs per agar plate. Plates were incubated overnight at 35 °C and the inhibition zone around the discs was measured.

3.5 Antioxidant Activity test

3.5.1 FRAP (Ferric reducing antioxidant power) assay

Total antioxidant activity of henna flower extracts was measured by reducing antioxidant activity power assay as described by Benzie and Strain 1996. The principle of this assay is the reduction of ferric into ferrous ion by the antioxidants.

FRAP reagent was prepared by mixing stock solutions in the ratio 10:1:1 at the time of use. Stock solutions included 300 mM acetate buffer (pH 3.6), 10 mM TPTZ (2,4,6-tripyridyl-s-triazine) solution in 40 mM HCl, and 20 mM $FeCl_3\_6H_2O$ solution. The mixed solution was incubated at 37 °C for 30 min in a water bath (Memmert, D-91126, Schwabach, Germany). 0.5 ml from each extract was diluted in 1.5 ml of ethanol. A sample (150 µl) of extract at each extraction temperature and pressure was mixed with 2850 µl of FRAP solution and kept for 30 min in the dark at room temperature. The absorbance of the ferrous tripyridyltriazine complex (coloured product) was measured at

wavelength 593 nm. A sample blank at each concentration was prepared by omitting $FeCl_3$ from the FRAP solution and distilled water was used instead. The standard curve was prepared using ascorbic acid ranging from 0 to 100 ppm. The activity was expressed as mg Ascorbic acid equivalents (AA)/100 g of henna flowers extracts.

3.5.2 DPPH radical scavenging activity

1.5 ml of this samples (about 0.5 ml of henna extract at each extraction condition was added to 1.5 ml of ethanol) was mixed with 1.5 ml of 0.15 mM 2,2-diphenyl-1-picryl hydrazyl (DPPH) in 95% ethanol. The mixture was mixed vigorously and allowed to stand at room temperature in the dark for 30 min. The absorbance of the resulting solution was measured at 517 nm using a UV-1601 spectrophotometer (Shimadzu, Kyoto, Japan). The sample blank at each concentration was prepared in the same manner except that ethanol was used instead of DPPH solution. A standard curve was prepared using ascorbic acid in the range of 0–100 ppm. The activity was calculated and expressed as mg Ascorbic Acid equivalents (AA)/100 g henna flower extracts.

4 RESULTS AND DISCUSSION

In this study first henna flower oil was extracted by supercritical carbon dioxide. The extraction experiments were performed under different temperatures and pressures while keeping the flow rate of SC-CO_2 and cooling temperature constant. Effect of other extraction parameters including the cooling temperature and the flow rate of SC-CO_2 were also studied. Appendix A includes the raw data for the experiments. The extracts were analyzed by GC for their composition and their antibacterial and antioxidant activities were measured.

4.1 Supercritical carbon dioxide extraction of henna flower

The operating conditions that were investigated, the maximum yield, and solubility of extract in SC-CO_2 for each of conditions are tabulated in Table 4 .The maximum yield was calculated by dividing the final extract weight over the charged sample weight (2g). The solubility of extract in SC-CO_2 was calculated from the initial slope of the extraction curve (mass of extract versus mass of CO_2 passed). The highest yield was (30.88%) obtained at 45 ^{o}C and 120 bar, while the lowest yield (18.29%) was found at the lowest temperature (35 ^{o}C) and pressure (80 bar).

Table 4 Maximum yields and solubility of SFE of Henna flower extract

T (°C)	P (bar)	F (ml/min)	$T_{cooling}$ (°C)	ρ (kg/m^3)	μ (Pa.s) x10^5	ν (m^2/s) x 10^8	Maximum Yield (%)	Solubility ($g_{extract}$/g CO_2)x 10^3
35	80	1	-40	419.09	2.98	7.12	18.29	0.541
35	100	1	-40	712.81	5.77	8.09	20.53	0.657
35	120	1	-40	767.07	6.55	8.54	21.66	0.742
45	80	1	-40	241.05	2.10	8.73	23.3	0.757
45	100	1	-40	498.25	3.60	7.23	28.88	0.913
45	120	1	-40	657.74	5.13	7.79	30.88	1
55	80	1	-40	203.64	2.02	9.91	23.13	0.756
55	100	1	-40	325.07	2.53	7.79	27.79	0.853
55	120	1	-40	504.51	3.70	7.33	25.4	2.9
55	100	2	-40	325.07	2.53	7.79	13.51	0.04
55	120	2	-40	504.51	3.70	7.33	17.94	1.2
45	100	1	-25	498.25	3.60	7.23	14.06	0.6
35	80	1	-25	419.09	2.98	7.12	4.52	0.1
55	80	1	-25	203.64	2.0	9.91	13.56	0.5

The cooling temperature was found to have a significant effect on both extraction yield and solubility. As can be seen in Table 4, increasing the cooling temperature from -40 to -25 °C reduces the extraction yield, which may be due to the loss of some of the volatile compounds. Figures 6 and 7 illustrate the significant effect of the cooling temperature on extraction yield.

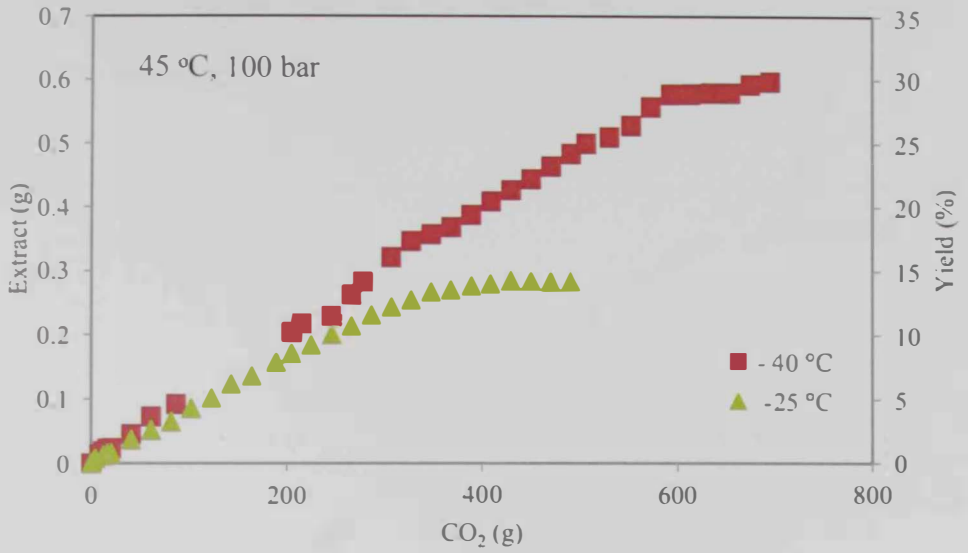

Figure 6 Effect of cooling temperature at 45 °C and 100 bar

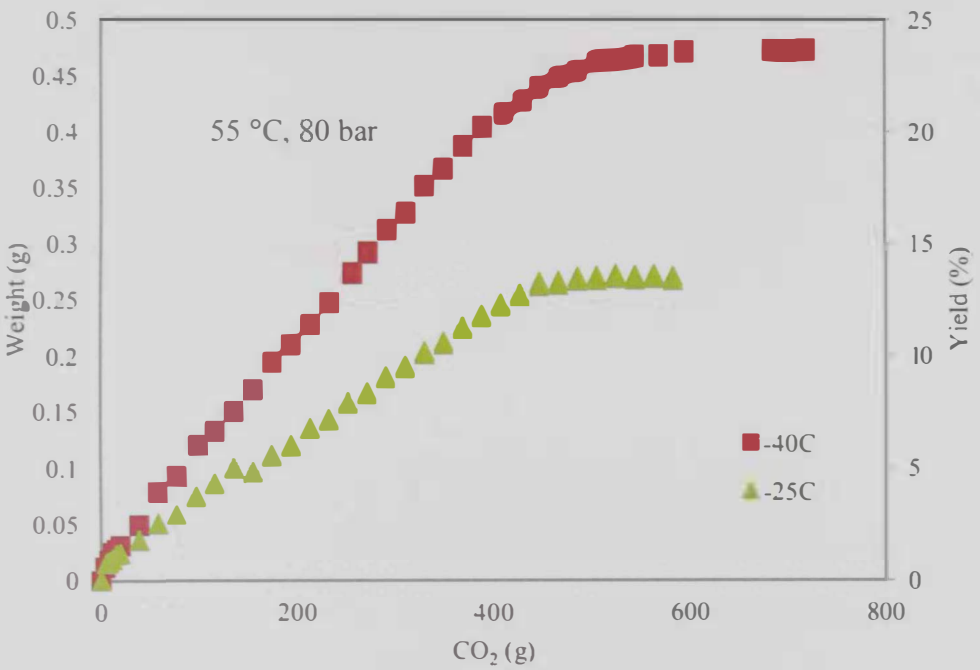

Figure 7 Effect of cooling temperature at 55 °C and 80 bar

The flow rate of SC-CO_2 affected the extraction yield significantly. As shown in figures 8 and 9, increasing the flow rate decreased the extraction yield drastically. For example an increase of the flow rate from 1 ml/min to 2 ml/min dropped the extraction yield by 7 %

at 55 °C and 120 bar (Table 4). The reason behind this trend is the longer contact time between the sample and SC-CO_2 at the lower flow rate.

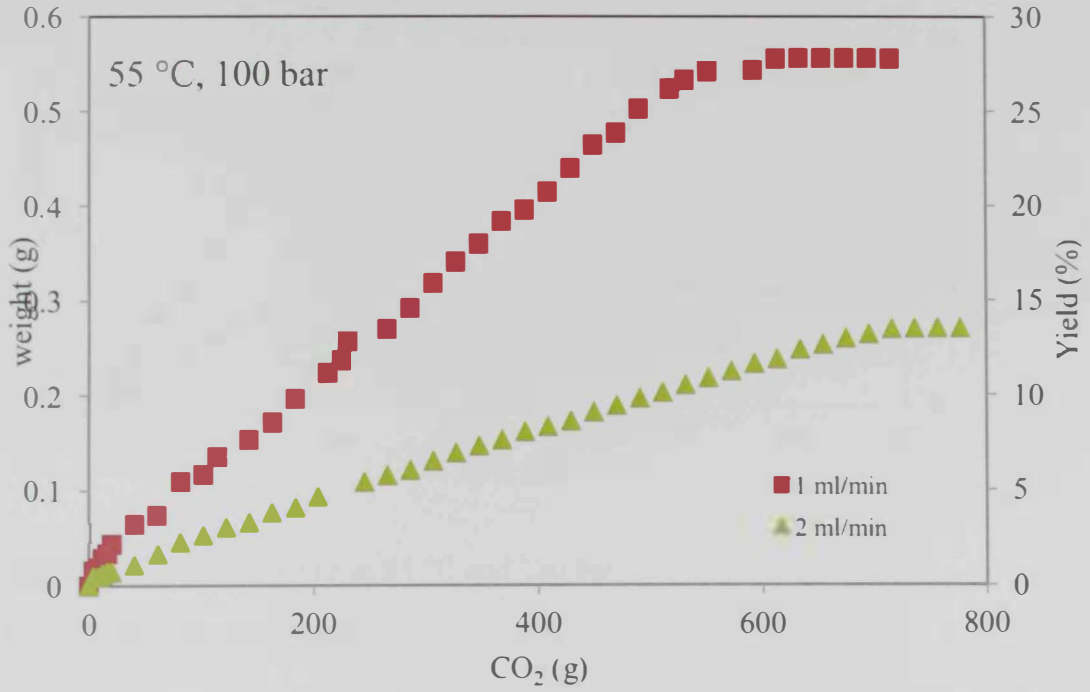

Figure 8 Effect of flow rate at 55 °C and 100 bar

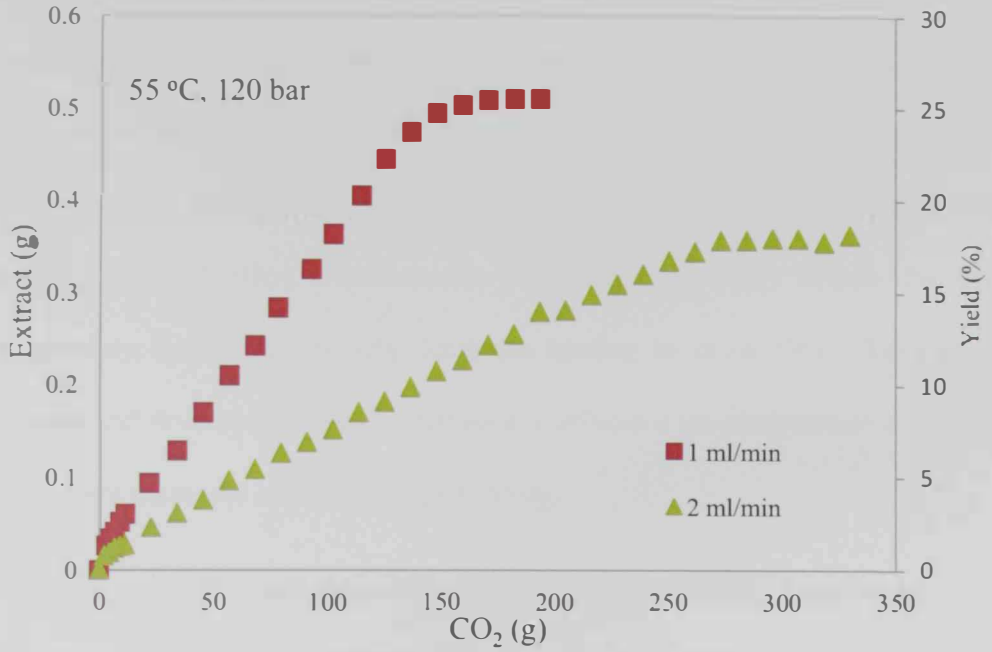

Figure 9 Effect of flow rate at 55 °C and 120 bar

4.1.1 Effect of temperature

The effect of temperature on the extraction yield is shown in figures 10-12. The extraction curves for all runs exhibited a similar trend, starting with a linear part for which the rate of extraction was constant followed by a continuous decrease in the rate of extraction until reaching a final maximum yield value after which no more extracts obtained. However, the initial slope and the final (maximum) yield value of extraction yield were different for the different conditions studied in this work. This is expected as the operating condition (temperature and pressure) affect fluid properties (i.e. volatility) and transport properties (i.e. diffusion coefficient), all of which affect the extraction process.

In almost all cases, the temperature had a direct effect on the extraction process since the yield increased with an increase in temperature. As temperature increases, density

increases inversely affecting the solubility of solute and extraction yield. However, temperature is directly related to volatility of the solute, which directly affects the solubility of the solute and hence the extraction yield. Therefore, temperature affects the solubility and extraction yield in trend opposite ways through two competing factors (density and volatility). Furthermore, temperature inversely affects the viscosity (as temperature increases, viscosity decreases leading to easier flow). Temperature is also directly and favorably related to diffusion coefficient (as temperature increases diffusion coefficient increases leading to higher yield).

As a result of all these factors, for most of the conditions studied in this work, the temperature had a direct influence on the extraction yield, suggesting that the effect of volatility, viscosity and transport coefficient was higher than the unfavorable effect of density change with temperature.

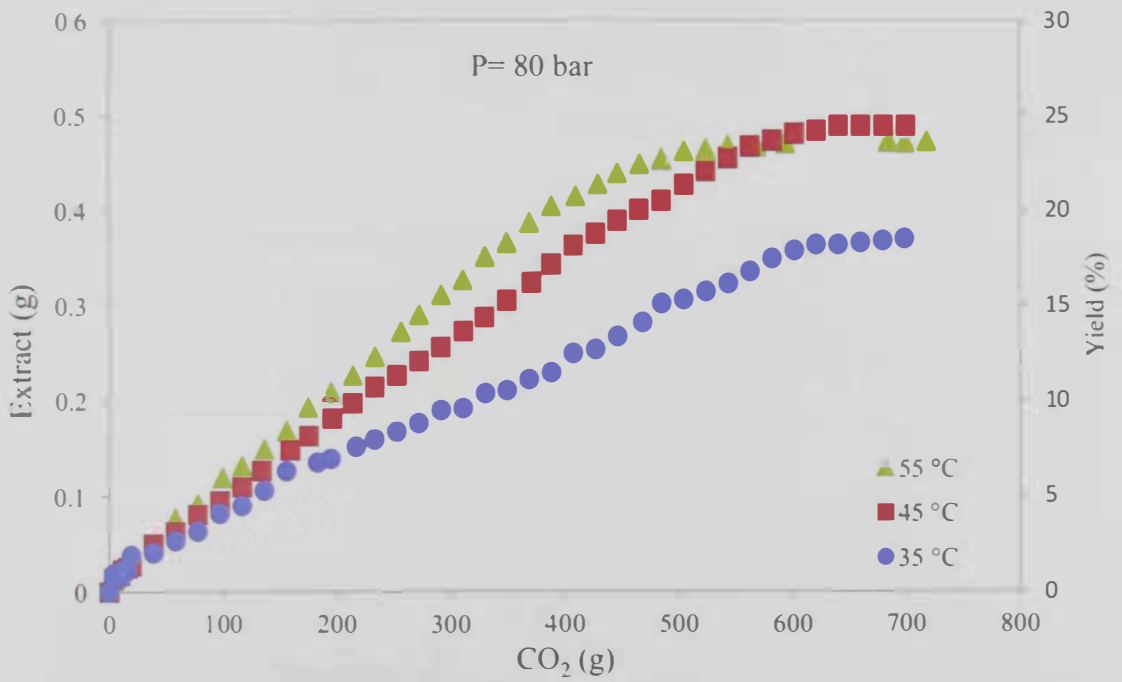

Figure 10 Effect of temperature on the extraction yield at 80 bar

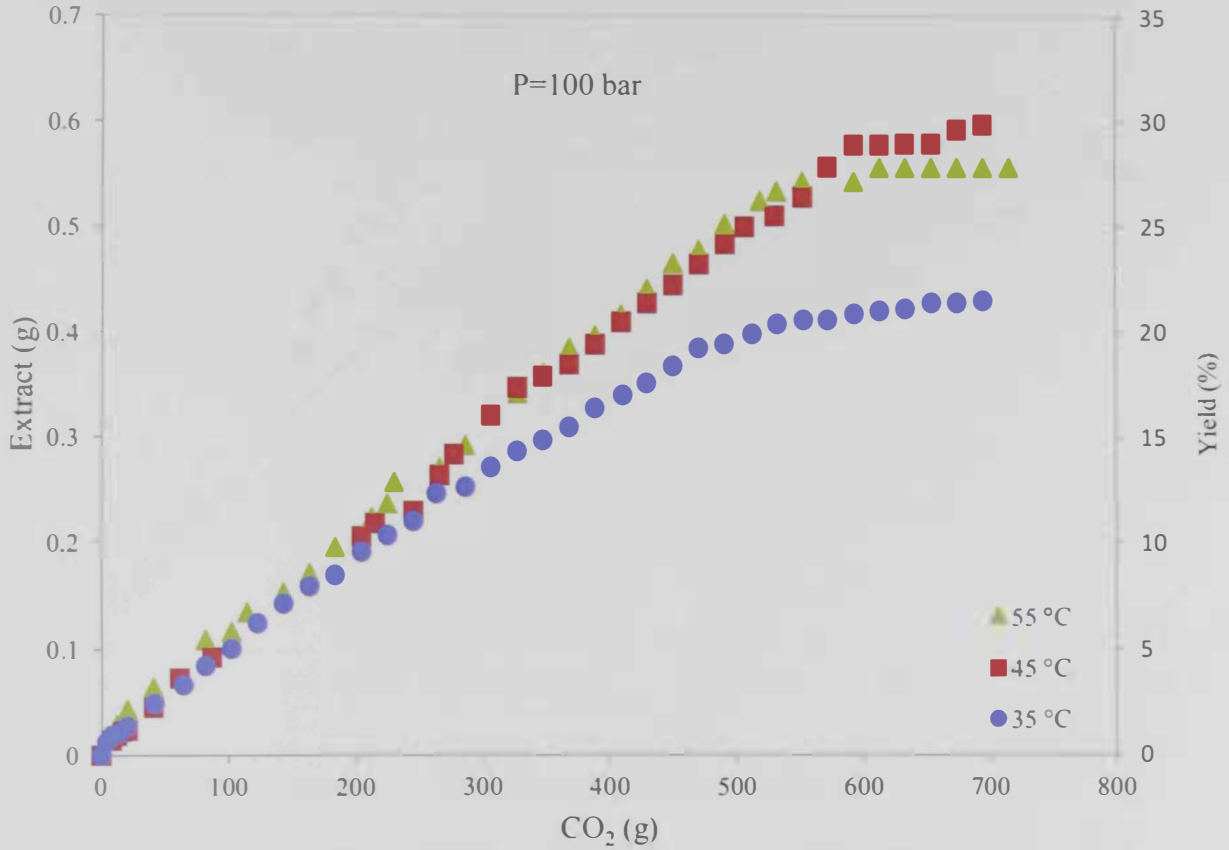

Figure 11 Effect of temperature on the extraction yield at 100 bar

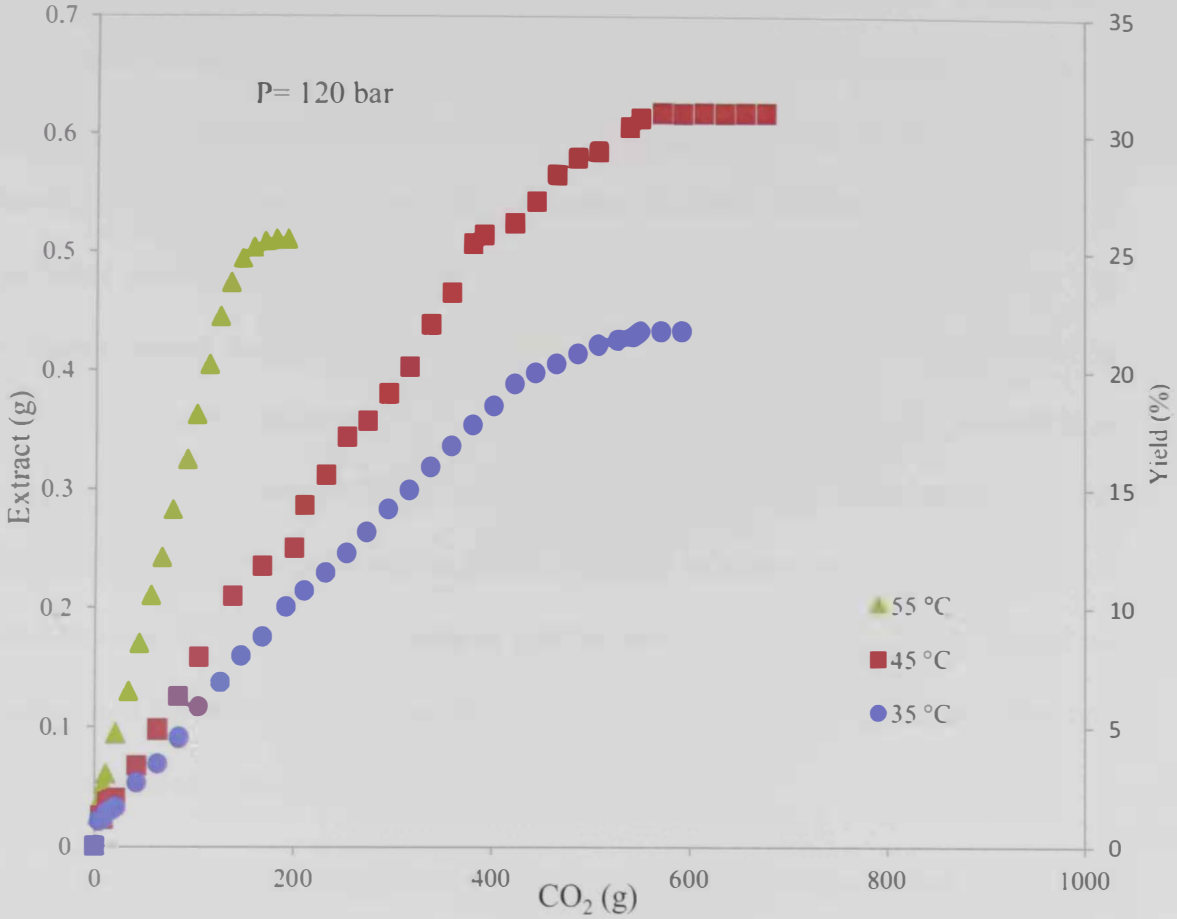

Figure 12 Effect of temperature on the extraction yield at 120 bar

The solubility of henna flower extract in SC-CO_2 (extract weight/CO_2 weight) was calculated at each condition using the initial slope of experimental extraction curves. As shown in Figure 13. solubility of the extract increased with both temperature and pressure, which matches the trend of the extraction yield. Pressure directly affects the solubility of solutes on SC-CO_2. As the pressure increases, the fluid density increases, enhancing the solvent power of CO_2 which leads to higher solubility on solutes as shown in Figure 13. Therefore, as a result of higher solubility, the extraction yield increases as the pressure is increased (Figures 10-12).

Temperature affects the solubility by two competing factors (density and volatility). As the temperature increases the density of CO_2 decreases, reducing its solvent power, which leads to lower solubility of the solute in CO_2. On the other hand, as the temperature increases, the volatility of solutes increases, leading to high solubility of the solute in CO_2. For all the conditions studied in this work, the volatility effect was dominant causing the solubility to increase with temperature as shown in Figure 13. The increase in solubility of henna flower extracts in SC-CO_2 with temperature resulted in an increase in the extraction yield with temperature (Figure 10-12). These results show that extraction process is directly related to the solubility of extract in SC-CO_2. The highest solubility was 2.9 $mg_{extract}/g_{CO2}$ found at 120 bar and 55 °C. This was also the fastest run leading to a yield of 25.4 % using only around 400 ml of CO_2 compared to other runs which consumed about twice as much CO_2.

Moreover, the solubility results revealed that at the highest pressure studied in this work the effect of temperature is more noticeable compared to those at lower pressures. At 120 bar, the solubility jumped from 1 to 2.9 $mg_{extract}/g_{CO2}$ when the temperature was increased from 45 to 55 °C, however at 80 bar no significant change on the solubility was observed for the same change in temperature.

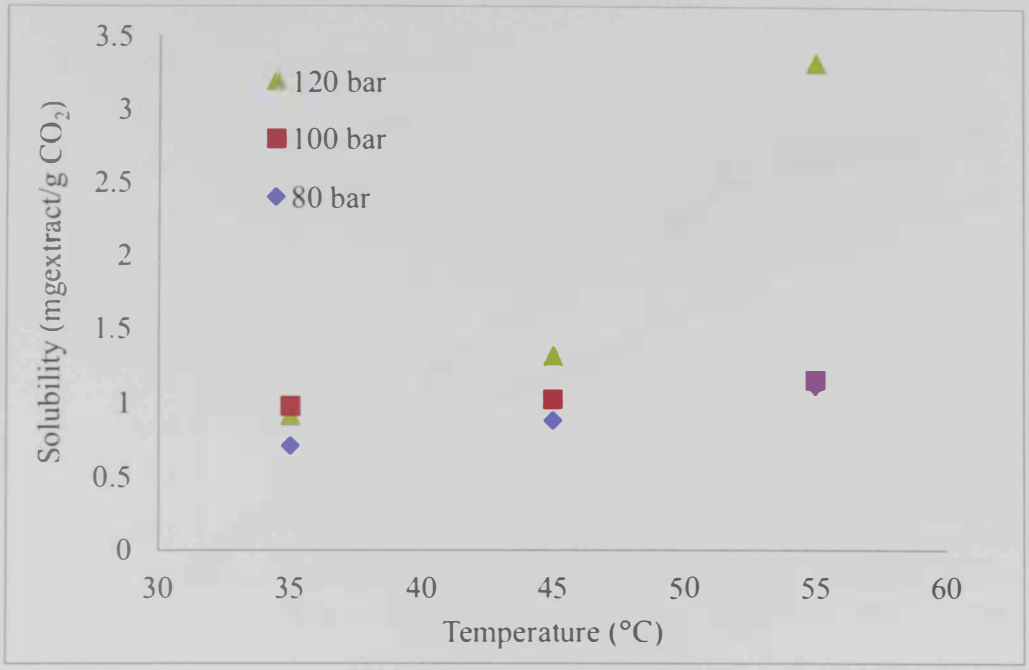

Figure 13 Effect of temperature and pressure on solubility of henna flower extract in SC-CO_2

4.1.2 Effect of pressure

Figures 14-16 show the effect of pressure on the extraction yield. At a constant temperature, the extraction yield was improved as increasing pressure. This behavior was expected since increasing the pressure increases the solvent density and hence the solvating power of SC-CO_2 which increases the amount of dissolved extract, leading to higher yield. Figure 13 is in agreement with the results presented in figures 14-16. As the pressure is increased the solubility increases (Figure 13) leading to higher extraction rate.

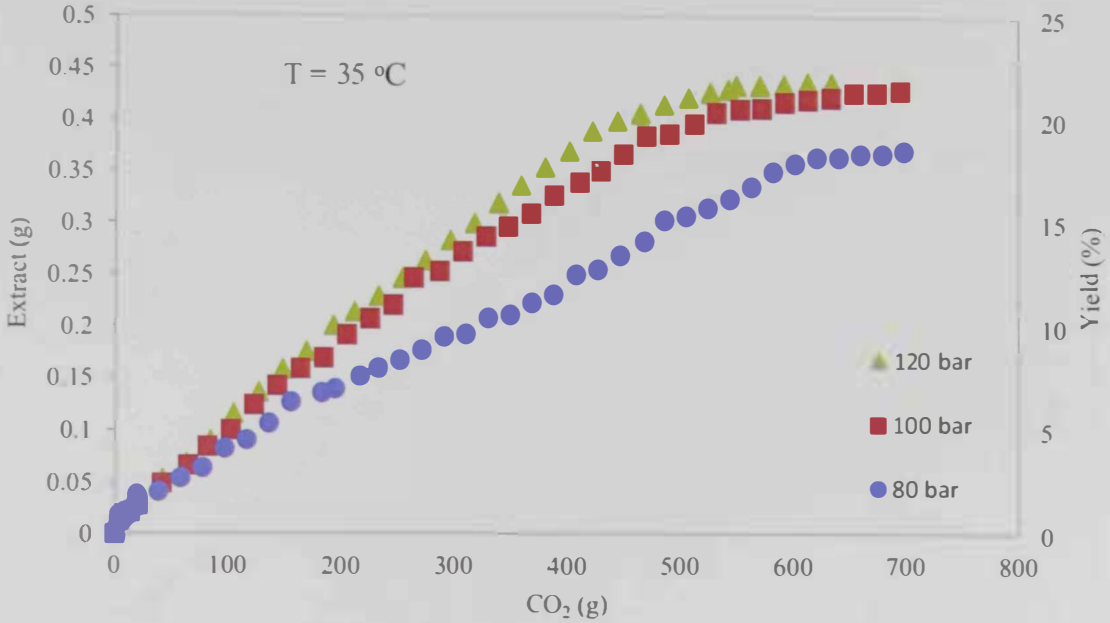

Figure 14 Effect of pressure on the extraction yield at 35 °C

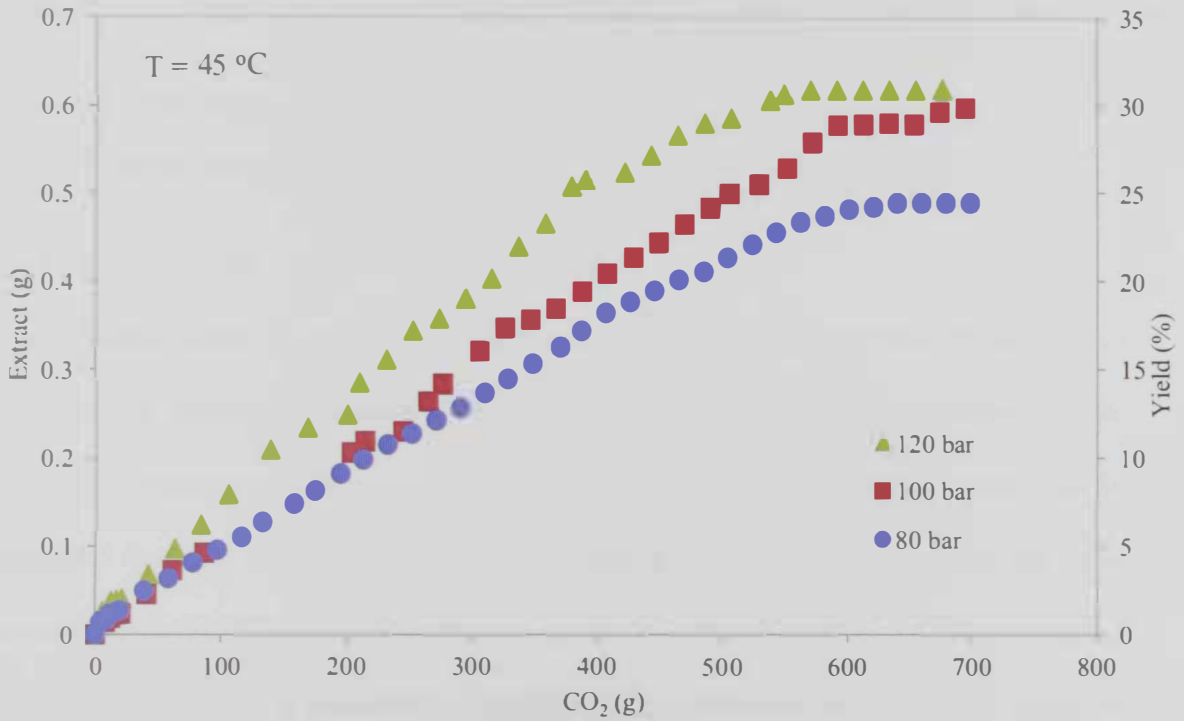

Figure 15 Effect of pressure on the extraction yield at 35 °C

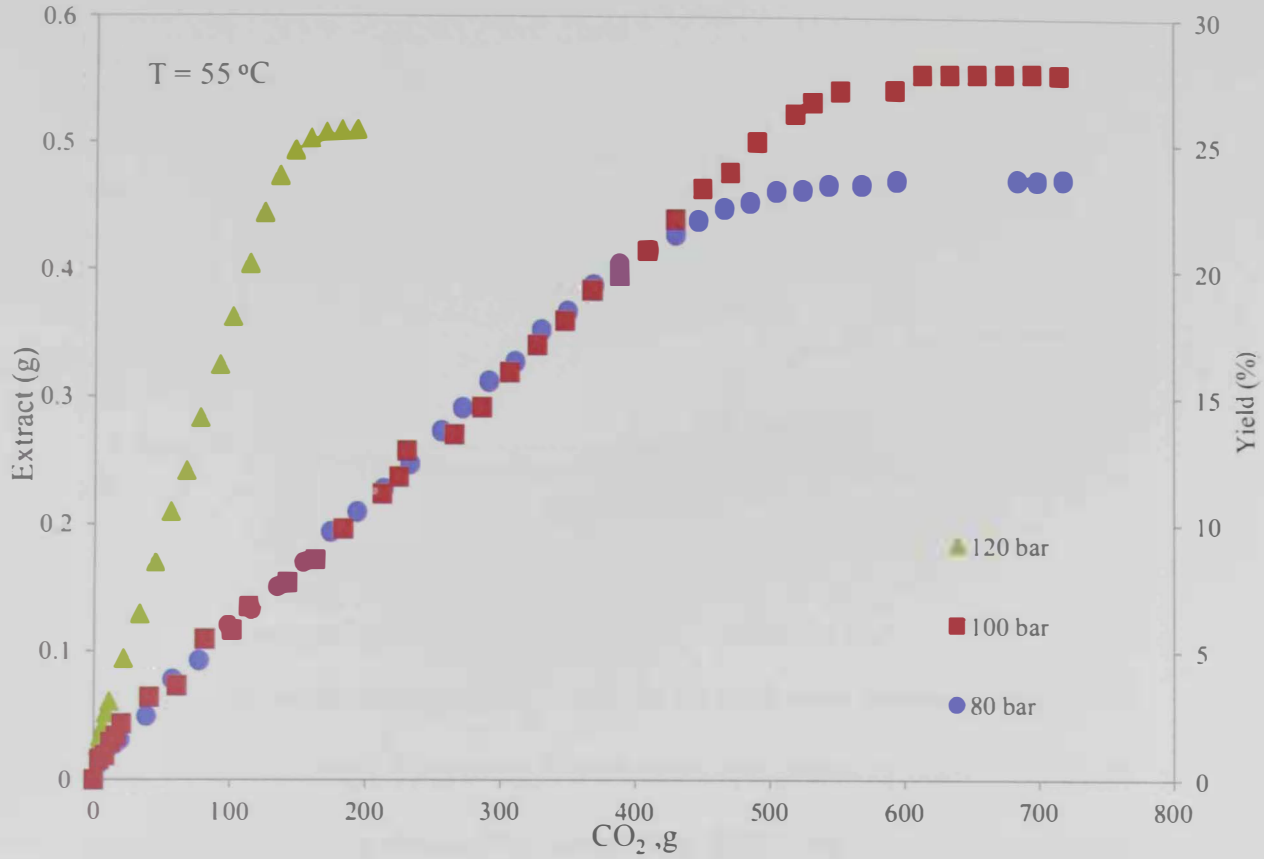

Figure 16 Effect of pressure on the extraction yield at 55 °C

4.2 Extract Analysis

4.2.1 GC-Analysis

Henna flower extracts were analyzed by GC for their compositions. From a list of 40 available standard chemicals essential oils, 27 components were observed in the extracts at various conditions in addition to about 79 components that could not be identified but they appeared in the GC chromatograms with unique peaks and were considered in the calculation of extract composition (Table 5). Figure 17 shows a typical GC chromatogram. The unidentified compounds are marked as unknowns and should be identified by GC-MS and other techniques for future studies.

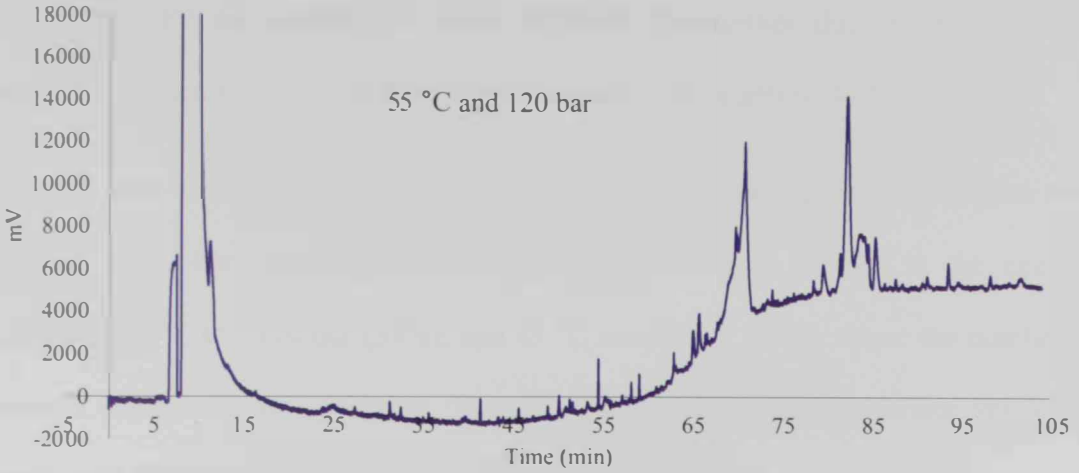

Figure 17 GC chromatogram for extract obtained at 55 °C and 120 bar

The identified components in the extracts obtained by SFE were compared with those obtained by Wong and Tong (1995) using solvent extraction (Table 1). Some compounds were observed in the extracts obtained by supercritical fluid extraction in this work were also presented in the extracts reported by Wong and Tong such as; limonene, eugenol, and linalool. On the other hand, β-ionone was reported by both techniques, but higher composition was obtained by supercritical fluid extraction. Moreover, some components existed only in the SFE extracts with high percentage and not found in Wong and Tong extracts (e.g. eugenol acetate).

The extract composition varied significantly at different conditions suggesting different quality for different extracts. For example β-ionone is a major component of henna flower extract. This component constituted about 28 % of the extract obtained at 55 °C and 80 bar, whereas at 120 bar, and at the same temperature only 1.49% of β-ionone was observed. Another example is eugenol acetate, for which the best condition to

operate was 55 °C and 120 bar resulting in 25.6% composition. Different extracts obtained by SFE are expected to show different bioactivities due to their different compositional quality. This is evident from the results of the antioxidant activity.

In some extracts, the compositions of some unknown components are higher than identified ones. For example unknown, Un_{64} is abundantly present in the extracts obtained at 55 °C and 120 bar (33%), and 45 °C and 80 bar (63%). Since the number of unknown compounds is significant, it would be useful to conduct further studies to identify and isolate some of the unknown compounds present in the extracts, especially the extracts that show significant antioxidant activity.

Table 5 Compositional analysis of extract from henna flower by GC

emperature (°C)		55	55	55	45	45	45	35	35	35
essure (bar)		100	120	80	80	100	120	80	100	120
ame	Time (min)									
n_1	25.84	-	-	-	-	-	-	-	10.312	
exanal	27.27	-	0.285	-	-	-	0.676	0.895		0.954
n_2	29.59	-	-	-	-	-	-	-	0.211	-
n_3	29.9	-	-	-	-	-	-	-	0.336	-
n_4	30.26	-	-	-	-	-	-	-	0.172	-
n_5	31.22	1.698	0.782	-	-	-	-	-	0.3	-
n_6	32.45	-	0.723	1.429	-	1.048	0.636	1.415	-	-
s-3-Hexenol	33.3	-	-	-	-	-	-	-	-	0.374
ns-2-Hexenol	33.88	-	-	-	-	-	-	-	-	-
n_7	34.24	-	-	-	-	-	-	-	0.12	-
n_8	34.46	-	-	-	-	-	-	-	0.13	-
n_9	34.83	-	-	-	-	-	-	-	0.216	-
n_{10}	35.53	-	0.479	-	-	1.31	0.712	0.751	-	0.829
n_{11}	36.24	-	-	1.801		1.037	-	-	-	-
pinene	37.21	-	-				-	-	-	-
n_{12}	41.3	-	1.048	4.004	1.337	3.628	1.788	4.111		0.628
-pinene	41.74	-		0.197		0.122				
n_{13}	43.11	-	-	-	-	-	0.314	-	0.13	
n_{14}	43.89	-					0.709			
ethyl Oxalate	44.56	-	0.621							
monene-S+R	45.61	-		1.973		0.44	1.607	7.424	0.188	0.727
n_{15}	45.76	-		0.06		0.199	0.143	0.321		
neole	46.55	-							3.648	
n_{16}	47.14	-							0.366	
n_{17}	48.05	-							0.293	
rtemisia ketone	48.72	-	0.46	1.158	0.576	1.039	0.655	1.246	0.167	
n_{18}	48.99	-		0.159		0.222		0.18	0.581	
n_{19}	49.36	-							9.576	

able 5 Compositional analysis of extract from henna flower by GC *(cont.)*

n_{20}	49.62	-						0.427	9.919	
n_{21}	50.04	1.736	1.245						21.778	
enzyl Alcohol	50.3	-		1.719						
n_{22}	50.82	-			0.305					0.108
n_{23}	50.94	-								0.194
n_{24}	51.25	-	0.471			1.373	0.927	0.873		0.837
inalool	51.63	-	0.525		0.888	1.979	1.699	1.588	0.41	
n_{25}	51.87	-				0.244	0.7	0.448	1.912	0.438
n_{26}	52.22	-							1.185	
n_{27}	54.43	-	1.548	3.838	2.34	3.442	2.082	3.753	0.207	0.841
Phenylethanol	54.71	-		2.488		0.108				0.057
n_{28}	55.34	-			0.785					0.265
n_{29}	55.56	-	3.646			0.685	0.433	0.605		0.412
enthone	55.87	-								
enthol	56.57	-					2.745			
orneol	57.02	-	0.314							0.392
ethyl Salicylate	57.97	0.513		5.217	0.548		0.879		0.141	0.775
ihydrocarvone	58.3	-								0.039
hyl nicotinate	58.83	7.522	0.907	3.709	1.279	1.785	1.194	1.928		1.011
n_{30}	59.08	-	0.775						0.132	
n_{31}	59.36	-								0.209
arvone	60.44	-					0.344			0.27
enthyl acetate	60.86	-				0.495	0.362			0.364
ornyl acetate	61.16	-								
obornyl Acetate	61.46	-							1.065	
n_{32}	62.07	-		3.37		2.156		4.086		2.911
n_{33}	62.42	9.38			2.914			3.305	0.289	
n_{34}	62.82	1.348	0.52	1.074	0.881	1.238	0.681	1.095	4.301	0.658
n_{35}	63.08	-	0.345	0.351			0.304		1.401	
n_{36}	63.29	0.416		0.499			0.172		0.092	
n_{37}	63.44						0.336			
zulene	63.89						0.231		0.092	
n_{38}	64.42						0.347		0.403	
igenol	64.84		2.445	0.524		4.458	4.887	4.06	2.114	
n_{39}	65.25	4.907		13.429					3.164	3.904
n_{40}	65.7	2.045				6.178	6.776	4.386	0.639	6.745
n_{41}	66.31	0.452	0.302	0.406	0.459		0.439		0.929	
caryophyllene	66.52	0.288	0.425	0.641		0.675		0.816		0.538
n_{42}	66.72	0.967		4.659	2.913		1.029			2.511
n_{43}	67.47			0.394						
hydro-B-Ionone	67.69		0.459	1.834	0.541		1.182	1.107		0.79
Humulene	67.89		0.315	0.913				0.571		0.353
n_{44}	68.09						1.089			
n_{45}	68.72	0.913				3.456				1.119
rsenene	69.28									
Ionone	69.74	1.491	0.834	28.019	10.12		14.307	10.99	0.939	31.112
n_{46}	69.88		0.335			0.326			0.044	
n_{47}	70.27			0.507			0.129	0.512	0.539	
n_{48}	70.49				2.433		0.203			
igenol acetae	70.84		25.684	2.804	1.284	16.341	3.972	3.198	0.725	2.979
n_{49}	71.24	47.063		3.457					0.175	
n_{50}	72.26								1.609	
n_{51}	72.73		0.176				0.343		0.796	
n_{52}	73.24						0.457			
n_{53}	73.73	0.499	0.533	0.91	0.475	0.559	0.592	0.92	1.208	0.901
n_{54}	74.06			0.217						

able 5 Compositional analysis of extract from henna flower by GC *(cont.)*

iethyl Phthalate	74.44			0.985			0.406			
arophyllene oxide	75.2			0.681						
n_{55}	75.4	0.774					0.377		0.092	0.496
n_{56}	76.2		0.383	0.605		0.602	0.381	0.661		
n_{57}	77.1						0.561			
n_{58}	78.04	0.545		1.877						
n_{59}	78.34	0.62		1.198	0.579	1.173	1.433	0.64		1.197
n_{60}	79.29		0.772			6.136			4.335	
n_{61}	79.48		3.79				1.593	2.132		1.734
n_{62}	80.41								0.331	
n_{63}	81.38	8.842	1.735		3.642	10.209	5.207	20.697	1.244	7.076
n_{64}	82.19		33.297		62.666	13.629	19.796	1.087	0.75	10.259
n_{65}	83.47		1.145							
n_{66}	83.75					1.553		1.355		
n_{67}	84.19	0.418		0.708		3.746	2.406	3.717	2.332	2.414
n_{68}	84.56		1.441			1.48	0.993	1.15		0.816
n_{69}	85.36	1.211	7.023			6.928	8.054	2.696	5.569	8.574
n_{70}	87.01			1.32						
n_{71}	87.55		0.638				0.443			
n_{72}	88.32			0.865	0.904					
n_{73}	90.35								0.342	
n_{74}	91.05		0.822						0.303	
n_{75}	93.43		1.849				2.267	2.386	0.509	1.894
n_{76}	94.31								1.238	
n_{77}	95.77				1.005					
n_{78}	98.12		0.902		1.124					
n_{79}	101.58	6.351						2.471		1.293
Total		100.00	100.00	100.00	100.00	100.00	100.00	100.00	100.00	100.00

4.2.2 Antibacterial activity

The antibacterial activity test showed that no inhibition zone existed for the henna flower extract, suggesting no antibacterial activity for the flower extracts. However, other researchers reported that the leaves extracts exhibited significant antibacterial activity. Figure 18 shows the results of antibacterial test where no inhibition zones against E.coli strains around the extracts discs (discs where numbered 1 to 9) compared to antibiotic control.

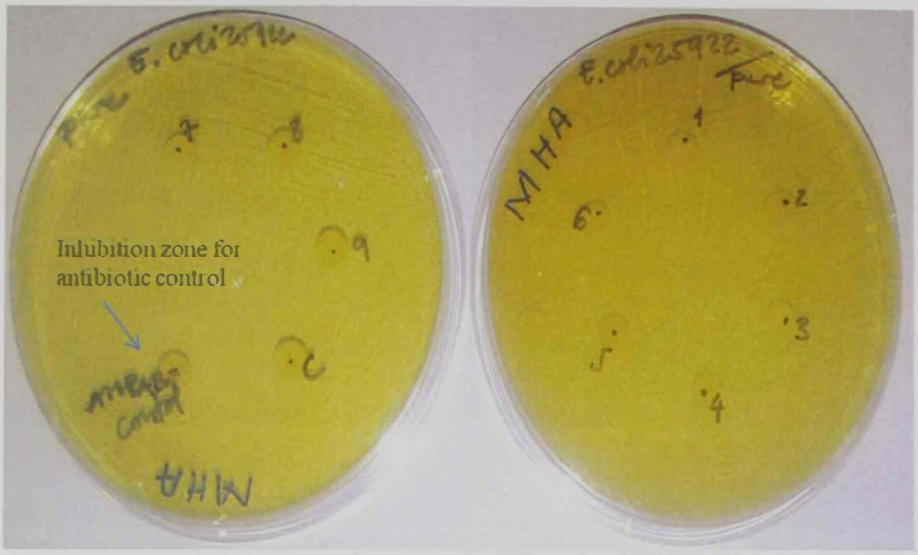

Figure 18 Results of antibacterial test

4.2.3 Antioxidant activity

4.2.3.1 FRAP (Ferric reducing antioxidant power) assay

The FRAP assay measures the ability of the extract to reduce a ferric salt (TPTZ-Fe (III) to a ferrous product (TPTZ-Fe(II). The reaction mechanism is electron transfer reaction shown in Figure 19. The reduction is due to the existence of antioxidants in the extract which involves electron-denoting groups such as hydroxyl group. The formation of the ferrous product is noticed as the color gets deeper from yellow to intense blue and quantitatively measured by the absorbance at 539 nm wavelength.

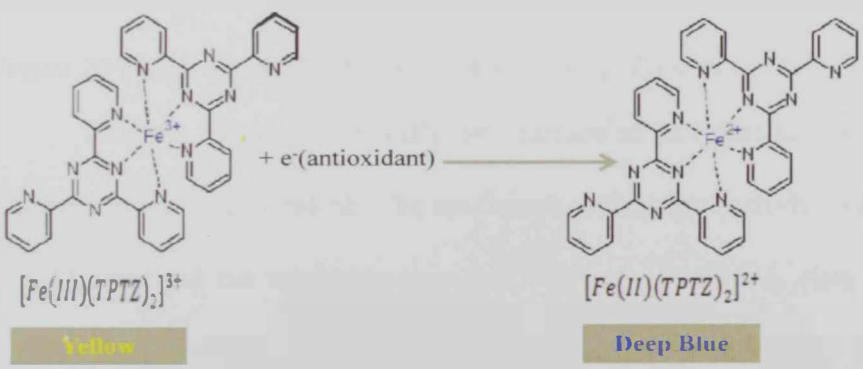

Figure 19 FRAP Reduction reaction

The absorbance of each extract mixed with the FRAP solution was measured and the concentration of antioxidants were calculated as ascorbic acid equivalent from a calibration curve (Appendix C). The results of FRAP assay for extracts at each extraction condition are shown in Figure 20. The FRAP assay revealed that compounds obtained by SFE of henna flowers exhibited antioxidant activity.

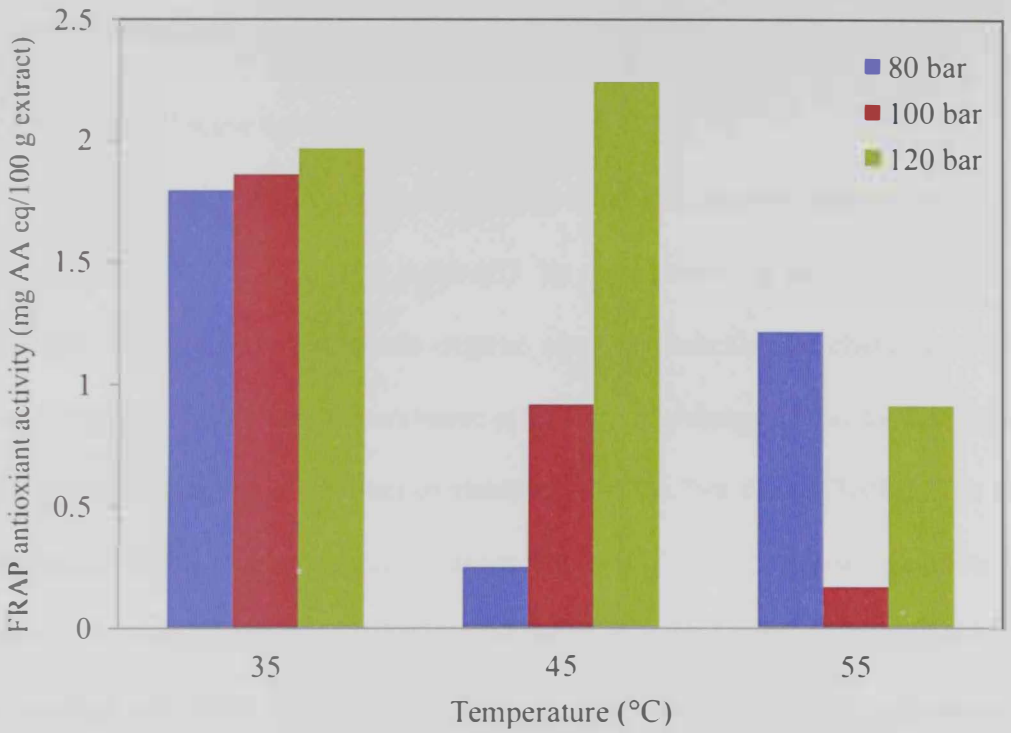

Figure 20 FRAP assay results for extract of henna flowers

Extracts obtained at different extraction temperature and pressure showed different antioxidant content. The maximum antioxidant activity was observed at 45 °C and 120 bar and the minimum was at 55 °C and 100 bar. A clear trend of antioxidant activity with extraction pressure can be observed at 35 and 45 °C. However, at elevated

temperature of 55 °C, lowest antioxidant activity was obtained at 100 bar. The variations in the antioxidant activity of different extracts are expected to be due to the differences in the composition of compounds in the extracts. For example the extract at 35 °C and 80 bar has the highest composition of compounds such as; Limonene-S+R and the unknown Un_{63}. The extract obtained at 45 °C and 120 bar is the only extract that contains menthol, unknowns UN_{14}, UN_{44}, and UN_{57}, and has the highest composition of carvone. It would be interesting to identify, fractionate and then test the antioxidant properly of these unknown compounds.

4.2.3.2 DPPH scavenging activity

The chemistry behind this assay is the reduction reaction that occurs to the DPPH molecule (2,2-diphenyl-1-picryl hydrazyl) by antioxidants in the substance. The DPPH molecule is one of the few stable organic nitrogen radicals and characterized by deep purple color with maximum absorbance at 517 nm wavelength. This method assesses the radical scavenging activity of antioxidants against the free radical DPPH. The reduction reaction of DPPH and by an antioxidant is shown in Figure 21. Upon reduction, the color fades as the odd electron of DPPH radical becomes paired with a free radical scavenging antioxidant and form the reduced DPPH-H. The loss in color is proportional to the antioxidant concentration; the higher the antioxidant concentration the more the color loss (the more the DPPH scavenging activity). The antioxidant concentration was calculated as ascorbic acid equivalent (AA eq) from a calibration curve (Appendix C) and the antioxidant or antiradical activity values were expressed as mm AA eq/100g of extract.

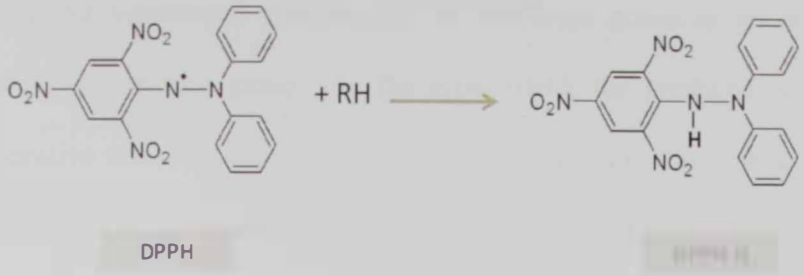

DPPH

Figure 21 DPPH reduction by antioxidant

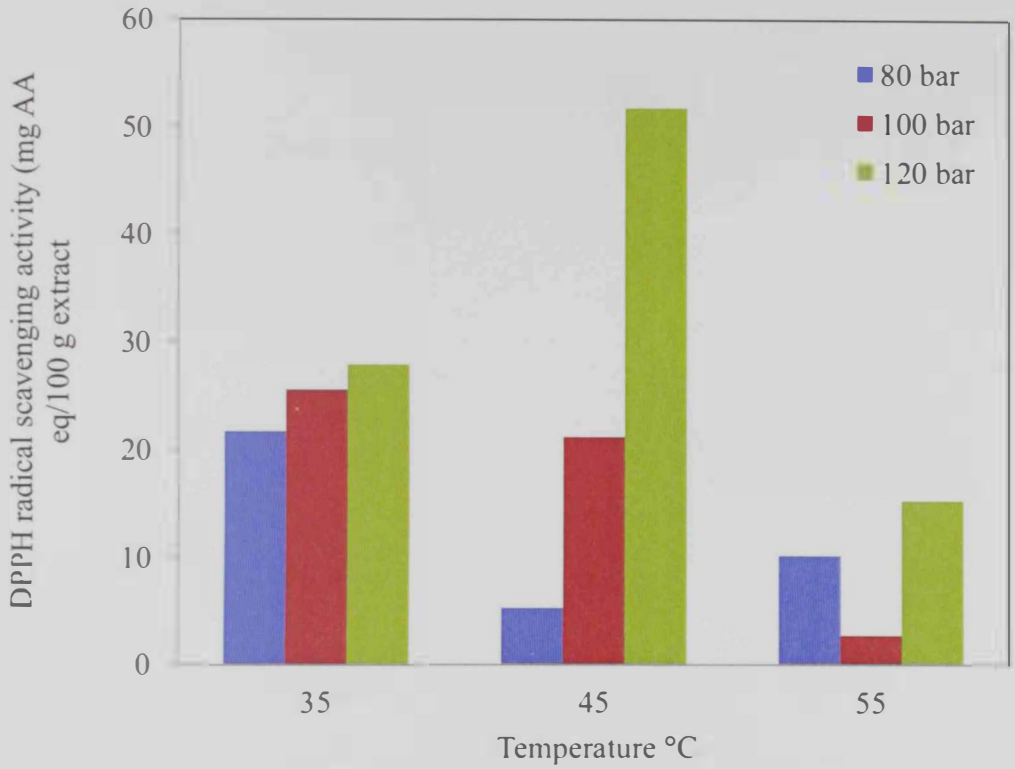

Figure 22 DPPH assay results for extracts of henna flowers

The results of DPPH assay agrees with the results obtained by FRAP assay, indicating that henna flower extracts obtained by SFE exhibit antioxidant activity (Figure 22). Similar to the results of the FRAP assay, the extract obtained at 45 °C and 120 bar has the highest radical scavenging activity while the extract obtained at 55 °C and 100 bar exhibited the lowest activity. The effect of antioxidants on DPPH radical scavenging is generally due to their hydrogen donating ability. This can be attributed to the presence of

adjacent substituted groups such as methoxyl group in an aromatic ring which is as electron-donating group. On the other hand, the presence of a carboxyl group has a negative effect on the antioxidant activity since it is an electron-withdrawing group. Such groups exist in henna flower extracts as shown from the GC analysis.

5 DATA MODELING

5.1 Description of the extraction mechanism

It is well known that the extraction process is the result of mass transfer which is promoted by concentration gradient. Figure 23 presents the steps involved in the supercritical fluid extraction process. At the beginning, supercritical carbon dioxide fills the extraction vessel and equilibrates with sample material where free solutes are dissolved in SC-CO_2. This equilibrium stage is to ensure the constant temperature, pressure, and composition within the extraction system. In step (a) the solutes present in the solid particles dissolve in SC-CO_2 within particle pores. This step is governed by solubility of solutes in SC-CO_2 or adsorption/desorption mechanism. Then, the solutes diffuse through the particle pores to the particle surface as shown in step (b). In step (c), the solutes transfer from the particle surface to the bulk phase through a film. Finally, the solutes diffuse within the bulk phase along the extraction vessel (Step d). The solutes leaving the extraction bed are collected and accumulated by depressurizing the supercritical solution to ambient pressure in the collection vial.

It is clear from the above explanation that the extraction process is governed by two phenomena, namely the solubility of solutes in SC-CO_2 and diffusion of the solutes within the particle and the bulk fluid phase.

Step a : Diffusion of Solutes from solid to pores

Step (b): Diffusion of solutes within the particle to the particle surface forming a film

Step (C): Diffusion of solutes from the particle surface to the bulk phase

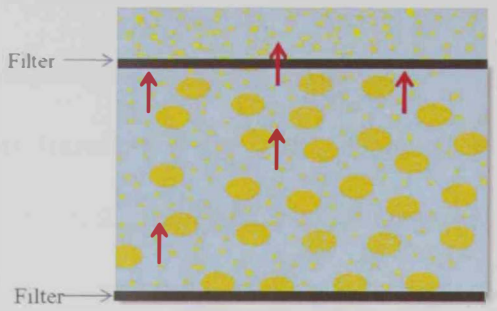

Step (d): Diffusion of solutes within the bulk along the extraction bed

Figure 23 Mechanism of SFE process

5.2 Theoretical principles of the extraction process

It is clear from section 5.1 that the extraction process takes place in two phases namely; particle phase, and fluid phase. The proposed mathematical model of the current extraction process is based on the law of conservation of mass. Derivation of the model equations starts by applying mass balance around a thin shell perpendicular to the transfer direction in each phase. The general equation of mass balance is:

$$\begin{pmatrix}\text{Rate of}\\ \text{mass in}\end{pmatrix} - \begin{pmatrix}\text{Rate of}\\ \text{mass out}\end{pmatrix} \pm \begin{pmatrix}\text{Rate of}\\ \text{mass generated or consumed}\end{pmatrix} = \begin{pmatrix}\text{Rate of}\\ \text{accumulated mass}\end{pmatrix} \quad (23)$$

The following assumptions were used to simplify the model equations:

1. The system is isothermal and isobaric; therefore, supercritical fluid properties such as; diffusivity coefficients, density, and viscosity are constant along the bed.
2. The particles have spherical geometry and solute is distributed uniformly.
3. Radial concentration gradients are neglected in the fluid phase
4. Solute concentration gradient in the particles is in r coordinate only.
5. Bed and particle porosities are fixed during the extraction process.
6. Local equilibrium is established at the interface of fluid and solid phase.

5.2.1 Particle Phase mass transfer

Mass transfer on the particle phase occurs through two steps as mentioned previously. When the fluid fills the particle pores, solute transfers from the solid phase to the fluid phase inside the particle pores, due to the concentration gradient (high solute concentration in the solid phase compared to that in the pores). This is usually expressed as an equilibrium relation by solubility or adsorption/desorption mechanism. Then the solute transfer to the particle surface by diffusing through the pores. This step can be described by molecular diffusion equation. A detailed description for each step is found in the coming sections.

5.2.1.1 Transfer of solute from solid phase

In this step, the fluid and the solid are competing in keeping the solute. This kind of competition is expressed by adsorption/desorption process. Many researchers expressed the adsorption/desorption process in the supercritical regions using different models such as Langmuir-like isotherm and BET type equilibrium equation (Jia et al., 2009b; Papamichail et al., 2000; Ruetsch et al., 2003) . Also the adsorption/desorption

process can be expressed simply by either analogy to interphase mass transfer as shown schematically in Figure 24, or using kinetics principles as discussed later.

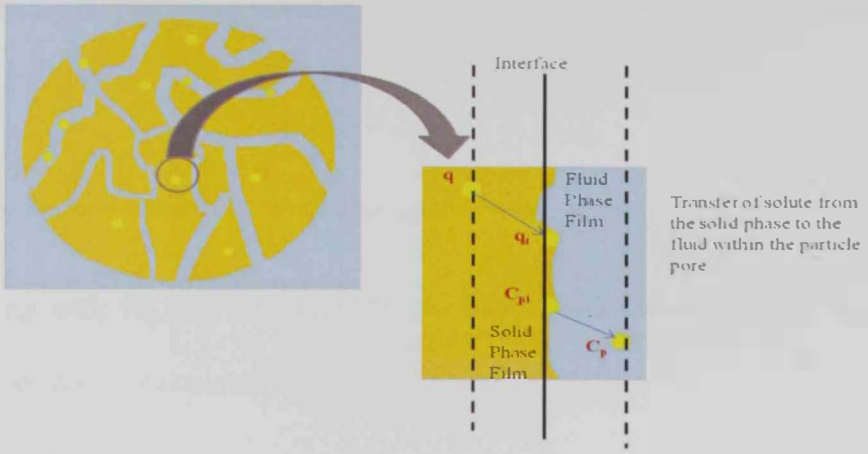

Figure 24 Interphase mass transfer mechanism

There are two phases in the interphase mass transfer mechanism; solid phase, and fluid phase separated by an interfacial surface. The interphase mass transfer involves three transfer steps; the transfer of solute through the solid phase film to the interfacial surface, transfer across the interface into the fluid phase within the pores, and transfer of solute through the fluid phase film to the bulk phase within the pores. The mathematical representation of this theory acquires two assumptions; (1) on each side of the interface, the transfer of solute is governed by the rates of diffusion through the phases, (2) there is no resistance to the mass transfer across the interface. Consequently, the two concentrations at the interface (q_i from the solid side and C_{pi} from the particle side) are in equilibrium as a result of the infinite contact time of the two phases. Assuming that the equilibrium relation is linear (Eq.24) the rate of mass transfer from solid phase to particles pore can be written as (Eq.25).

$$q_i = KC_{pi} \tag{24}$$

$$\frac{dq}{dt} = k_a(C_P - C_P^*) \quad (25)$$

Where K is the slope of the equilibrium curve. k_a is the overall mass transfer capacity coefficient, C_P^* is the concentration in the pore of the particle in equilibrium with q.

$$q = KC_p^* \quad (26)$$

The equilibrium relation (Eq.24) can be used to relate C_P^* to q.

Substituting with Eq.(26) into Eq.(25), the rate of mass transfer from solid phase to particle pore can be calculated from:

$$\frac{dq}{dt} = -k_a(C_p - \frac{q}{K}) \quad (27)$$

Another way to express the transfer of solute from solid phase to pore of the particle is through adsorption/desorption mechanism using the reaction kinetics principles by implementing the following reversible reaction with 1st order rate constants for both directions:

$$C_p \underset{k_d}{\overset{k_a}{\rightleftharpoons}} q$$

$$\frac{dq}{dt} = k_a C_p - k_d q$$

Defining $K = \frac{k_a}{k_d}$ leads to

$$\frac{dq}{dt} = -k_a(C_p - \frac{q}{K}) \quad (28)$$

Both approaches (interphase mass transfer and adsorption/desorption) resulted in the same form of the mass transfer equation (Eq. 27 and 28), with different physical meaning for their constants. In this study parameters k_a and K were fitted to the experimental data.

5.2.1.2 Diffusion within particle pores

Solute that is transferred from the solid phase to the pore will diffuse within the pores towards the surface of the particle due to a concentration gradient. Molecular mass transfer is described by Fick's law and since the pore sizes are not uniform in the particle, effective diffusion coefficient is used in the flux equation:

$$j_A = -D_e \frac{dC_p}{dr} \tag{29}$$

Applying equation 23 (mass balance) around a spherical shell of thickness Δr within a single particle as shown in Figure 25,the following equation can be obtained:

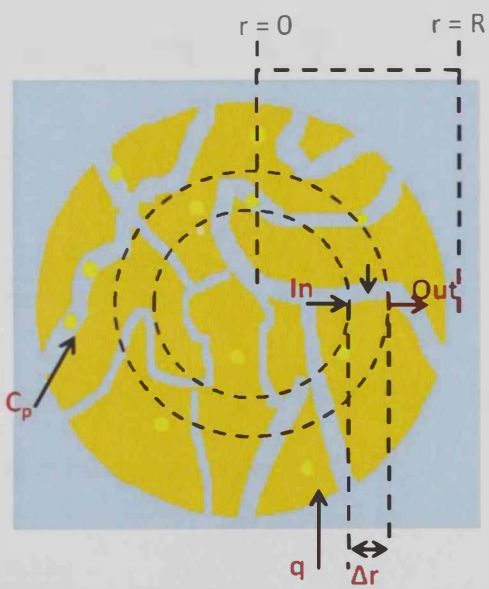

Figure 25 Mass transfer in the particle phase

$$\varepsilon_P 4\pi r^2 N_A(r) - \varepsilon_P 4\pi r^2 N_A(r+\Delta r) - 4\pi r^2 \Delta r \frac{dq}{dt}(1-\varepsilon_P) = \varepsilon_P 4\pi r^2 \Delta r \frac{dC_p}{dt} \qquad (30)$$

Dividing both sides by $4\pi\Delta r$

$$\frac{(\varepsilon_P r^2 N_A(r) - \varepsilon_P r^2 N_A(r+\Delta r))}{\Delta r} - r^2 \frac{dq}{dt}(1-\varepsilon_P) = \varepsilon_P r^2 \frac{dC_p}{dt}$$

$$\lim_{\Delta r \to 0}\left[\frac{(\varepsilon_P r^2 N_A(r) - \varepsilon_P r^2 N_A(r+\Delta r))}{\Delta r}\right] - r^2 \frac{dq}{dt}(1-\varepsilon_P) = \varepsilon_P r^2 \frac{dC_p}{dt}$$

Rearranging

$$-\varepsilon_P \frac{d}{dr} r^2 N_A = \varepsilon_P r^2 \frac{dC_p}{dt} + r^2 \frac{dq}{dt}(1-\varepsilon_P)$$

Since there is no convective mass transfer (lower flow) in the pores $N_A = j_A$

Applying Fick's law of diffusion $j_A = -D_e \frac{dC_p}{dr}$

$$D_e \varepsilon_p \frac{d}{dr}\left(r^2 \frac{dC_p}{dr}\right) = \varepsilon_p r^2 \frac{dC_p}{dt} + r^2\left(1-\varepsilon_p\right)\frac{dq}{dt}$$

Dividing both sides by $\varepsilon_p r^2$

$$\frac{D_e}{r^2}\left[\frac{d}{dr}\left(r^2 \frac{dC_p}{dr}\right)\right] - \frac{(1-\varepsilon_p)}{\varepsilon_p}\frac{dq}{dt} = \frac{dC_p}{dt}$$

Since both C_P and q are functions of two variables (r,t), the ordinary derivatives are converted to partial derivatives and rearranged:

$$\frac{\partial C_p}{\partial t} = \frac{D_e}{r^2}\frac{\partial}{\partial r}\left(r^2 \frac{\partial C_p}{\partial r}\right) - \frac{(1-\varepsilon_p)}{\varepsilon_p}\frac{\partial q}{\partial t} \qquad (31)$$

Eq.31 can also be written as

$$\frac{\partial C_P}{\partial t} = \frac{D_e}{r^2}\left[2r\frac{\partial C_P}{\partial r} + r^2\frac{\partial^2 C_P}{\partial r^2}\right] - \frac{(1-\varepsilon_P)}{\varepsilon_P}\frac{\partial q}{\partial t} \qquad (32)$$

Equation 32 is a partial differential equation with two dimensions and has the following initial and boundary conditions:

$at\ t = 0\ and\ 0 \leq r \leq R$:

$$C_p = C_{po}\ , \qquad q = q_o$$

$$at\ r = 0\ ; \frac{\partial C_p}{\partial r} = 0$$

$$at\ r = R\ ;\ -D_e\frac{\partial C_p}{\partial r} = k_f a\left(C_{pR} - C\right)$$

5.2.2 Fluid Phase mass transfer

Diffusion of the solute in the fluid phase is controlled by its transfer from the particle phase, which involves two steps; (1) transfer of solute from surface of the particle to the bulk fluid phase in the extraction vessel which is represented by film diffusion and (2) transfer of solute along the extraction vessel, which is governed by molecular and convective mass transfer. These steps are schematically demonstrated in Figure 26.

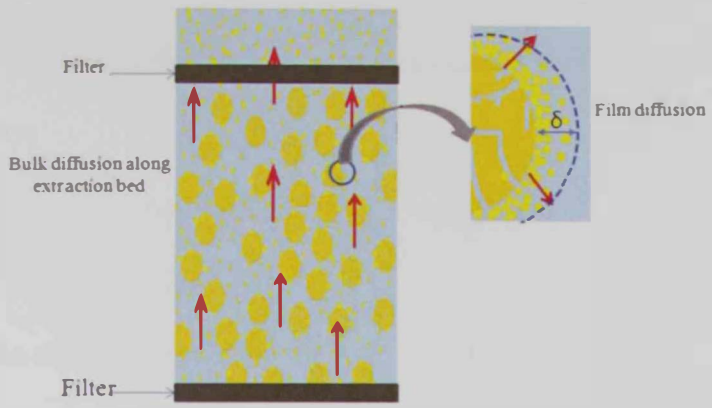

Figure 26 Fluid phase mass transfer mechanism

5.2.2.1 Film diffusion

Film diffusion is based upon the assumption that the entire resistance to diffusion from the particle surface to the bulk fluid phase occurs in a stagnant or laminar film of constant thickness δ as shown in Figure 26. Mass transfer takes place as a result of the concentration gradient between the particle surface (high concentrations) and the film boundary in the fluid phase (low concentration). The mass transfer flux through the film can be described as shown in Eq.33

$$\frac{dC}{dt} = k_f a\left(C_{pR} - C\right) \tag{33}$$

5.2.2.2 Bulk diffusion along the extraction bed

Since the fluid is flowing within the extraction vessel, mass transfer is the result of molecular diffusion plus convective mass transfer (bulk flow), which can be described as:

$$N_A = j_A + C\vartheta_i$$

Where ϑ_i is the interstitial velocity and can be calculated from the superficial velocity and the bed porosity:

$$\vartheta_i = \frac{\vartheta_s}{\varepsilon_b}$$

Figure 27 shows the mass balance along the extraction bed.

Applying mass balance (Eq.23) over a control volume in the extraction bed as shown in Figure 27 yields:

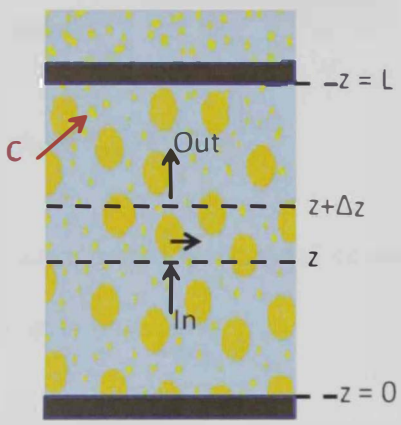

Figure 27 Mass transfer in the fluid phase

$$\varepsilon_b A N_A(z) - \varepsilon_b A N_A(z+\Delta z) + (1-\varepsilon_b) A \Delta z k_f a\left(C_{pR} - C\right) = \varepsilon_b A \Delta z \frac{dC}{dt}$$

Dividing both sides by $\varepsilon_b A \Delta z$

$$\frac{N_{A(z)} - N_{A(z+\Delta z)}}{\Delta z} + \frac{(1-\varepsilon_b)}{\varepsilon_b} k_f a\left(C_{pR} - C\right) = \frac{dC}{dt}$$

$$\lim_{\Delta z \to 0} \left(\frac{N_{A(z)} - N_{A(z+\Delta z)}}{\Delta z}\right) + \frac{(1-\varepsilon_b)}{\varepsilon_b} k_f a\left(C_{pR} - C\right) = \frac{dC}{dt}$$

$$-\frac{dN_A}{dz} + \frac{(1-\varepsilon_b)}{\varepsilon_b} k_f a\left(C_{pR} - C\right) = \frac{dC}{dt}$$

Substituting the flux by $N_A = j_A + C\vartheta_i$

$$-\frac{\partial(j_A+C\vartheta_i)}{\partial z}+\frac{(1-\varepsilon_b)}{\varepsilon_b}k_f a\left(C_{pR}-C\right)=\frac{\partial C}{\partial t} \quad (34)$$

Recalling Equation 33

$$j_A = -D_{ax}\frac{dC}{dz}$$

Where

$$-\frac{\partial}{\partial z}\left(-D_{ax}\frac{\partial C}{\partial z}\right)-\vartheta_i\frac{\partial C}{\partial z}+\frac{(1-\varepsilon_b)}{\varepsilon_b}k_f a\left(C_{pR}-C\right)=\frac{\partial C}{\partial t}$$

Further rearrangements results

$$D_{ax}\frac{\partial^2 C}{\partial z^2}-\vartheta_i\frac{\partial C}{\partial z}+\frac{(1-\varepsilon_b)}{\varepsilon_b}k_f a\left(C_{pR}-C\right)=\frac{\partial C}{\partial t} \quad (35)$$

Equation 35 is second order partial differential equation for solute concentration in the fluid phase as a function of two variables (z,t).

Boundary and initial conditions are as follows:

$$at\ t = 0; all\ zC = C_o = 0$$

$$at\ z = 0; all\ tC = 0$$

$$at\ z = L; t > 0, \frac{dC}{dz} = 0$$

Equations 32 and 35 are the mathematical expressions for the proposed model and were solved numerically by the finite element method

Values of C_{po}, and q_o were calculated from their corresponding definitions which take into account; the amount of oil dissolved initially in the fluid phase; amount of oil in the sample, and the geometry of the particle and the bed as expressed in equations 39 and 40.

$$q_o = \frac{(1-f_o)M_o}{AL(1-\varepsilon_b)(1-\varepsilon_p)} \quad (39)$$

$$C_{po} = \frac{f_o M_o}{AL(1-\varepsilon_b)\varepsilon_p} \quad (40)$$

The fraction of solute initially dissolved in the fluid phase after the equilibrium time, f_o, was assumed to be 0. Equations 36-38 can be solved simultaneously from $q(r,t)$, $C_P(r,t)$, and $C(z,t)$ profiles. Once the fluid phase concentration profile, $C(z,t)$, is obtained, the extract mass can be calculated from:

$$M(t) = \int_0^t C(z=L,t)\vartheta_s A dt$$

Where ϑ_s is the superficial velocity and A is the cross sectional area of the extraction vessel. Since both ϑ_s and A are constants:

$$M(t) = \vartheta_s A \int_0^t C(z=L,t)dt \quad (41)$$

Superficial velocity ϑ_s can be calculated from

$$\vartheta_s = \frac{m}{\rho A}$$

Where $\dot{m}$ and ρ are the mass flow rate and density of the fluid, respectively, at the extraction operating conditions. The fluid is mainly CO_2 since the extract solubility is low in CO_2 ($<3x10^{-3}$ g/g_{CO2}). Therefore, fluid properties are assumed to be the same as for

pure CO_2. The process can be assumed continuous and at steady state for CO_2, therefore, mass flow rate of CO_2 in the extraction vessel can be assumed equal to that at the syringe pump, which is at 25 °C and system pressure (P). Since volumetric flow rate (F) is controlled and recorded at the syringe pump. Mass flow rate of CO_2 ($\dot{m}$) can be calculated from its density at temperature and pressure of CO_2 of the syringe pump (25°C, system P):

$$\dot{m} = \rho_{25^oC,P} F$$

Therefore,

$$\vartheta_s = \frac{\rho_{25^oC,P} F}{\rho A}$$

Finally extraction yield is calculated from:

$$Yield\ (\%) = \frac{M_\infty}{M_{sample}} \times 100 \qquad (42)$$

The properties of SC-CO_2 namely; density and viscosity were obtained from NIST Chemistry webbook and tabulated in Table 4. The density values were used for the calculation of mass flow rate and supercritical velocity.

5.2.2.3 Model parameters

The model equations require the knowledge of parameters such as effective diffusion coefficient (D_e), film coefficient (k_f), axial dispersion coefficient (D_{ax}), and constants of the kinetics model (K_a, K). The axial dispersion coefficient at each extraction condition was calculated using the correlation proposed by Tan and Liou in 1989. Their investigation revealed that the axial dispersion is affected by the interstitial velocity,

particle diameter, and reduced density and viscosity of supercritical carbon dioxide. The correlation is shown in equation 43 and has about 8.5% deviation from experimental results.

$$D_{ax} = 0.085\vartheta_i^{0.914} d_p^{0.388} \rho_r^{0.725} \mu_r^{0.676} \quad (43)$$

With $\rho_r = \frac{\rho}{\rho_c}$ and $\mu_r = \frac{\mu}{\mu_c}$

Effective diffusion coefficient is usually related to binary diffusion coefficient and particle porosity:

$$D_e = D_{12}\varepsilon_P$$

However, since henna flower extracts contain many unknown compounds, calculation or experimental determination of the binary diffusion coefficient is difficult and time consuming.

Therefore, D_e and other parameters (k_f, k_a, and K) were adjusted to fit experimental extraction data by minimizing the following objective function, which is the summation of squared relative error.

$$f_{Obj} = \sum_i \left(\frac{Y_i^{cal} - Y_i^{exp}}{Y_i^{cal}}\right)^2 \quad (43)$$

Where Y_i^{exp} is the experimental and Y_i^{cal} the calculated extraction yield and i refers to data points used in the fitting.

6 MODELING RESULTS

The model equations (36-38) and extraction yield (Eq.42) were solved using Excel Visual Basic Applications-Mocro (VBA-Macro). Furthermore, Powell minimization method using subroutine available was used for fitting the model parameters to the experimental extraction data using objective function (Eq.44). The VBA-Macro code is shown in Appendix D. The calculation for the adjustable parameters at each condition using Powell's minimization method usually took 1-2 days on a personal computer (DELL Inspiron 1564, AE).

The model was applied to each experimental condition and the results are shown in figures 28-30 showing the effect of temperature and pressure. Results showed good agreements between calculated extraction yield by the mathematical model and the experimental data.

The difference between experimental and calculated extraction curve, R^2 was calculated for each condition using equation (44).

$$R^2 = \frac{\sum_i \left(Y_i^{exp} - Y_i^{cal}\right)^2}{\sum_i Y_i^{exp} - \overline{Y^{exp}}} \qquad (44)$$

Values of R^2 ranged from 0.96 to 0.99 as seen in Table 6. The best agreement between experimental and calculated extraction curve was found at 45 °C and 80 bar with R^2 of 0.998, while the worst agreement was at 55 °C and 80 bar with R^2 of 0.96.

Four fitting parameters (D_e, k_f, k_a, and K) were used and their values were adjusted to the experimental data using Powell's minimization method. Values of these parameters obtained from the model are given in Table 6 at their corresponding conditions

along with the optimum objective function and R^2 values. The fitting method revealed that the objective function (f_{Obj}) was sensitive to D_e and k_f, while K and K_a were not affecting the objective function significantly.

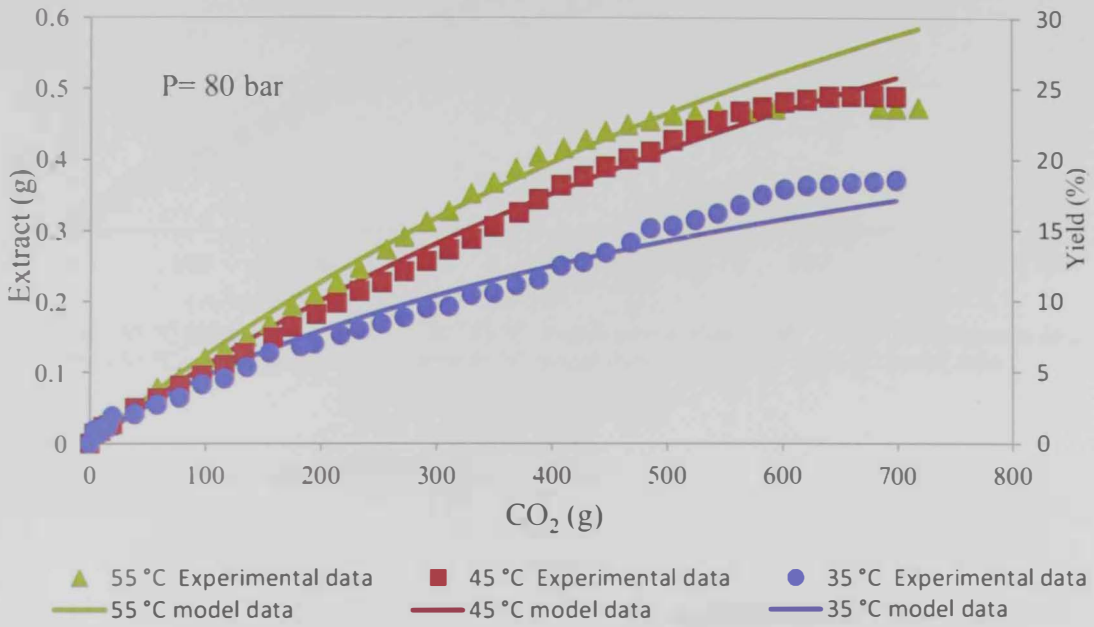

Figure 28 Extraction curves at 80 bar

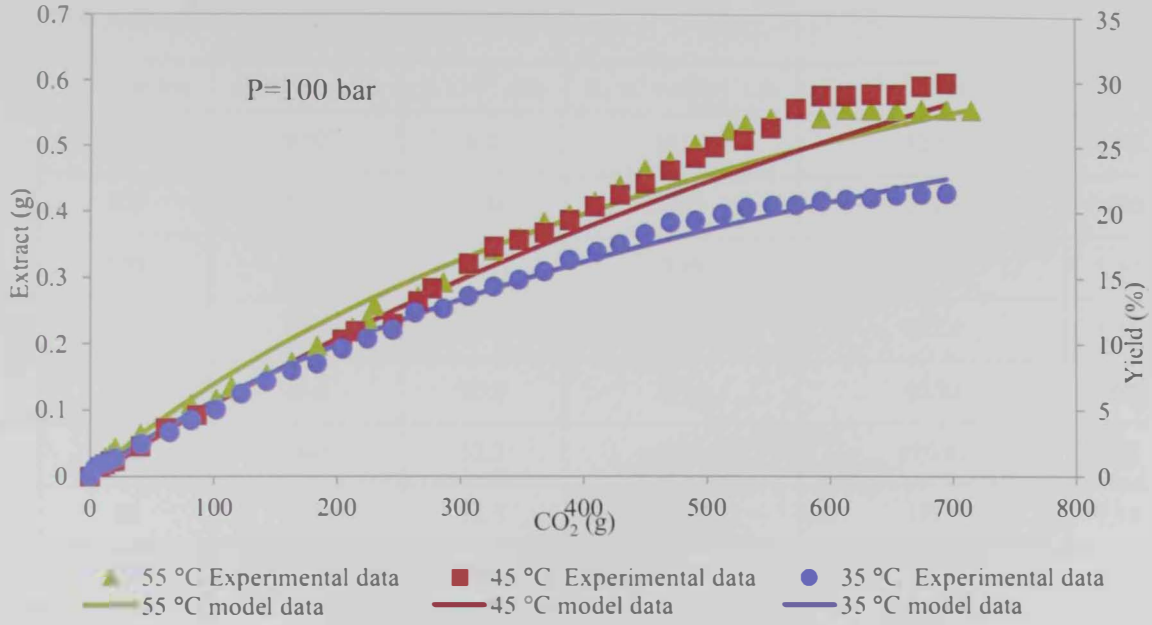

Figure 29 Extraction curves at 100 bar

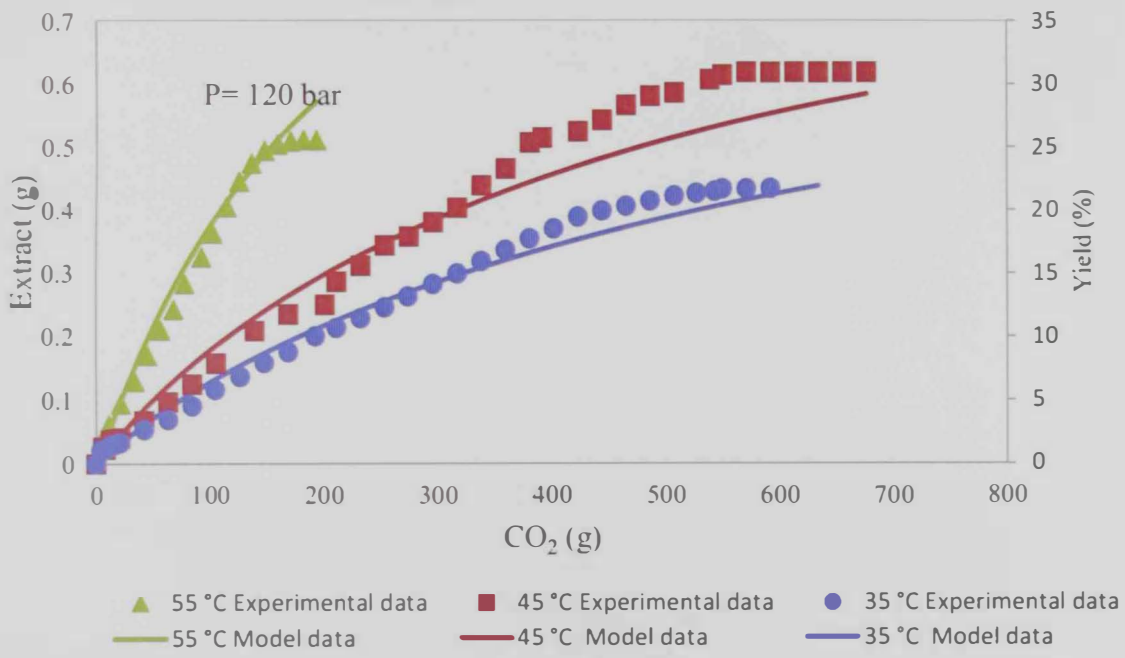

Figure 30 Extraction curves at 120 bar

Table 6 Adjustable model parameters

perature °C	Pressure bar	D_e x10^{12}, m^2/s	k_fx10^8, m/s	K, m^3 void/m^3 s.p.	K_a, $s^{-1}m^3$ void/m^3 s.p.	*OBJF*	R^2
35	80	9.50	6.0	141.2	320.8	1.60	0.97127
35	100	5.24	7.88	90.3	519.3	0.992	0.9939
35	120	0.496	0.702	3.49	1.046	1.30	0.98519
45	80	16.3	9.42	150.3	197.1	1.35	0.99838
45	100	20.3	10.9	139.6	45.91	0.403	0.97439
45	120	0.685	12.2	69.0	320.02	1.08	0.96052
55	80	21.9	13.7	179.8	198.5	1.38	0.96216
55	100	9.47	16.4	139.9	122.2	1.41	0.97971
55	120	25.5	5.01	34.05	519.1	0.826	0.98388

7 Conclusion and recommendations

Volatile components of henna flowers were extracted using supercritical fluid extraction technique over temperature and pressure ranges of 35-55 °C and 80-120 bar, respectively. Extraction operating conditions showed significant effects on the solubility of extracts in SC-CO_2 and extraction yield. An extraction yield 31% was obtained at 45 °C and 120 bar. The maximum solubility of 2.9 $mg_{extract}/g$ CO_2 was observed at 55 °C and 120 bar. Other extraction parameters including; extract cooling temperature, and SC-CO_2 flow rate were also found to have effects on the extraction yield.

Compositional analysis of extracts obtained at different conditions revealed the presence of many compounds in the extracts. Over 100 compounds, 79 of which were not identified were detected by GC. Henna flower extracts did not exhibit any antibacterial activity against *S. aureus* and *E. coli* since no inhibition zone was detected when performing disc diffusion test. The FRAP and DPPH tests revealed that extracts of henna flower contain antioxidants. This assay has a great interest in nutraceutical and pharmaceutical fields.

The proposed mathematical model could fit the experimental extraction curve very well at all conditions. The model was derived according to mass transfer principles where two mass balance equations (one for the particle phase and one for the fluid phase) governed the extraction phenomenon. The parameters; film coefficient, effective diffusivity coefficients, adsorption and equilibrium constants were adjustable parameters and fitted to match the experimental result by Powell's minimization method an objective function defined as the minimum sum of squared relative errors. The model can be used for a feasibility study of a large scale process or selection of better conditions that yield

higher extract quality. Moreover, the proposed model can be tested to model supercritical extraction of other plants materials.

8 REFERENCES

Abourriche, A., Oumam, M., Hannache, H., Adil, A., Pailler, R., Naslain, R., Birot, M., & Pillot, J. P. (2009). Effect of toluene proportion on the yield and composition of oils obtained by supercritical extraction of Moroccan oil shale. The Journal of Supercritical Fluids, 51(1), 24-28.

Anitescu, G., & Tavlarides, L. L. (1997). Solubilities of solids in supercritical fluids: I. New quasistatic experimental method for polycyclic aromatic hydrocarbons (PAHs) + pure fluids. The Journal of Supercritical Fluids, 10(3), 175-189.

Armstrong, S. D. (1999). Microwave-Assisted Extraction for the Isolation of Trace Systemic Fungicides from Woody Plant Material. Faculty of the Virginia Polytechnic Institute and State University, Virginia.

Ashraf-Khorassani, M., Taylor, L. T., & Zimmerman, P. (1990). Nitrous oxide versus carbon dioxide for supercritical-fluid extraction and chromatography of amines. Analytical Chemistry, 62(11), 1177-1180.

B.Gupta, R., & Shim, J.-J. (2007). Solubility in supercritical carbon dioxide (1 ed.). New York: Taylor and Francis Group.

Bernardo-Gil, M. G., & Casquilho, M. (2007). Modeling the supercritical fluid extraction of hazelnut and walnut oils. AIChE Journal, 53(11), 2980-2985.

Bernardo-Gil, M. G., Lopes, I. M. G., Casquilho, M., Ribeiro, M. A., Esquivel, M. M., & Empis, J. (2007). Supercritical carbon dioxide extraction of acorn oil. The Journal of Supercritical Fluids, 40(3), 344-348.

BH., A., AK., B., & MO., T. (1995). inflammatory, antipyretic, and analgesic effects of Lawsonia inermis L. (henna) in rats. Journal of pharmacology, 51, 356-363.

Brunner, G. (2009). Near and supercritical water. Part II: Oxidative processes. The Journal of Supercritical Fluids, 47(3), 382-390.

Campos, L. M. A. S., Michielin, E. M. Z., Danielski, L., & Ferreira, S. R. S. (2005). Experimental data and modeling the supercritical fluid extraction of marigold (Calendula officinalis) oleoresin. The Journal of Supercritical Fluids, 34(2), 163-170.

Ceni, G., Silva, P. C. d., Lerin, L., Charin, R. M., Oliveira, J. V., Toniazzo, G., Treichel, H., Oestreicher, E. G., & Oliveira, D. d. (2010). Enzyme-catalyzed production of 1-glyceryl benzoate in compressed n-butane. Enzyme and Microbial Technology, 46(6), 513-519.

Chan, C.-H., Yusoff, R., Ngoh, G.-C., & Kung, F. W.-L. (2011). Microwave-assisted extractions of active ingredients from plants. Journal of Chromatography A, 1218(37), 6213-6225.

Chaudhary, G., Goyal, S., & Poonia, P. (2010). Lawsonia inermis Linnaeus: A Phytopharmacological Review. International Journal of Pharmaceutical Sciences and Drug Research, 2(2), 91-98.

Chen, P.-Y., Chen, W.-H., Lai, S.-M., & Chang, C.-M. J. (2011). Solubility of Jatropha and Aquilaria oils in supercritical carbon dioxide at elevated pressures. The Journal of Supercritical Fluids, 55(3), 893-897.

Chihara, K., Sumitomo, K., Omote, M., Simokawatoko, T., Takubo, M., Kono, K., & Kawai, T. (2012). Supercritical propane regeneration of activated carbon fiber adsorbed by heavy oil

Chrastil, J. (1982). Solubility of solids and liquids in supercritical gases. The Journal of Physical Chemistry, 86(15), 3016-3021.

Crank, J. (1975). The Mathematics of diffusion (2 ed.). New York: Oxford University Press.

Damjanovic, B., Lepojevic, Z., Zivkovic, V., & Tolic, A. (2005). Extraction of fennel (Foeniculum vulgare Mill.) seeds with supercritical CO2: Comparison with hydrodistillation. Food Chemistry, 92(1), 143-149.

Del Valle, J. M., & Aguilera, J. M. (1988). An improved equation for predicting the solubility of vegetable oils in supercritical carbon dioxide. Industrial & Engineering Chemistry Research, 27(8), 1551-1553.

Doker, O., Salgın, U., Sanal, I., U. Mehmetoglu, & Calımlı, A. (2004). Modeling of extraction of beta-carotene from apricot bagasse using supercritical CO_2 in packed bed extractor. The Journal of Supercritical Fluids, 28(1), 11-19.

Duvernag, W. H., Assad, J. M., Sabiov, C. M., Lima, M., & Xu, Z. (2005). Microwave Extraction of Antioxidants Components from Rice Bran. The official Journal of ISPE, 25(4).

Endrini, S., Rahmat, A., Ismail, P., & Taufiq-Yap, Y. H. (2007). Comparing of the cytotoxicity properties and mechanism of lawsonia inermis and strobilanthes crispus extract against severak cancer cell lines. Journal of medical sciences, 7(7), 1098-1102.

Esmaeilzadeh, F., Asadi, H., & Lashkarbolooki, M. (2009). Calculation of the solid solubilities in supercritical carbon dioxide using a new Gex mixing rule. The Journal of Supercritical Fluids, 51(2), 148-158.

Esquivel, M. M., Bernardo-Gil, M. G., & King, M. B. (1999). Mathematical models for supercritical extraction of olive husk oil. The Journal of Supercritical Fluids, 16(1), 43-58.

Fischer, A., Mallat, T., & Baiker, A. (1999). Synthesis of 1,4-Diaminocyclohexane in Supercritical Ammonia. Journal of Catalysis, 182(2), 289-291.

Franke, M., Winek, C. L., & Kingston, H. M. (1996). Extraction of selected drugs from serum using microwave irradiation. Forensic Science International, 81(1), 51-59.

Ganzer, K., Salgo, A., & Valko, K. (1986). Microwave Extraction: Anovel Sample Preparation method for Chromatography. Journal of Chromatography 371, 299-306.

García-Risco, M. R., Vicente, G., Reglero, G., & Fornari, T. (2011). Fractionation of thyme (Thymus vulgaris L.) by supercritical fluid extraction and chromatography. The Journal of Supercritical Fluids, 55(3), 949-954.

Gaspar, F., Lu, T., Santos, R., & Al-Duri, B. (2003). Modelling the extraction of essential oils with compressed carbon dioxide. The Journal of Supercritical Fluids, 25(3), 247-260.

Gonen, M., Balkose, D., & Ulku, S. (2011). Supercritical ethanol drying of zinc borates of $2ZnO{\cdot}3B_2O_3{\cdot}3H_2O$ and $ZnO{\cdot}B_2O_3{\cdot}2H_2O$. The Journal of Supercritical Fluids, 59(0), 43-52.

Gong, X.-Y., & Cao, X.-J. (2009). Measurement and correlation of solubility of artemisinin in supercritical carbon dioxide. Fluid Phase Equilibria, 284(1), 26-30.

Goto, M., Roy, B. C., & Hirose, T. (1996). Shrinking-core leaching model for supercritical-fluid extraction. The Journal of Supercritical Fluids, 9(2), 128-133.

Gracia, I., Garcia, M. T., Rodriguez, J. F., Fernandez, M. P., & de Lucas, A. (2009). Modelling of the phase behaviour for vegetable oils at supercritical conditions. The Journal of Supercritical Fluids, 48(3), 189-194.

Grosso, C., Coelho, J. P., Pessoa, F. L. P., Fareleira, J. M. N. A., Barroso, J. G., Urieta, J. S., Palavra, A. F., & Sovov, H. (2010). Mathematical modelling of supercritical CO2 extraction of volatile oils from aromatic plants. Chemical Engineering Science, 65(11), 3579-3590.

Gui, M. M., Lee, K. T., & Bhatia, S. (2009). Supercritical ethanol technology for the production of biodiesel: Process optimization studies. The Journal of Supercritical Fluids, 49(2), 286-292.

Guiochon, G., & Tarafder, A. (2011). Fundamental challenges and opportunities for preparative supercritical fluid chromatography. Journal of Chromatography A, 1218(8), 1037-1114.

Handa, S. S., Khanuja, S. P. S., Longo, G., & Rakesh, D. D. (2008). Extraction Technologies for Medicinal and Aromatic Plants (1 ed.). Trieste: INTERNATIONAL CENTRE FOR SCIENCE AND HIGH TECHNOLOGY.

Hashimoto, T., Fujito, K., Haskell, B. A., Fini, P. T., Speck, J. S., & Nakamura, S. (2005). Growth of gallium nitride via fluid transport in supercritical ammonia. Journal of Crystal Growth, 275(12), e525-e530.

Hsouna, A. B., Trigui, M., Culioli, G. r., Blache, Y., & Jaoua, S. (2011). Antioxidant constituents from Lawsonia inermis leaves: Isolation, structure elucidation and antioxidative capacity. Food Chemistry, 125(1), 193-200.

Huang, Z., Yang, M.-J., Liu, S.-F., & Ma, Q. (2011). Supercritical carbon dioxide extraction of Baizhu: Experiments and modeling. The Journal of Supercritical Fluids, 58(1), 31-39.

Hwang, G. C., Kim, B. K., Bae, S. Y., Yi, S. C., & Kumazawa, H. (1999). Degradation of Polystyrene in Supercritical Acetone. Journal of Industrial and Engineering Chemistry, 5(2), 150-154.

Jallad, K. N., & Espada-Jallad, C. (2008). Lead exposure from the use of Lawsonia inermis (Henna) in temporary paint-on-tattooing and hair dying. Science of The Total Environment, 397(13), 244-250.

Jia, D., Li, S., & Xiao, L. (2009a). Supercritical CO_2 extraction of Plumula nelumbinis oil: Experiments and modeling. Journal of Supercritical Fluids, 50, 229-234.

Jia, D., Li, S., & Xiao, L. (2009b). Supercritical CO_2 extraction of Plumula nelumbinis oil: Experiments and modeling. The Journal of Supercritical Fluids, 50(3), 229-234.

Joung, S., Park, S., Kim, S., Yoo, K.-P., & Bae, S. (1999). Thermolysis of scrap tire using supercritical toluene. Korean Journal of Chemical Engineering, 16(5), 602-607.

Khajeh, M., Yamini, Y., Bahramifar, N., Sefidkon, F., & Reza Pirmoradei, M. (2005). Comparison of essential oils compositions of Ferula assa-foetida obtained by supercritical carbon dioxide extraction and hydrodistillation methods. Food Chemistry, 91(4), 639-644.

Kipcak, E., Kıpcak, E., Sogut, O. O., & Akgun, M. (2011). Hydrothermal gasification of olive mill wastewater as a biomass source in supercritical water. The Journal of Supercritical Fluids, 57(1), 50-57.

Kruse, A., & Dinjus, E. (2007). Hot compressed water as reaction medium and reactant: 2. Degradation reactions. The Journal of Supercritical Fluids, 41(3), 361-379.

Lachance, R., Paschkewitz, J., DiNaro, J., & Tester, J. W. (1999). Thiodiglycol hydrolysis and oxidation in sub- and supercritical water. The Journal of Supercritical Fluids, 16(2), 133-147.

Langa, E., Cacho, J., Palavra, A. M. F., Burillo, J., Mainar, A. M., & Urieta, J. S. (2009). The evolution of hyssop oil composition in the supercritical extraction curve: Modelling of the oil extraction process. The Journal of Supercritical Fluids, 49(1), 37-44.

Langa, E., Porta, G. D., Palavra, A. M. F., Urieta, J. S., & Mainar, A. M. (2009). Supercritical fluid extraction of Spanish sage essential oil: Optimization of the process parameters and modelling. The Journal of Supercritical Fluids, 49(2), 174-181.

Lee, S.-B., & Hong, I.-K. (1998). Depolymerization Behavior for cis-Polyisoprene Rubber in Supercritical Tetrahydrofuran. Journal of Industrial and Engineering Chemistry, 4(1), 26-30.

Letellier, S., Marias, F., Cezac, P., & Serin, J. P. (2010). Gasification of aqueous biomass in supercritical water: A thermodynamic equilibrium analysis. The Journal of Supercritical Fluids, 51(3), 353-361.

Leusbrock, I., Metz, S. J., Rexwinkel, G., & Versteeg, G. F. (2010). The solubilities of phosphate and sulfate salts in supercritical water. The Journal of Supercritical Fluids, 54(1), 1-8.

Liu, J., Lin, S., Wang, Z., Wang, C., Wang, E., Zhang, Y., & Liu, J. (2010). Supercritical fluid extraction of flavonoids from Maydis stigma and its nitrite-scavenging ability. Food and Bioproducts Processing, 89(4), 333-339.

Luque de Castro, M. D., & Garcia• Ayuso, L. E. (1998). Soxhlet extraction of solid materials: an outdated technique with a promising innovative future. Analytica Chimica Acta, 369(12), 1-10.

Luque de Castro, M. D., & Priego-Capote, F. (2010). Soxhlet extraction: Past and present panacea. Journal of Chromatography A, 1217(16), 2383-2389.

Madras, G. (2004). Thermodynamic modeling of the solubilities of fatty acids in supercritical fluids. Fluid Phase Equilibria, 220(2), 167-169.

Mandal, V., Mohan, Y., & Hemalatha, S. (2007). Microwave assisted extraction - An innovative and promising extraction tool for medicinal plant research. Pharmacognosy Reviews, 1(1), 7-18.

Marias, F., Letellier, S., Cezac, P., & Serin, J. P. (2011). Energetic analysis of gasification of aqueous biomass in supercritical water. Biomass and Bioenergy, 35(1), 59-73.

Martinez-Correa, H. A., Gomes, D. C. A., Kanehisa, S. L., & Cabral, F. A. (2010). Measurements and thermodynamic modeling of the solubility of squalene in supercritical carbon dioxide. Journal of Food Engineering, 96(1), 43-50.

McHugh, M. A., & Krukonis, V. J. (1994). Supercritical Fluid Extraction (2 ed.). Washington: Butterworth-Heinemam.

Mikhaeil, B. R., Badria, F. A., Maatooq, G. T., & Amer, M. M. A. (2004). Antioxidant and immunomodulatory constituents of henna leaves. Journal of biosciences, 59(7-8), 468-476

Naik, S. N., Lentz, H., & Maheshwari, R. C. (1989). Extraction of Perfumes and Flavours from Plant materials with liquid Carbon dioxide under liquid-vapor Equilibrium Conditions. Fluid Phase Equilibria, 49, 115-126.

Nei, H. Z. N., Fatemi, S., Mehrnia, M. R., & Salimi, A. (2008). Mathematical modeling and study of mass transfer parameters in supercritical fluid extraction of fatty acids from Trout powder. Biochemical Engineering Journal, 40(1), 72-78.

Okubo, M. (2005). Polymer Particles (1 ed.). The Netherlands: Springer-Verlag Berlin Heidelberg.

Oliveira, E. L. G., Silvestre, A. J. D., & Silva, C. M. (2011). Review of kinetic models for supercritical fluid extraction. Chemical Engineering Research and Design, 89(7), 1104-1117.

Otsu, J., & Oshima, Y. (2005). New approaches to the preparation of metal or metal oxide particles on the surface of porous materials using supercritical water:: Development of supercritical water impregnation method. The Journal of Supercritical Fluids, 33(1), 61-67.

Ozkal, S. G., Yener, M. E., & Bayındırlı, L. (2005). Mass transfer modeling of apricot kernel oil extraction with supercritical carbon dioxide. The Journal of Supercritical Fluids, 35(2), 119-127.

Pan, Z. Y., Bao, Z., & Chen, Y. X. (2006). Depolymerization of Poly(bisphenol A carbonate) in Subcritical

and Supercritical Toluene. Chinese Chemical Letters, 17(4), 545-548.

Papamichail, I., Louli, V., & Magoulas, K. (2000). Supercritical fluid extraction of celery seed oil. The Journal of Supercritical Fluids, 18(3), 213-226.

Park, H. S., Choi, H.-K., Lee, S. J., Park, K. W., Choi, S.-G., & Kim, K. H. (2007). Effect of mass transfer on the removal of caffeine from green tea by supercritical carbon dioxide. Journal of Supercritical Fluids 42, 205-211.

Poh, S., Hernandez, R., Inagaki, M., & Jessop, P. G. (1999). Oxidation of Phosphines by Supercritical Nitrous Oxide. Organic Letters, 1(4), 583-586.

Priya, R., Ilavenil, S., Kaleeswaran, B., Srigopalram, S., & Ravikumar, S. (2011). Effect of Lawsonia inermis on tumor expression induced by Daltons lymphoma ascites in Swiss albino mice. Saudi Journal of Biological Sciences, 18(4), 353-359.

Quesada-Medina, J., & Olivares-Carrillo, P. (2011). Evidence of thermal decomposition of fatty acid methyl esters during the synthesis of biodiesel with supercritical methanol. The Journal of Supercritical Fluids, 56(1), 56-63.

Reis-Vasco, E. M. C., Coelho, J. A. P., Palavra, A. M. F., Marrone, C., & Reverchon, E. (2000). Mathematical modelling and simulation of pennyroyal essential oil supercritical extraction. Chemical Engineering Science, 55(15), 2917-2922.

Reverchon, E. (1997). Supercritical fluid extraction and fractionation of essential oils and related products. The Journal of Supercritical Fluids, 10(1), 1-37.

Reverchon, E., Donsi, G., & Sesti Osseo, L. (1993). Modeling of supercritical fluid extraction from herbaceous matrices. Industrial & Engineering Chemistry Research, 32(11), 2721-2726.

Reverchon, E., & Marrone, C. (2001). Modeling and simulation of the supercritical CO_2 extraction of vegetable oils. Journal of Supercritical Fluids 19, 161-175.

Rezaei, K. A., & Temelli, F. (2000). Using supercritical fluid chromatography to determine diffusion coefficients of lipids in supercritical CO_2. The Journal of Supercritical Fluids, 17(1), 35-44.

Royon, D., Locatelli, S., & Gonzo, E. E. (2011). Ketalization of glycerol to solketal in supercritical acetone. The Journal of Supercritical Fluids, 58(1), 88-92.

Ruetsch, L., Daghero, J., & Mattea, M. (2003). Supercritical extraction of solid matrices. Model formulation and experiments. Latin American applied research, 33, 103-107.

Sangon, S., Ratanavaraha, S., Ngamprasertsith, S., & Prasassarakich, P. (2006). Coal liquefaction using supercritical toluenetetralin mixture in a semi-continuous reactor. Fuel Processing Technology, 87(3), 201-207.

Santiago, J. M., & Teja, A. S. (1999). The solubility of solids in supercritical fluids. Fluid Phase Equilibria, 160, 501-510.

Savage, P. E. (2009). A perspective on catalysis in sub- and supercritical water. The Journal of Supercritical Fluids, 47(3), 407-414.

Sawangkeaw, R., Bunyakiat, K., & Ngamprasertsith, S. (2009). A review of laboratory-scale research on lipid conversion to biodiesel with supercritical methanol (2001-2009). The Journal of Supercritical Fluids, 55(1), 1-13.

Shao, L., Bai, Y., Huang, X., Gao, Z., Meng, L., Huang, Y., & Ma, J. (2009). Multi-walled carbon nanotubes (MWCNTs) functionalized with amino groups by reacting with supercritical ammonia fluids. Materials Chemistry and Physics, 116(23), 323-326.

Sharma, A., & Sharma, K. (2011). Assay of Antifungal Activity of Lawsonia inermis Linn. and Eucalyptus citriodora Hook. Journal of Pharmacy Research, 4(5), 1313-1314.

Sotelo, J. L., Rodríguez, A., & .I. Águeda, P. G. (2010). Supercritical fluids as reaction media in the ethylbenzene disproportionation on ZSM-5. The Journal of Supercritical Fluids, 55(1), 241-245.

Sovova, H., Stateva, R. P., & Galushko, A. A. (2001). Essential oils from seeds: solubility of limonene in supercritical CO_2 and how it is affected by fatty oil. The Journal of Supercritical Fluids, 20(2), 113-129.

Sun, L., & Lee, H. K. (2003). Optimization of microwave-assisted extraction and supercritical fluid extraction of carbamate pesticides in soil by experimental design methodology. Journal of Chromatography A, 1014(165-177).

Taathke, P., & Y.Jaiswal (2011). An Overview of Microwave Assisted Extraction and its Application in Herbal Drug Research. Research Journal of Medicinal Plants, 5(1), 21-31.

Tan, K. T., Lee, K. T., & Mohamed, A. R. (2010). Effects of free fatty acids, water content and co-solvent on biodiesel production by supercritical methanol reaction. The Journal of Supercritical Fluids, 53(13), 88-91.

Uddin, N., Siddiqui, B. S., Begum, S., Bhatti, H. A., Khan, A., Parveen, S., & Choudhary, M. I. (2011). Bioactive flavonoids from the leaves of Lawsonia alba (Henna). Phytochemistry Letters, 4(4), 454-458.

Valerio, A., Fiametti, K. G., Rovani, S., Franceschi, E., Corazza, M. L., Treichel, H., de Oliveira, D. b., & Oliveira, J. V. (2009). Enzymatic production of mono- and

diglycerides in compressed n-butane and AOT surfactant. The Journal of Supercritical Fluids, 49(2), 216-220.

van Bennekom, J. G., Venderbosch, R. H., Assink, D., & Heeres, H. J. (2011). Reforming of methanol and glycerol in supercritical water. The Journal of Supercritical Fluids, 58(1), 99-113.

Vaquero, E. M., Beltrn, S., & Sanz, M. T. (2006). Extraction of fat from pigskin with supercritical carbon dioxide. The Journal of Supercritical Fluids, 37(2), 142-150.

Vogel, F. d. r., Blanchard, J. L. D., Marrone, P. A., Rice, S. F., Webley, P. A., Peters, W. A., Smith, K. A., & Tester, J. W. (2005). Critical review of kinetic data for the oxidation of methanol in supercritical water. The Journal of Supercritical Fluids, 34(3), 249-286.

Vogelaar, B. M., Makkee, M., & Moulijn, J. A. (1999). Applicability of supercritical water as a reaction medium for desulfurisation and demetallisation of gasoil. Fuel Processing Technology, 61(3), 265-277.

Vyalov, I., Kiselev, M., Tassaing, T., Soetens, J. C., Federov, M., Damay, P., & Idrissi, A. (2011). Reorientation relaxation in supercritical ammonia. Journal of Molecular Liquids, 159(1), 31-37.

Wang, C., Chen, W., Wang, W., Wu, Y., Chi, R., & Tang, Z. (2011). Experimental study on methanol recovery through flashing vaporation in continuous production of biodiesel via supercritical methanol. Energy Conversion and Management, 52(2), 1454-1458.

Wang, J., Chen, J., & Yang, Y. (2004). Solubility of titanocene dichloride in supercritical propane. Fluid Phase Equilibria, 220(2), 147-151.

Wang, S., Bonrath, W., Pauling, H., & Kienzle, F. (2000). The synthesis of d,l-tocopherol in supercritical media. The Journal of Supercritical Fluids, 17(2), 135-143.

Wang, S., Karpf, M., & Kienzle, F. (1999). Ammonolysis with supercritical NH_3. The Journal of Supercritical Fluids, 15(2), 157-164.

Wong, K. C., & Tong, Y. E. (1995). Volatile components of lawsonia inermis L. flowers. Journal of essential oils research, 7, 425-428.

Yazdizadeh, M., Eslamimanesh, A., & Esmaeilzadeh, F. (2011). Thermodynamic modeling of solubilities of various solid compounds in supercritical carbon dioxide: Effects of equations of state and mixing rules. The Journal of Supercritical Fluids, 55(3), 861-875.

Yeo, S.-D., & Kiran, E. (2005). Formation of polymer particles with supercritical fluids: A review. The Journal of Supercritical Fluids, 34(3), 287-308.

Yoneyama, Y., Sun, X., Zhao, T., Wang, T., Iwai, T., Ozaki, K., & Tsubaki, N. (2009). Direct synthesis of isoparaffin from synthesis gas under supercritical conditions. Catalysis Today, 149(12), 105-110.

Yoshida, T., Oshima, Y., & Matsumura, Y. (2004). Gasification of biomass model compounds and real biomass in supercritical water. Biomass and Bioenergy, 26(1), 71-78.

Zhang, P., Huang, Y., Shen, B., & Wang, R. Z. (2011). Flow and heat transfer characteristics of supercritical nitrogen in a vertical mini-tube. International Journal of Thermal Sciences, 50(3), 287-295.

Zheng, Q. X., Li, B., Xue, M., Zhang, H. D., Zhan, Y. J., Pang, W. S., Tao, X. T., & Jiang, M. H. (2008). Synthesis of YVO_4 and rare earth-doped YVO4 ultra-fine particles in supercritical water. The Journal of Supercritical Fluids, 46(2), 123-128.

Zhou, C., Wang, C., Wang, W., Wu, Y., Yu, F., Chi, R. a., & Zhang, J. (2010). Continuous Production of Biodiesel from Soybean Oil Using Supercritical Methanol in a Vertical Tubular Reactor: 1. Phase Holdup and Distribution of Intermediate Product along the Axial Direction. Chinese Journal of Chemical Engineering, 18(4), 626-629.

Zhuang, M. S., & Thies, M. C. (1999). Extraction of Petroleum Pitch with Supercritical Toluene: Experiment and Prediction. Energy & Fuels, 14(1), 70-75.

9 APPENDICES

Appendix A

Experimental data of SFE of volatile components from flower of henna

This section includes the values of extraction yields for each run that were obtained experimentally and mathematically at each extraction condition.

35 °C and 80 bar

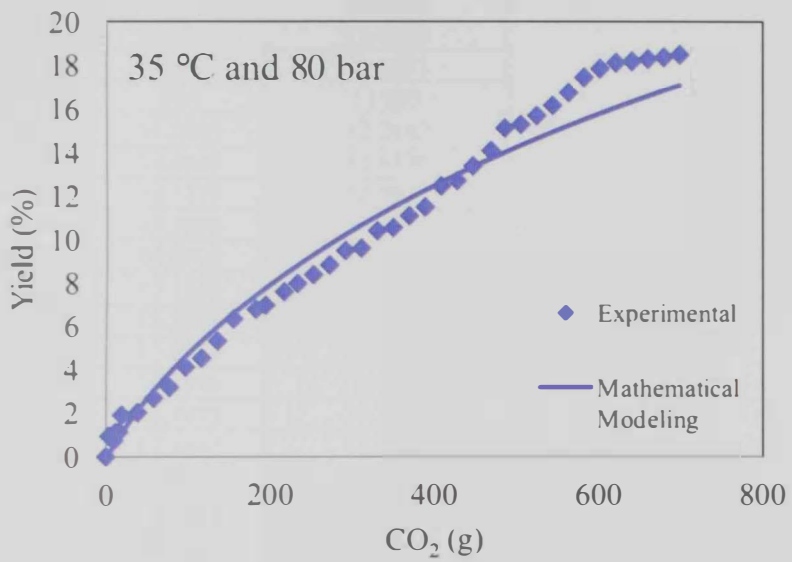

CO_2 g	% Y_{exp}	% Y_{cal}
0	0	0
3.8832	0.94119	0.13012
9.85556	0.74199	0.51273
11.6496	1 10552	0.62474
15.5328	1.13042	0.85989
19.416	1.90728	1.08612
38.832	2 02679	2.11617
58.248	2.68413	3.02577
77.664	3.17713	3.85056
97.08	4 11334	4.61004
116.496	4.52169	5.31666
135.912	5.31846	5.97904
155.328	6.33435	6.60353
182.51	6.78253	7.42322
194.16	6.97176	7.75727
216.683	7.58926	8.37701
232.992	7.97271	8.80614
252.408	8.38106	9.29743
271.824	8.83422	9.76918
291.24	9.49156	10.223
310.656	9.60112	10.6601
330.072	10.4029	11.0818
349.488	10.5473	11.4891
368.904	11.1	11.883
388.32	11.5034	12.2642
407.736	12.4645	12.6336
427.152	12.7135	12.9917
446.568	13.3858	13.3393
468.314	14.0929	13.7167
485.4	15.1188	14.0048
504.816	15.2881	14.3237
524.232	15.6964	14.634
543.648	16.1596	14.936
563.064	16.7472	15.2301
582.48	17.4643	15.5167
601.896	17.8577	15.796
621.312	18.1216	16.0684
640.728	18.1863	16.3342
660.144	18.2909	16.5935
679.56	18.3656	16.8466
698.976	18.4802	17.0938

35 °C and 100 bar

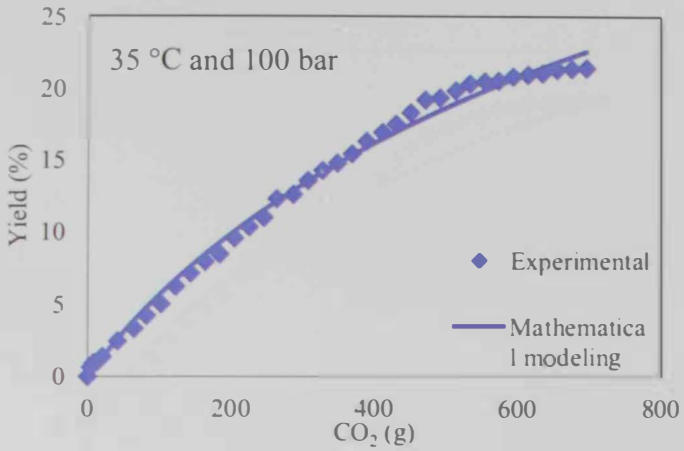

CO_2 (g)	% Y_{exp}	% Y_{cal}
0	0	0
4.08815	0.6331	0.15841
8.1763	0.9322	0.45262
13.8997	1.05683	0.85095
20.4408	1.3659	1.28566
41.6991	2.44267	2.59119
64.5928	3.31007	3.86637
81.763	4.21236	4.75634
102.204	5.00997	5.75564
122.645	6.21137	6.69921
143.085	7.1336	7.59451
163.526	7.93619	8.44718
183.967	8.44965	9.26166
204.408	9.56132	10.0415
224.848	10.329	10.7898
245.289	10.987	11.5089
263.277	12.2931	12.1193
286.171	12.5972	12.8681
306.611	13.5593	13.5116
327.052	14.2722	14.133
347.493	14.7856	14.7337
367.934	15.4287	15.3147
388.374	16.3011	15.8771
410.45	16.9292	16.4646
429.256	17.5025	16.9496
449.697	18.2901	17.4613
470.137	19.1874	17.9578
490.578	19.332	18.4395
512.409	19.8355	18.9384
532.277	20.319	19.3791
553.127	20.4786	19.8283
572.341	20.5284	20.2308
592.782	20.8225	20.6473
613.223	20.9472	21.0522
633.663	21.0518	21.4459
654.104	21.2961	21.8287
674.545	21.3659	22.2011
694.986	21.4307	22.5633

35 °C and 120 bar

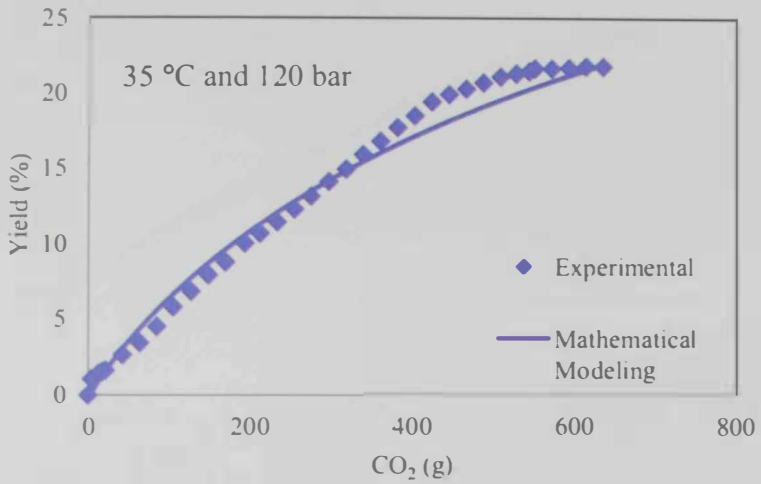

CO_2 g	% Y_{exp}	% Y_{cal}
0	0	0
4.22735	1.06107	0.19915
9.30017	1.18063	0.63856
12.6821	1.41477	0.91757
16.9094	1.52436	1.25305
21.1368	1.63894	1.57622
42.2735	2.66514	3.05587
63.4103	3.45223	4.37269
84.547	4.51828	5.57233
104.838	5.80353	6.63693
126.821	6.81977	7.71074
147.957	7.91073	8.67678
169.094	8.75262	9.58621
192.767	9.99801	10.5456
211.368	10.6556	11.26
232.504	11.4078	12.0338
253.641	12.2596	12.7707
273.932	13.1165	13.446
295.915	14.0879	14.1449
317.051	14.9148	14.7871
338.188	15.8862	15.4022
359.325	16.7729	15.9918
380.462	17.6796	16.5576
401.598	18.4617	17.1008
422.735	19.3982	17.6228
443.872	19.8864	18.1247
465.009	20.2551	18.6075
486.145	20.6685	19.0722
507.282	21.0621	19.5196
526.728	21.2713	19.9166
542.792	21.4307	20.2346
549.556	21.62	20.3658
570.692	21.62	20.766
591.829	21.6599	21.1518
612.966	21.7695	21.5238
634.103	21.7595	21.8826

45 °C and 80 bar

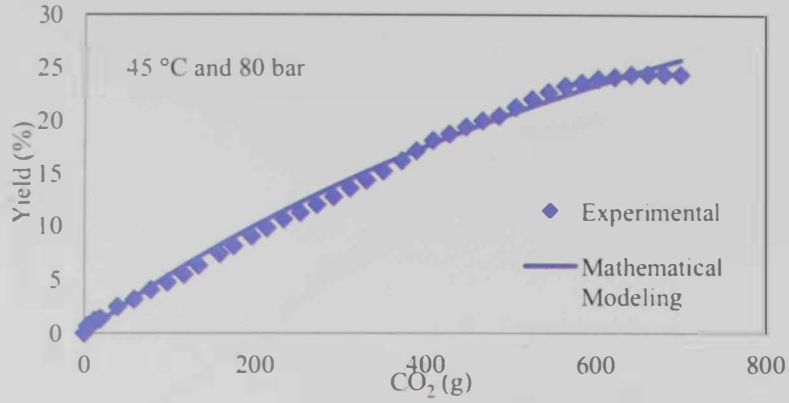

CO_2 g	% Y_{exp}	% Y_{cal}
0	0	0
3.8832	0.70247	0.13127
9.31968	0.86688	0.47518
11.6496	1.15584	0.62009
16.3094	1.27043	0.90564
19.416	1.36509	1.09322
38.832	2.48107	2.22518
58.248	3.16361	3.30171
77.664	4.05042	4.33378
97.08	4.77282	5.32772
116.496	5.5002	6.28778
133.582	6.34217	7.10711
158.435	7.43822	8.25969
174.744	8.17557	8.99257
195.713	9.0823	9.90925
213.576	9.87445	10.6686
232.992	10.7065	11.4726
252.408	11.3242	12.2553
271.824	12.0815	13.0176
291.24	12.8189	13.7604
310.656	13.6309	14.4843
330.072	14.3882	15.19
349.488	15.2551	15.8781
371.234	16.2216	16.6287
388.32	17.1682	17.2038
407.736	18.1397	17.8424
427.152	18.7625	18.4654
446.568	19.4251	19.0733
465.984	20.008	19.6664
485.4	20.4813	20.2452
504.816	21.2983	20.8101
524.232	22.0506	21.3613
543.648	22.7232	21.8994
563.064	23.321	22.4245
582.48	23.6299	22.937
601.896	23.9886	23.4372
621.312	24.163	23.9255
640.728	24.3922	24.4021
660.144	24.4271	24.8673
679.56	24.437	25.3214
698.976	24.4071	25.7646

45 °C and 100 bar

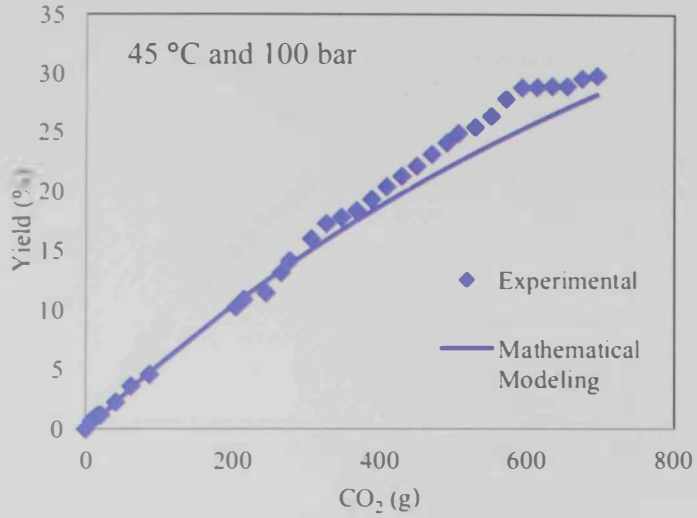

CO_2 (g)	% Y_{exp}	% Y_{cal}
0	0	0
8.1763	0.71325	0.2842
12.2645	0.93271	0.53151
16.3526	1.13223	0.77855
20.4408	1.1821	1.02352
40.8815	2.26944	2.21752
61.3223	3.6311	3.36835
86.6688	4.6137	4.74577
204.408	10.2649	10.5836
215.037	10.9033	11.072
245.289	11.4519	12.4308
265.73	13.1528	13.3238
277.177	14.1453	13.8152
306.611	16.0158	15.0516
327.052	17.2876	15.8875
347.493	17.8163	16.7055
367.934	18.385	17.5059
388.374	19.3376	18.2893
408.815	20.4	19.0559
429.256	21.2878	19.8063
449.697	22.1457	20.5407
470.137	23.1483	21.2595
490.578	24.1259	21.9631
506.113	24.9339	22.4879
529.824	25.4576	23.2726
551.9	26.3604	23.9858
572.341	27.8318	24.6318
592.782	28.8294	25.264
613.223	28.8543	25.8829
633.663	28.9491	26.4888
654.104	28.9391	27.0818
674.545	29.5925	27.6623
694.986	29.8319	28.2306

45 °C and 120 bar

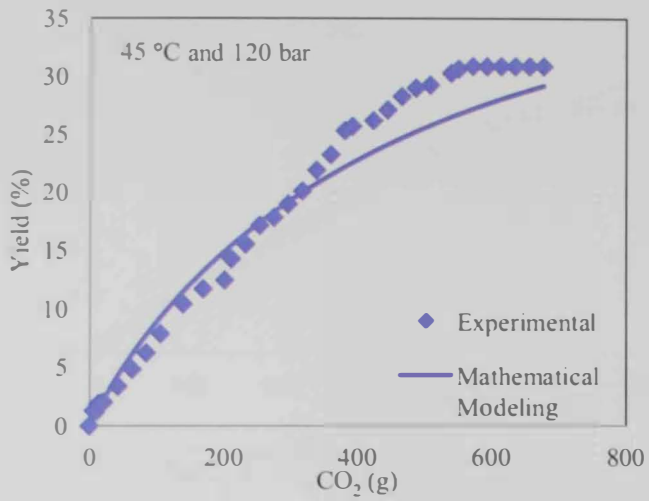

CO_2 g	% Y_{exp}	% Y_{cal}
0	0	0
5.91829	1.29715	0.49525
8.4547	1.14748	0.804
12.6821	1.87088	1.29932
16.9094	1.94572	1.77279
21.1368	2.02055	2.22804
42.2735	3.38256	4.30077
63.4103	4 84434	6.12902
84.547	6.24626	7.78103
105.684	7.88266	9.29422
139.503	10.4271	11.484
169.094	11.7242	13.2093
201.222	12.4726	14.9161
211.368	14.2836	15.4233
232.504	15.5508	16.4358
253.641	17.1622	17.3928
274.778	17.8408	18.299
295.915	18.9832	19.1582
317.051	20.1207	19.9738
338.188	21.9118	20.7488
359.325	23.2389	21.4859
380.462	25.3143	22.1874
391.453	25.6935	22.5389
422.735	26.1824	23.4921
443.872	27.0904	24 0989
465.009	28.2628	24.6775
486.145	28.9862	25.2294
507.282	29.2556	25.7561
538.564	30.2934	26.4918
549.556	30.6476	26.7385
570.692	30.8821	27.1966
591.829	30.8571	27.6339
612.966	30.8821	28.0516
634.103	30.8721	28.4505
655.239	30.8821	28.8316
676.376	30.8821	29.1955

55 °C and 80 bar

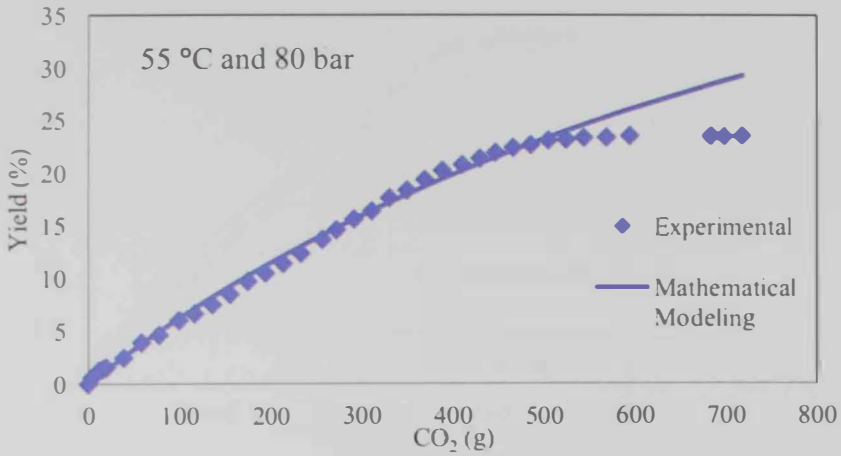

CO_2 (g)	% Y_{exp}	% Y_{cal}
0	0	0
3.8832	0.60709	0.15138
7.7664	0 90565	0.42975
11.6496	1.249	0.70395
15.5328	1.37838	0.97362
19.416	1.54757	1.23936
38.832	2.4582	2.52052
58.248	3.88635	3.73863
77.664	4.60788	4.90589
99.4099	5.98627	6.16147
116.496	6.60828	7.1138
135.912	7.4791	8.1627
155.328	8.44447	9.17877
174 744	9.66361	10.1642
194.16	10.4399	11.1208
213.576	11.3406	12.05
232.992	12.3109	12.9533
256.291	13.6246	14.0044
271.824	14.5253	14.6862
291.24	15.5603	15.5177
310.656	16.3266	16.3272
330.072	17.5707	17.1154
349.488	18.3021	17.8828
368.904	19.3173	18.6303
388.32	20.1732	19.3584
410.066	20.7454	20.1515
429.482	21.3376	20.8403
446.568	21.9098	21.4317
465.984	22.3726	22.0876
485.4	22.6363	22.7267
504.816	23.0693	23.3495
524.232	23.1389	23.9563
543.648	23.3181	24.5476
568.5	23.3479	25.2826
594.13	23.4972	26.0154
684.22	23.5569	28.4023
698.976	23.5271	28.7667
718.392	23.5768	29.2355

55 °C and 100 bar

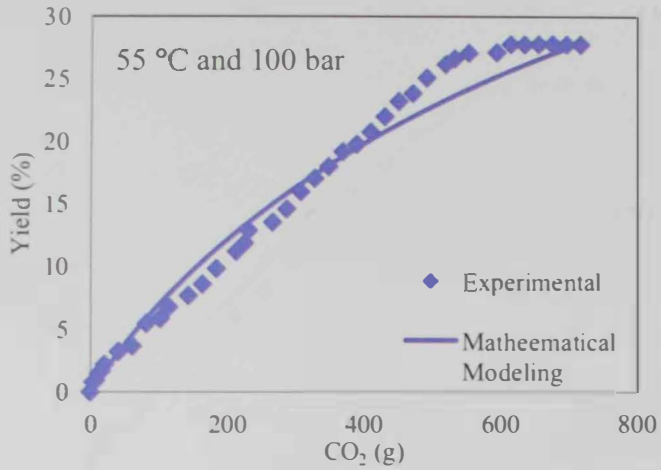

CO_2 (g)	% Y_{exp}	% Y_{cal}
0	0	0
4.08815	0.78854	0.19453
8.1763	0.93826	0.55102
12.2645	1.44732	0.89976
16.3526	1.68688	1.23798
20.4408	2.17597	1.56711
40.8815	3.20407	3.10737
61.3223	3.64825	4.51565
81.763	5.43495	5.82469
102.204	5.80925	7.05312
114.468	6.73754	7.75677
143.085	7.65085	9.31396
163.526	8.55917	10.362
183.967	9.79688	11.3626
212.584	11.1643	12.6919
224.848	11.8231	13.2382
230.572	12.8462	13.4886
265.73	13.505	14.9676
286.171	14.568	15.7838
306.611	15.9455	16.5703
327.052	17.0185	17.329
347.493	17.9668	18.0614
367.934	19.1645	18.7689
388.374	19.7535	19.4528
408.815	20.7416	20.1141
429.256	21.9694	20.754
449.697	23.1971	21.3735
470.137	23.8309	21.9733
490.578	25.0786	22.5543
518.377	26.1666	23.3158
531.46	26.6307	23.6631
551.9	27.0799	24.1921
592.782	27.1348	25.2027
613.223	27.7936	25.6853
633.663	27.7736	26.1536
654.104	27.7886	26.608
674.545	27.8036	27.0489
694.986	27.7886	27.4769
715.426	27.7786	27.8923

55 °C and 120 bar

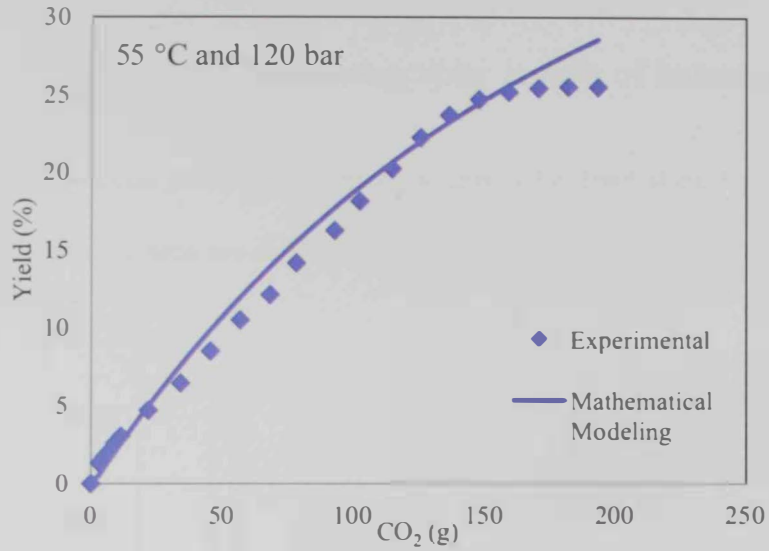

CO_2 g	% Y_{exp}	% Y_{cal}
0	0	0
3.1829	1.327677	0.541789
5.0017	1.707013	1.003844
6.8205	2.066384	1.457106
9.094	2.600449	2.013066
11.3675	3.039681	2.558561
21.8256	4.696781	4.954133
34.1025	6.443723	7.564377
45.47	8.485151	9.811672
56.8375	10.47667	11.91037
68.205	12.09384	13.8712
78.2084	14.13027	15.49012
92.7588	16.22161	17.67913
102.3075	18.11829	19.0159
114.5844	20.20464	20.62656
125.4972	22.2261	21.96263
136.41	23.66858	23.21459
147.7775	24.6868	24.43499
159.145	25.16596	25.57547
170.5125	25.41552	26.64127
181.88	25.51036	27.63728
193.2475	25.50537	28.56806

Appendix B

Gas Chromatography results of henna flower extracts

This section presents the chromatogram of extract at each condition obtained by GC. The chromatograms are shown in the following figures:

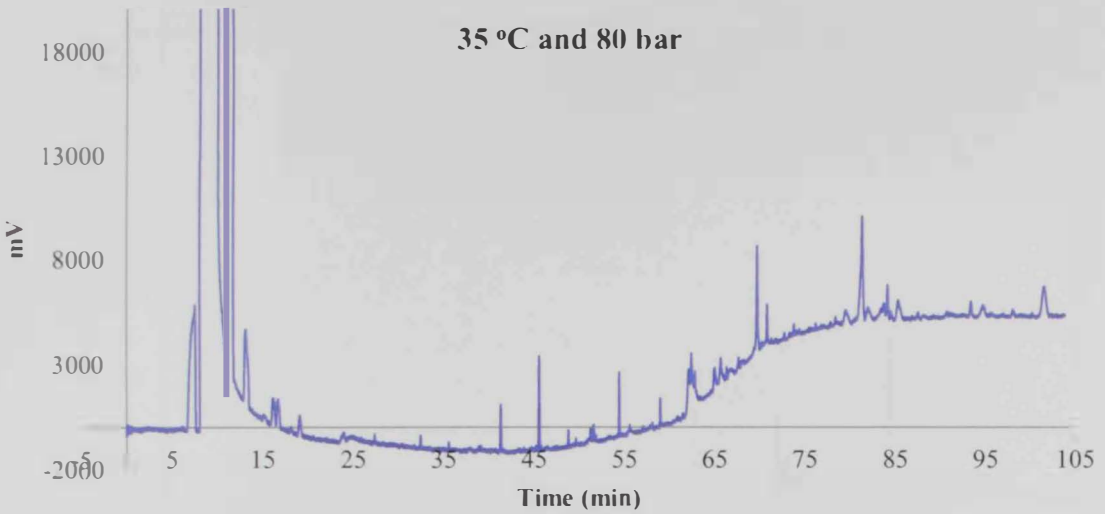

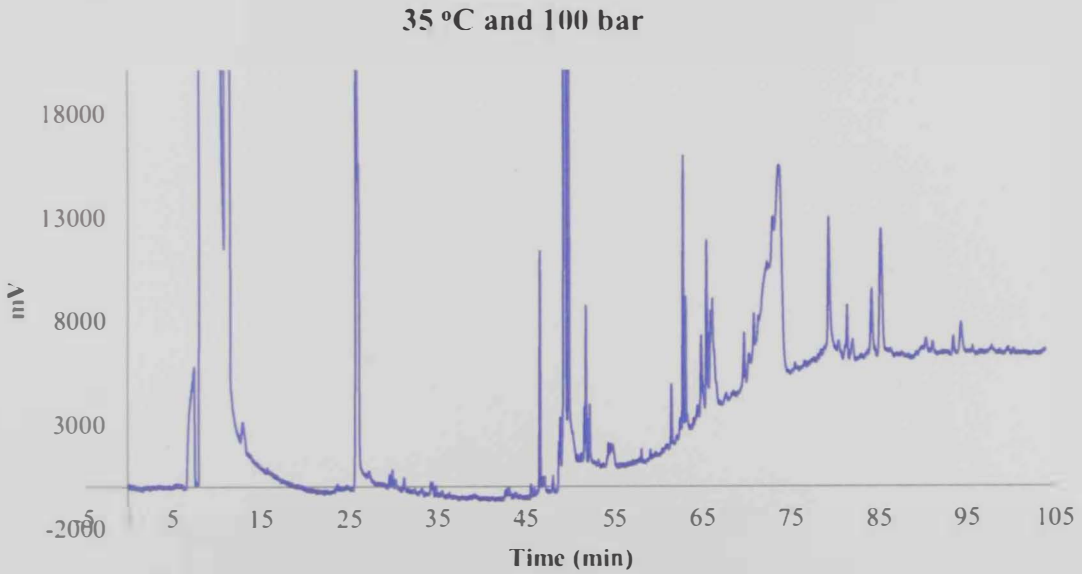

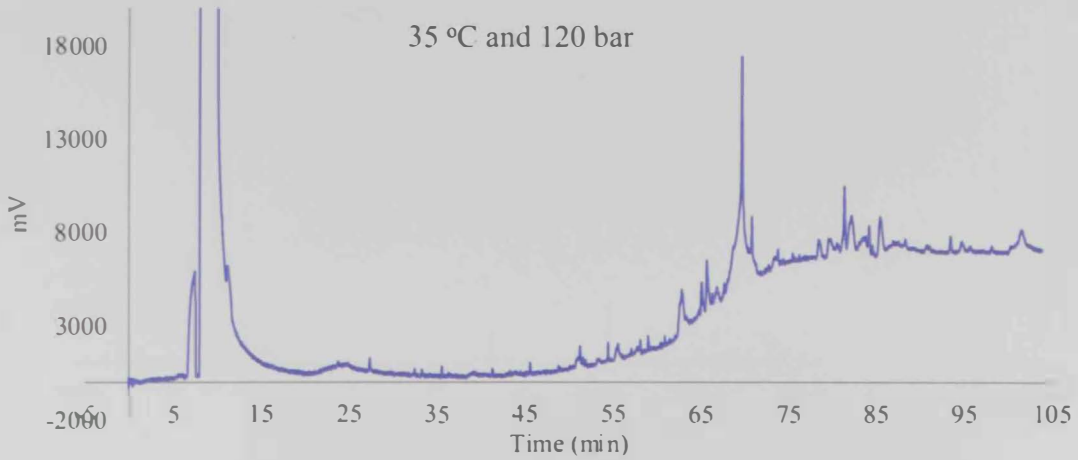
35 °C and 120 bar
18000
13000
8000
3000
-2000
mV
5
15
25
35
45
55
65
75
85
95
105
Time (min)

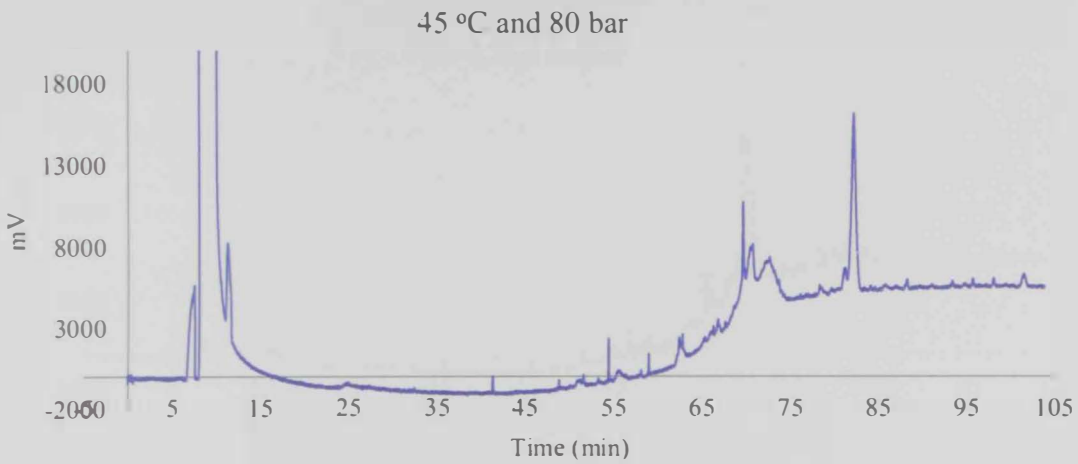
45 °C and 80 bar
18000
13000
8000
3000
-2000
mV
5
15
25
35
45
55
65
75
85
95
105
Time (min)

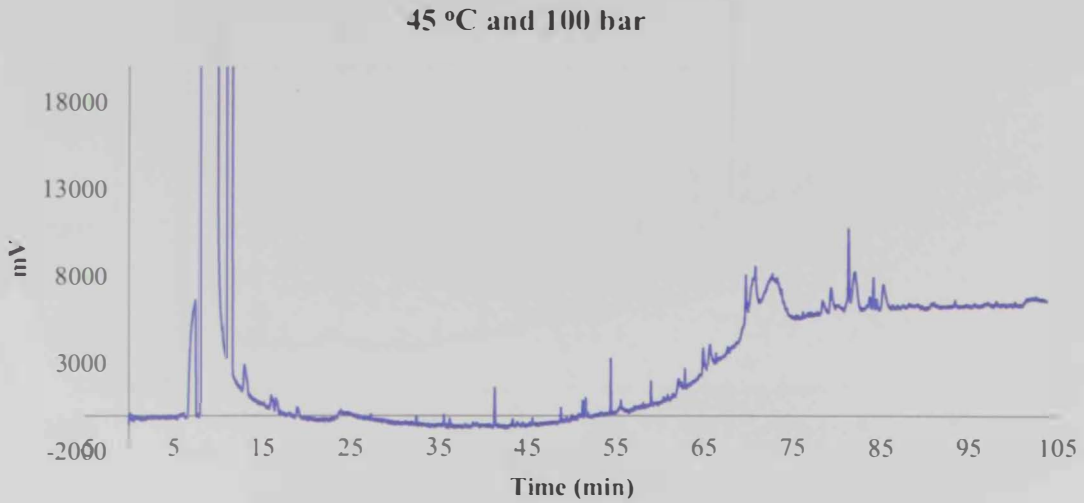
45 °C and 100 bar
18000
13000
8000
3000
-2000
mV
5
15
25
35
45
55
65
75
85
95
105
Time (min)

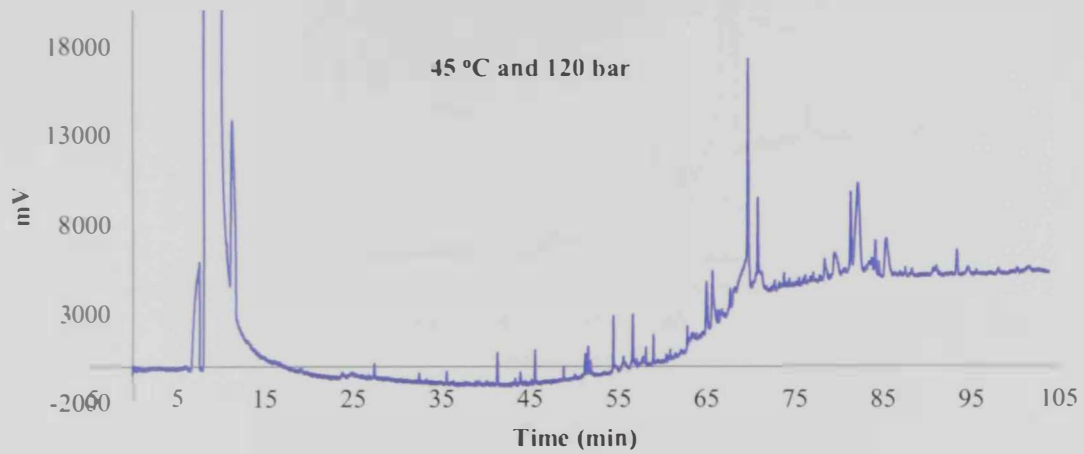
45 °C and 120 bar
18000
13000
8000
3000
-2000
mV
5
15
25
35
45
55
65
75
85
95
105
Time (min)

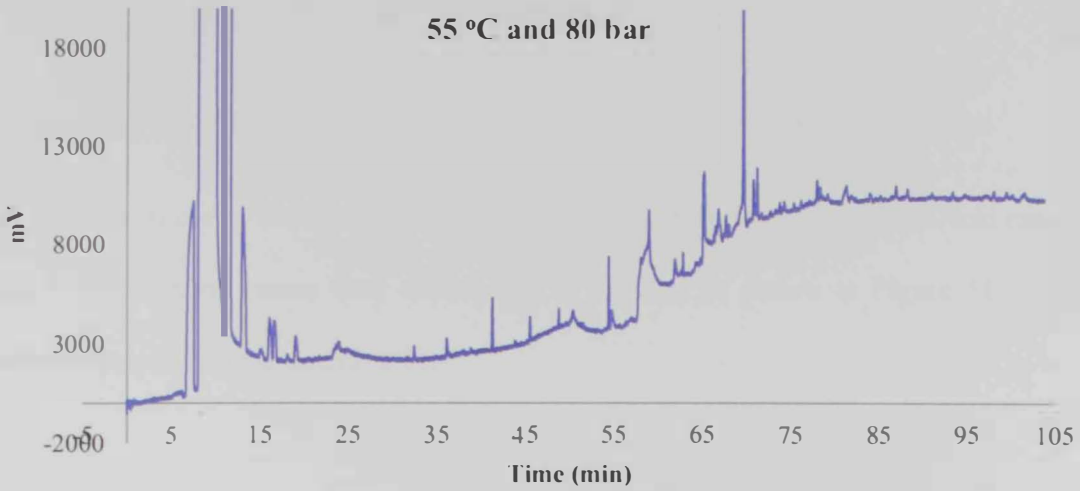
55 °C and 80 bar
18000
13000
8000
3000
-2000
mV
5
15
25
35
45
55
65
75
85
95
105
Time (min)

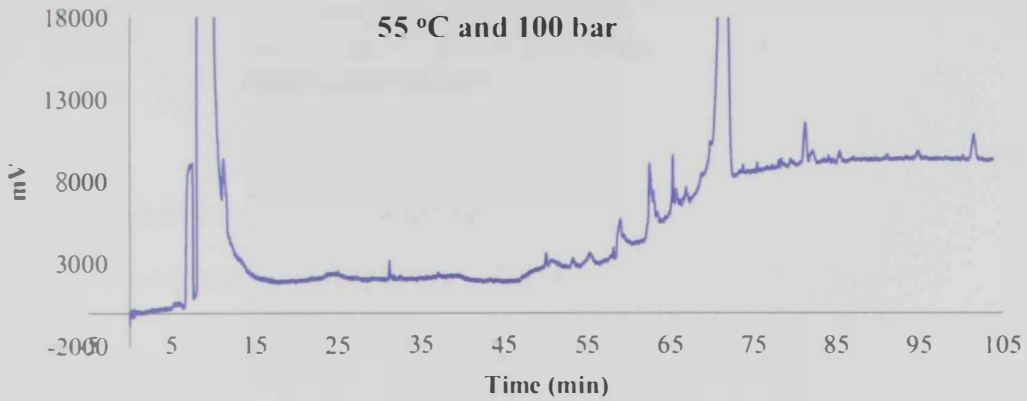
55 °C and 100 bar
18000
13000
8000
3000
-2000
mV
5
15
25
35
45
55
65
75
85
95
105
Time (min)

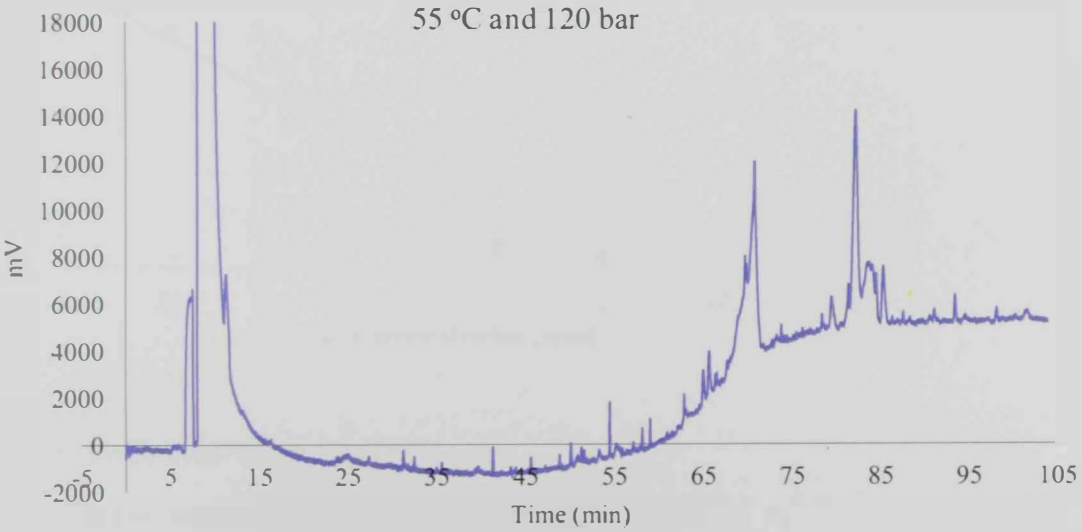
55 °C and 120 bar
18000
16000
14000
12000
10000
8000
6000
4000
2000
0
-2000
mV
5
15
25
35
45
55
65
75
85
95
105
Time (min)

Appendix C

This section presents the calibration curves obtained for FRAP and DPPH assays.

The calibration curve was prepared by plotting concentrations of Ascorbic Acid ranging from 0 to 100 ppm versus their absorbance at 539 nm as shown in Figure 31 and the calibration equation was found to be:

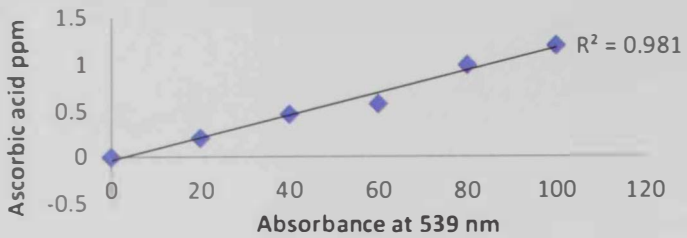

Figure 31 Calibration curve for FRAP assay

$$Concentration\ (ppm) = 0.0121\ Abs - 0.0342$$

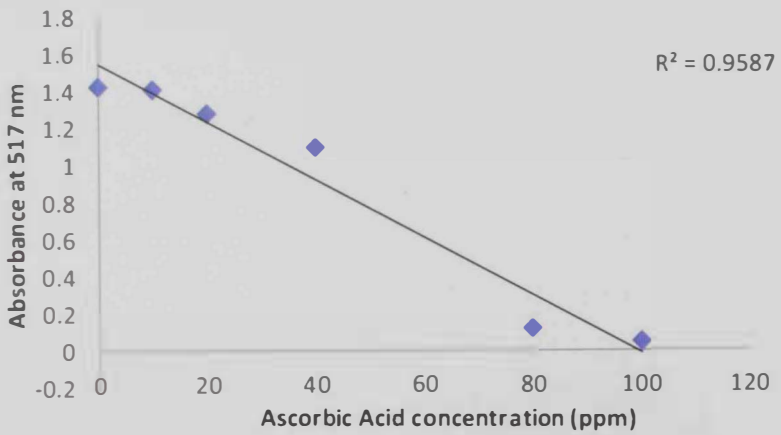

Figure 32 Calibration curve for DPPH assay

$$Absorbance = -0.0156\ concentration\ (ppm) + 1.5474$$

Appendix D

Solution to the model equations

In the particle phase:

Recalling equations 32 and 28:

$$\frac{\partial C_p}{\partial t} = \frac{D_e}{r^2}\left[2r\frac{\partial C_p}{\partial r} + r^2\frac{\partial^2 C_p}{\partial r^2}\right] - \frac{(1-\varepsilon_p)}{\varepsilon_p}\frac{\partial q}{\partial t} \tag{32}$$

$$\frac{\partial q}{\partial t} = -k_a\left(C_p - \frac{q}{K}\right) \tag{28}$$

let n and k present the time and radius domains respectively,

$$\frac{\partial C_p}{\partial t} = \frac{C_{p\,k,n+t} - C_{p\,k,n}}{\Delta t}$$

$$\frac{\partial C_p}{\partial r} = \frac{C_{p\,k+1,n} - C_{p\,k-1,n}}{2\Delta r}$$

$$\frac{\partial^2 C_p}{\partial r^2} = \frac{C_{p\,k+1,n} - 2C_{p\,k,n} + C_{p\,k-1,n}}{\Delta r^2}$$

Starting with Equation 28:

$$\frac{\partial q}{\partial t} = \frac{q_{\,k,n+t} - q_{\,k,n}}{\Delta t}$$

$$\frac{q_{\,k,n+t} - q_{\,k,n}}{\Delta t} = k_a\left(C_{p\,k,n} - \frac{q_{\,k,n}}{K}\right)$$

Rearranging yields

$$q_{\,k,n+t} = q_{\,k,n}\left(1 - \Delta t\frac{k_a}{K}\right) + \Delta t k_a C_{p\,k,n} \tag{36}$$

Equation 32 can be rearranged and converted to finite elements as follows:

$$\frac{\partial C_P}{\partial t} = \frac{D_e}{r^2}\left[2r\frac{\partial C_P}{\partial r} + r^2\frac{\partial^2 C_P}{\partial r^2}\right] - \frac{(1-\varepsilon_P)}{\varepsilon_P}\frac{\partial q}{\partial t}$$

$$\frac{D_e}{r^2}\left[2r\frac{dC_p}{dr} + r^2\frac{d^2 C_p}{dr^2}\right] - \frac{(1-\varepsilon_p)}{\varepsilon_p}\frac{dq}{dt} = \frac{dC_p}{dt}$$

$$\frac{C_{p\,k,n+t} - C_{p\,k,n}}{\Delta t} = \frac{2D_e}{k\Delta r}\left(\frac{C_{p\,k+1,n} - C_{p\,k-1,n}}{2\Delta r}\right) + D_e\frac{C_{p\,k+1,n} - 2C_{p\,k,n} + C_{p\,k-1,n}}{\Delta r^2} - \frac{(1-\varepsilon_p)}{\varepsilon_p}\frac{q_{k,n+t} - q_{k,n}}{\Delta t}$$

Rearranging results

$$C_{p\,k,n+t} = C_{p\,k,n} + \frac{2D_e}{k\Delta r^2}\left(C_{p\,k+1,n} - C_{p\,k-1,n}\right) + \frac{\Delta t D_e}{\Delta r^2}\left(C_{p\,k+1,n} - 2C_{p\,k,n} + C_{p\,k-1,n}\right) - \frac{(1-\varepsilon_p)}{\varepsilon_p}\left(q_{k,n+t} - q_{k,n}\right)$$

Substituting with $q_{k,n+t}$ from equation 36:

$$C_{p\,k,n+t} = \left(1 - \frac{2\Delta t D_e}{\Delta r^2} - \frac{(1-\varepsilon_p)}{\varepsilon_p}\Delta t k_a\right)C_{p\,k,n} + \left(\frac{\Delta t D_e}{\Delta r^2} - \frac{\Delta t D_e}{k\Delta r^2}\right)C_{p\,k-1,n} + \left(\frac{\Delta t D_e}{k\Delta r^2} + \frac{\Delta t D_e}{\Delta r^2}\right)C_{p\,k+1,n} + \frac{(1-\varepsilon_p)}{\varepsilon_p}\Delta t\frac{k_a}{K}q_{k,n}$$

Defining

$$M_1 = \frac{\Delta t D_e}{\Delta r^2},\ M_2 = \frac{(1-\varepsilon_p)}{\varepsilon_p}\Delta t k_a$$

$$C_{p\,k,n+t} = (1 - 2M_1 - M_2)C_{p\,k,n} + \left(M_1 - \frac{M_1}{k}\right)C_{p\,k-1,n} + \left(\frac{M_1}{k} + M_1\right)C_{p\,k+1,n} + \frac{M_2}{K}q_{k,n} \qquad (37)$$

The following criteria should be taken into account to ensure realistic physical results:

a) $(1 - 2M_1 - M_2) > 0$

$$\left(1 - \frac{2\Delta t D_e}{\Delta r^2} - \frac{(1-\varepsilon_p)}{\varepsilon_p}\Delta t k_a\right) > 0$$

$$1 > \frac{2\Delta t D_e}{\Delta r^2} + \frac{(1-\varepsilon_p)}{\varepsilon_p}\Delta t k_a$$

Hence,

$$\Delta t < \frac{1}{\frac{2D_e}{\Delta r^2}+\frac{(1-\varepsilon_p)}{\varepsilon_p}k_a}$$

b) $M_1 - \frac{M_1}{k} > 0$

$k > 1$

The initial and boundary conditions:

$at\ n = 0\ ;\ C_p = C_{po}\ ,\ q = q_o$

$at\ k = 0\ ;\ \frac{\partial C_p}{\partial r} = 0 = \frac{C_{p\,k+1,n} - C_{p\,k-1,n}}{2\Delta r}$

$hence\ C_{p\,k+1,n} = C_{p\,k-1,n}$

$\frac{\partial q}{\partial r} = 0 = \frac{q_{\,k+1,n} - q_{\,k,n}}{\Delta r}$

$therefore,\ q_{\,k+1,n} = q_{\,k,n}$

$at\ k = R\ ;$

$\because -D_e \frac{\partial C_p}{\partial r} = k_f a\left(C_{pR} - C\right)$

$\therefore -D_e \frac{C_{p\,R+1,n} - C_{p\,R,n}}{\Delta r} = k_f a\left(C_{pR,n} - C_{m,n}\right)$

$C_{p\,R+1,n} = -\frac{k_f a \Delta r}{D_e}\left(C_{pR,n} - C_{m,n}\right) + C_{pR,n}$

In the fluid phase:

Recalling Equation 35:

$$D_{ax}\frac{\partial^2 C}{\partial z^2} - \vartheta_i \frac{\partial C}{\partial z} + \frac{(1-\varepsilon_b)}{\varepsilon_b} k_f a\left(C_{pR} - C\right) = \frac{\partial C}{\partial t} \qquad (35)$$

let m presents the z domain

$$\frac{\partial C}{\partial t} = \frac{C_{m,n+1} - C_{m,n}}{\Delta t}$$

$$\frac{\partial C}{\partial z} = \frac{C_{m+1,n} - C_{m-1,n}}{2\Delta z}$$

$$\frac{\partial^2 C}{\partial z^2} = \frac{C_{m+1,n} - 2C_{m,n} + C_{m-1,n}}{\Delta z^2}$$

Substituting into Equation 35:

$$D_{ax}\left(\frac{C_{m+1,n} - 2C_{m,n} + C_{m-1,n}}{\Delta z^2}\right) - \vartheta_i\left(\frac{C_{m+1,n} - C_{m-1,n}}{2\Delta z}\right) + \frac{(1-\varepsilon_b)}{\varepsilon_b} k_f a\left(C_{pR,n} - C_{m,n}\right) = \frac{C_{m,n+1} - C_{m,n}}{\Delta t}$$

Rearranging yields:

$$C_{m,n+1} = \left(\frac{D_{ax}}{\Delta z^2} - \frac{\vartheta_i}{2\Delta z}\right)\Delta t C_{m+1,n} + \left(1 - \frac{(1-\varepsilon_b)}{\varepsilon_b} k_f a \Delta t - \frac{2D_{ax}}{\Delta z^2}\Delta t\right) C_{m,n} + \left(\frac{D_{ax}}{\Delta z^2} + \frac{\vartheta_i}{2\Delta z}\right)\Delta t C_{m-1,n} + \frac{(1-\varepsilon_b)}{\varepsilon_b} k_f a \Delta t C_{pR,n}$$

Defining $M_3 = \frac{D_{ax}}{\Delta z^2}$, $M_4 = -\frac{\vartheta_i}{2\Delta z}$, *and* $M_5 = \frac{(1-\varepsilon_b)}{\varepsilon_b} k_f a$

$$C_{m,n+1} = (M_3 + M_4)\Delta t C_{m+1,n} + (1 - M_5\Delta t - 2M_3\Delta t) C_{m,n} + (M_3 - M_4)\Delta t C_{m-1,n} + M_5 \Delta t C_{pR,n} \quad (38)$$

The following criteria should be valid for realistic results:

a) $M_3 + M_4 > 0$, $\frac{D_{ax}}{\Delta z^2} - \frac{\vartheta_i}{2\Delta z} > 0$

therefore $\Delta z < \frac{2D_{ax}}{\vartheta_i}$

b) $(1 - M_5\Delta t - 2M_3\Delta t) > 0$

$$\Delta t < \frac{1}{M_5 + 2M_3}$$

$$\Delta t < \frac{1}{\frac{(1-\varepsilon_b)}{\varepsilon_b} k_f a + 2\frac{D_{ax}}{\Delta z^2}}$$

Initial and boundary conditions:

$at\ n = 0; C = 0$

$at\ m = 0; C = 0$

$at\ m = L;$

$\frac{\partial C}{\partial z} = 0 = \frac{C_{m+1,n} - C_{m,n}}{\Delta z}$

$hence,\ C_{m+1,n} = C_{m,n}$

Excel Visual Basic Application Macro (VBA-Macro) Code

This section includes the code that was written in Excel VBA-Macro for mathematical modeling of SFE from henna flowers.

The code is as follows:

```
        Public pcom(50), xicom(50), ncom
Function FUNC(x)
Dim c(1001), c1(1001), Y(10000000), t(10000000), q1(151), cp1(151),
cp(151), q(151), texp(100), yexp(100), ycal(100)
Dim nt As Long, nz As Long, nr As Integer

fo = Worksheets("visual basic").Range("c36").Value
Minf = Worksheets("visual basic").Range("c37").Value
D12 = Worksheets("visual basic").Range("c57").Value
Dax = Worksheets("visual basic").Range("c61").Value
ep = Worksheets("visual basic").Range("c8").Value
F = Worksheets("visual basic").Range("c26").Value
density = Worksheets("visual basic").Range("c41").Value
Msample = Worksheets("visual basic").Range("c30").Value
ibn = Worksheets("visual basic").Range("n43").Value
Ndat = ibn

De = Abs(x(1)) * 0.000000000001
kf = Abs(x(2)) * 0.00000001
k = Abs(x(3))
ka = Abs(x(4))

For ib = 0 To ibn
texp(ib) = Worksheets("visual basic").Cells(5 + ib, 15).Value
yexp(ib) = Worksheets("visual basic").Cells(5 + ib, 17).Value
Next ib

ib = 1

dp = 0.000504
rp = dp / 2#
r = rp

L = 0.05
D = 0.016
pi1 = 3.141592654
a = pi1 * (D ^ 2) / 4#
us = F / (density * a)
porosity = 0.5
ui = us / porosity
Mo = 0.000619

co = 0
qo = (1 - fo) * Mo / (a * L * (1 - porosity) * (1 - ep))
```

```
Cpo = fo * Mo / (a * L * (1 - porosity) * ep)

tf = 60000
nr = 20
dr = r / nr

Worksheets("visual basic").Range("A100:B101").ClearContents
Worksheets("visual basic").Range("DC118:DE3000").ClearContents

dzmax = 2# * Dax / ui
dz = dzmax - (dzmax / 10)
nz = CLng(L / dz)
stepdr:
dtmax1 = 1# / (2# * Dax / (dz ^ 2#) + 3# * kf * (1# - porosity) / (rp *
porosity))
dtmax2 = 1# / ((2 * De / (ep * (dr ^ 2)) + (1 - ep) * ka / ep))
dtmax3 = k / ka
If dtmax1 < dtmax2 And dtmax1 < dtmax3 Then
dtmax = dtmax1
ElseIf dtmax2 < dtmax1 And dtmax2 < dtmax3 Then
dtmax = dtmax2
Else
dtmax = dtmax3
End If
dtmax = dtmax - (dtmax / 10)
dt = dtmax
If dt > 3 Then
dt = 3
End If


nt = CLng(tf / dt)
drmin = ((2 * De * dt) / (ep * (1 - ((1 - ep) * dt * ka / ep)))) ^ 0.5

drmax = De / kf
If dr < drmin Then
dr = drmin + (drmin / 10)
Worksheets("visual basic").Cells(100, 3).Value = "dr is small"
GoTo stepdr
End If
If dr > drmax Then
dr = drmax - (drmax / 10)
Worksheets("visual basic").Cells(100, 4).Value = "dr is large"
GoTo stepdr
End If

If (dz >= 2# * Dax / ui) Then
   Worksheets("visual basic").Cells(100, 1).Value = "dz is large"

End If
If (dt >= 1# / (2# * Dax / (dz ^ 2#) + 3# * kf * (1# - porosity) / (rp
* porosity))) Then
   Worksheets("visual basic").Cells(101, 1).Value = "dt is large"
End If
If (dt >= 1# / ((2 * De / (ep * (dr ^ 2)) + (1 - ep) * ka / ep))) Then
   Worksheets("visual basic").Cells(101, 2).Value = "dt is large"
End If
```

```
M1 = Dax / (dz ^ 2)
M2 = -ui / (2# * dz)
M3 = 3 * kf * (1 - porosity) / (r * porosity)
M4 = De * dt / (dr ^ 2)
M5 = (1 - ep) * dt * ka / ep

c1(0) = 0#
t(0) = 0#
Y(0) = 0#

For j = 1 To nz + 1
    c1(j) = co
Next j

For jr = 0 To nr
    q1(jr) = qo
    cp1(jr) = Cpo
Next jr

cp1(nr + 1) = cp1(nr) - dr * kf * (cp1(nr) - c1(0)) / De

M10 = 0#
Y10 = 0#

ycal(0) = 0#

For i = 0 To nt
    c(0) = c1(0)
    c(1) = c(0) + dz * ui * c(0) / Dax

    For j = 0 To nz
        q(0) = (1# - (dt * ka / k)) * q1(0) + dt * ka * cp1(0)
        q(1) = q(0)
        cp(1) = (M4 / 1# + M4) * cp1(2) + (1# - 2# * M4 - M5) * cp1(1)
+ (M4 - M4 / 1#) * cp1(0) + M5 * q1(1) / k
        cp(0) = cp(1)

        For jr = 2 To nr
            q(jr) = (1# - dt * ka / k) * q1(jr) + dt * ka * cp1(jr)
            cp(jr) = (M4 / jr + M4) * cp1(jr + 1) + (1# - 2# * M4 - M5)
* cp1(jr) + (M4 - M4 / jr) * cp1(jr - 1) + M5 * q1(jr) / k
        Next jr
        If (j < 2) Then GoTo stepz1
        c(j) = dt * (M1 + M2) * c1(j + 1) + (1# - 2# * M1 * dt - M3 *
dt) * c1(j) + dt * (M1 - M2) * c1(j - 1) + M3 * dt * cp1(nr + 1)

stepz1:
        cp(nr + 1) = cp(nr) - dr * kf * (cp(nr) - c(j)) / De

    Next j
    c(nz + 1) = c(nz)

    area = dt * (c(nz) + c1(nz)) / 2#
    M = M10 + area * us * a
    Y(i) = M * 100# / Msample
    t(i) = i * dt
```

```
    For j = 0 To nz + 1
        c1(j) = c(j)
        M10 = M
     Next j
     For jr = 0 To nr
        cp1(jr) = cp(jr)
        q1(jr) = q(jr)
     Next jr
     cp1(nr + 1) = cp(nr + 1)
    If i > 0 Then
    If t(i - 1) <= texp(ib) * 60 And t(i) > texp(ib) * 60 Then
     ycal(ib) = ((texp(ib) * 60 - t(i - 1)) / (t(i) - t(i - 1))) * (Y(i)
- Y(i - 1)) + Y(i - 1)
        ib = ib + 1
    End If
    End If

Next i
OBJF = 0#
For ib = 1 To ibn - 1
OBJF = OBJF + ((ycal(ib) - yexp(ib)) / yexp(ib)) ^ 2
Next ib
Worksheets("visual basic").Cells(5, 21).Value = OBJF
Worksheets("visual basic").Cells(6, 10).Value = OBJF
Worksheets("visual basic").Range("i6").Value = x(1)
Worksheets("visual basic").Range("i7").Value = x(2)
Worksheets("visual basic").Range("i8").Value = x(3)
Worksheets("visual basic").Range("i9").Value = x(4)

FUNC = OBJF
End Function
Sub Optimization()
     NDIM = 4
     Dim XP(4), xi(4, 4)
     FTOL = 0.000001
     np = NDIM
      For i = 1 To NDIM
        For j = 1 To NDIM
          xi(i, j) = 0#
        Next j
      Next i
      For i = 1 To NDIM
        xi(i, i) = 1#
      Next i
      De = Worksheets("visual basic").Range("c64").Value
      kf = Worksheets("visual basic").Range("c66").Value
      k = Worksheets("visual basic").Range("c67").Value
      ka = Worksheets("visual basic").Range("c68").Value

      XP(1) = De
      XP(2) = kf
      XP(3) = k
      XP(4) = ka

      Call powell(XP, xi, NDIM, np, FTOL, iter, fret)
```

```
    Worksheets("visual basic").Range("i6:k9").ClearContents
    Worksheets("visual basic").Range("i6").Value = XP(1)
    Worksheets("visual basic").Range("i7").Value = XP(2)
    Worksheets("visual basic").Range("i8").Value = XP(3)
    Worksheets("visual basic").Range("i9").Value = XP(4)
    Worksheets("visual basic").Range("j6").Value = FUNC(XP)
    Worksheets("visual basic").Range("j7").Value = fret
    Worksheets("visual basic").Range("k6").Value = iter
End Sub
Sub powell(P, xi, N, np, FTOL, iter, fret)
      NMAX = 20
      ITMAX = 200
      Dim pt(20), ptt(20), xit(20)
      fret = FUNC(P)
      For j = 1 To N
        pt(j) = P(j)
      Next j
      iter = 0
step1:
     iter = iter + 1
      fp = fret
      ibig = 0
      del = 0#
      For i = 1 To N
        For j = 1 To N
          xit(j) = xi(j, i)
        Next j
        fptt = fret
        Call linmin(P, xit, N, fret)
        If (Abs(fptt - fret) > del) Then

          del = Abs(fptt - fret)
          ibig = i
        End If
      Next i
      If (2# * Abs(fp - fret) <= FTOL * (Abs(fp) + Abs(fret))) Then
GoTo finish
      If (iter = ITMAX) Then GoTo finish2
      For j = 1 To N
        ptt(j) = 2# * P(j) - pt(j)
        xit(j) = P(j) - pt(j)
        pt(j) = P(j)
      Next j
      fptt = FUNC(ptt)
      If (fptt >= fp) Then GoTo step1
      t = 2# * (fp - 2# * fret + fptt) * (fp - fret - del) ^ 2# - del *
(fp - fptt) ^ 2#
      If (t >= 0#) Then GoTo step1
      Call linmin(P, xit, N, fret)
      For j = 1 To N
        xi(j, ibig) = xi(j, N)
        xi(j, N) = xit(j)
      Next j
      GoTo step1
finish2:
      Worksheets("visual basic").Range("l6").Value = "powell exceeding
maximum iterations"
```

```
finish:
End Sub
Sub linmin(P, xi, N, fret)
      NMAX = 50
      tol = 0.0001
      ncom = N
      For j = 1 To N
        pcom(j) = P(j)
        xicom(j) = xi(j)
      Next j
      ax = 0#
      xx = 1#
      Call mnbrak(ax, xx, bx, fa, fx, fb)
      fret = brent(ax, xx, bx, tol, xmin)
      For j = 1 To N
        xi(j) = xmin * xi(j)
        P(j) = P(j) + xi(j)
      Next j
End Sub
Sub mnbrak(ax, bx, cx, fa, fb, fc)
      GOLD = 1.618034
      GLIMIT = 100#
      TINY = 1E-20
      fa = fldim(ax)
      fb = fldim(bx)
      If (fb > fa) Then
        dum = ax
        ax = bx
        bx = dum
        dum = fb
        fb = fa
        fa = dum
      End If
      cx = bx + GOLD * (bx - ax)
      fc = fldim(cx)
step1:
      If (fb >= fc) Then
        r = (bx - ax) * (fb - fc)
        q = (bx - cx) * (fb - fa)
        maxqr = Application.WorksheetFunction.Max(Abs(q - r), TINY)
        u = bx - ((bx - cx) * q - (bx - ax) * r) / (2# * sign(maxqr, q
- r))
        ulim = bx + GLIMIT * (cx - bx)
        If ((bx - u) * (u - cx) > 0#) Then
          fu = fldim(u)
          If (fu < fc) Then
            ax = bx
            fa = fb
            bx = u
            fb = fu
            GoTo finish
          ElseIf (fu > fb) Then
            cx = u
            fc = fu
            GoTo finish
          End If
          u = cx + GOLD * (cx - bx)
```

```
        fu = f1dim(u)
      ElseIf ((cx - u) * (u - ulim) > 0#) Then
        fu = f1dim(u)
        If (fu < fc) Then
          bx = cx
          cx = u
          u = cx + GOLD * (cx - bx)
          fb = fc
          fc = fu
          fu = f1dim(u)
        End If
      ElseIf ((u - ulim) * (ulim - cx) >= 0#) Then
        u = ulim
        fu = f1dim(u)
      Else
        u = cx + GOLD * (cx - bx)
        fu = f1dim(u)
      End If
      ax = bx
      bx = cx
      cx = u
      fa = fb
      fb = fc
      fc = fu
      GoTo step1
    End If
finish:
    End Sub
    Function brent(ax, bx, cx, tol, xmin)
    ITMAX = 100
    CGOLD = 0.381966
    ZEPS = 0.0000000001
     a = Application.WorksheetFunction.Min(ax, cx)
     b = Application.WorksheetFunction.Max(ax, cx)
    v = bx
    w = v
    x = v
    E = 0#
    fx = f1dim(x)
    fv1 = fx
    fw = fx
    For iter = 1 To ITMAX
      xm = 0.5 * (a + b)
      tol1 = tol * Abs(x) + ZEPS
      tol2 = 2# * tol1
      If (Abs(x - xm) <= (tol2 - 0.5 * (b - a))) Then GoTo step3
      If (Abs(E) > tol1) Then
        r = (x - w) * (fx - fv1)
        q = (x - v) * (fx - fw)
        P = (x - v) * q - (x - w) * r
        q = 2# * (q - r)
        If (q > 0#) Then P = -P
        q = Abs(q)
        etemp = E
        E = D
        If (Abs(P) >= Abs(0.5 * q * etemp) Or P <= q * (a - x) Or P
>= q * (b - x)) Then GoTo step1
```

```
            D = P / q
            u = x + D
            If (u - a < tol2 Or b - u < tol2) Then D = sign(tol1, xm - x)
            GoTo step2
          End If
step1:
          If (x >= xm) Then
            E = a - x
          Else
            E = b - x
          End If
          D = CGOLD * E
step2:
          If (Abs(D) >= tol1) Then
            u = x + D
          Else
            u = x + sign(tol1, D)
          End If
          fu = f1dim(u)
          If (fu <= fx) Then
            If (u >= x) Then
              a = x
            Else
              b = x
            End If
            v = w
            fv1 = fw
            w = x
            fw = fx
            x = u
            fx = fu
          Else
            If (u < x) Then
              a = u
            Else
              b = u
            End If
            If (fu <= fw Or w = x) Then
              v = w
              fv1 = fw
              w = u
              fw = fu
            ElseIf (fu <= fv1 Or v = x Or v = w) Then
              v = u
              fv1 = fu
            End If
          End If
      Next iter
        GoTo finish2
step3:
        xmin = x
        brent = fx
finish2:
        Worksheets("visual  basic").Range("17").Value  =  "brent  exceeding
maximum iterations"
End Function
        Function f1dim(x)
```

```
      Dim xt(50)
      NMAX = 50
      For j = 1 To ncom
        xt(j) = pcom(j) + x * xicom(j)
      Next j
      fldim = FUNC(xt)
End Function
Function sign(a, b)
    If (b >= 0#) Then
       sign = Abs(a)
    Else
       sign = -Abs(a)
    End If
End Function
```

ملخص الأطروحة

استخدمت نبتة الحناء تقليديا في تلوين الأظافر, الجلد, و صبغة الشعر، كما أنها تعد من النباتات الطبية. تعتبر الموائع فوق الحرجة تقنية مضمونة كوسط للاستخلاص فضلا عن طرق الاستخلاص التقليدية الأخرى. في هذه الدراسة تم استخلاص المواد المتطايرة من زهرة الحناء باستخدام ثاني أكسيد الكربون فوق الحرج تحت ضغط مداه من 80 إلى 120 بار و درجات حرارة تتراوح من 35 و حتى 55 درجة مئوية. أعلى تحصيل للاستخلاص من 2 جم من ورود الحناء كان 31% تحت ضغط 120 بار و درجة حرارة 45 درجة مئوية. كما تم استكشاف تركيب المستخلص باستخدام تقنية الغاز كروماتوغرافي (Gas Chromatography). فحص النشاط المضاد للأكسدة و المضاد للبكتيريا لمستخلص ورود الحناء. لم يكشف فحص النشاط المضاد للبكتيريا عن وجود منطقة عزل للبكتيريا على الرغم من أن الدراسة كشفت عن احتواء مستخلص أزهار الحناء على مضادات أكسدة.

اشتق التمثيل الرياضي لمنحنى الاستخلاص باستخدام قوانين انتقال الكتلة لجميع ظروف الاستخلاص التي درست مخبريا. استخدمت طريقة Powell لحساب عوامل المعادلات الرياضية المشتقة و ذلك بتضبيطها للنتائج المخبرية. سجلت نتائج حساب التحصيل من المعادلات الرياضية توافقا جيدا مع نتائج التحصيل من التجارب المخبرية.

UAEU Faculty of Engineering

جامعة الإمارات العربية المتحدة
United Arab Emirates University

جامعة الإمارات العربية المتحدة

كلية الهندسة

برنامج ماجستير علوم البترول و الهندسة

استخلاص زيت زهرة الحناء باستخدام ثاني أكسيد الكربون فوق الحرج: عمليا، رياضيا و دراسة نشاطه المضاد للأكسدة.

مقدمة من

بشرى سعيد محمد دحي

رسالة مقدمة إلى

جامعة الإمارات العربية المتحدة

لاستكمال متطلبات

درجة الماجستير في علوم البترول والهندسة

Shrieen M Wolieed

Digitally signed by Shrieen M Wolieed
DN: cn=Shrieen M Wolieed, o=United Arab Emirates University, ou=UAEU Libraries, email=shrieen@uaeu.ac.ae, c=AE
Date: 2017.05.08 07:17:34 +04'00'

April 2012